Title
Molecular Engineering on Semiconducting Polymers for Enhancing Solar Cell Performance

Author
Chang, Wei-Hsuan

Publication Date
2016

Peer reviewed|Thesis/dissertation

UNIVERSITY OF CALIFORNIA

Los Angeles

Molecular Engineering on Semiconducting Polymers for Enhancing Solar Cell Performance

A dissertation submitted in partial satisfaction of the

requirements for the degree Doctor of Philosophy

in Materials Science and Engineering

by

Wei-Hsuan Chang

2016

ABSTRACT OF THE DISSERTATION

Molecular Engineering on Semiconducting Polymers for

Enhancing Solar Cell Performance

by

Wei-Hsuan Chang

Doctor of Philosophy in Materials Science and Engineering

University of California, Los Angeles, 2016

Professor Yang Yang, Chair

A promising solution to address the present-day energy crisis is photovoltaic technology. Currently, the market is dominated by inorganic-based materials such as silicon, III-V semiconductors, CIGS, etc. Despite their technical maturity, the energy generated from these devices is still low. This is partially due to the high production cost of these materials. Therefore, the search for next generation photovoltaic technologies that utilize earth-abundant elements with low-cost production processes has been an intensive research area.

Using solution-processable organic polymer semiconductors, polymer solar cells provide an opportunity to efficiently generate energy from sunlight at a reasonable cost. This is due to the

ease of synthesis/modification of organic molecules and polymers compared to that of inorganic materials, the easily scalable solution-based fabrication process, and the use of cost-effective, environmentally friendly carbon-based elements. Owing to the vast research efforts over the past decade, the power conversion efficiencies of single- and multi-junction polymer solar cells have recently surpassed the 10% milestone.

During this progression, materials development, driven by the desire to overcome the constraint of P3HT, has played a very important role in advancing the technology. To date, hundreds of photovoltaic polymers have been made through different combinations of conjugated building blocks and suitable functional groups. As a result, several state-of-the-art polymers, such as PTB7, PDPP3T, PBDTDPP and PffBT4T, have shown impressive performance. In order to keep this momentum going, further improvements and deeper insights into materials' property are certainly needed. In this dissertation, we particularly focus on improving the properties of several state-of-the-art photovoltaic polymers by resolving their shortcomings using innovative organic synthetic approaches. It is demonstrated that the materials' optoelectronic property as well as their fabrication process can be alternated through chemistry modification at a molecular scale, that is, by molecule engineering. This study paves a way not only to achieve high performance polymer solar cells, but also to provide novel synthetic strategies for researchers in the field to further push the boundaries of polymer solar cell technology in the future.

The dissertation of Wei-Hsuan Chang is approved.

Ya-Hong Xie

Yves F. Rubin

Yang Yang, Committee Chair

University of California, Los Angeles

2016

To my family

TABLE OF CONTENTS

LIST OF FIGURES

LIST OF SCHEMES

LIST OF TABLES

ACKNOWLEDGMENT

This dissertation cannot be completed without the unwavering support and guidance of many. I would like to express my deepest appreciation to everyone who has helped make my Ph.D. work possible.

First of all, I would like to give my sincere thanks to my Ph.D. advisor, Prof. Yang Yang, for the opportunity to join his distinguished research group. Under his guidance, I learned not only the methodology of scientific research, but also the significance of challenging real-world issues, ways to solve problems with teamwork and creativity, and the importance of conducting work with the correct attitude. Through sharing his experience, inspirational thoughts, and encouragement, Prof. Yang helped me pass through the ups and downs of my graduate study all these years. Without his endless support, I would not be able to have all these achievements, for which I thank him the most.

I also would like to thank my committee members, Prof. Yu Huang, Prof. Ya-Hong Xie, and Prof. Yves Rubin, for their mentorship and support to make the work better.

My current and former labmates in the Yang Yang research laboratory played a remarkable part in my graduate research life. I would like to first thank Dr. Letian Dou and Dr. Youjun He for bringing me to the field of synthetic semiconducting polymers; and I thank Dr. Yongsheng Liu, Dr. Eric Richard, and Dr. Shirong Lu for the helpful discussions on the synthetic problems that I have encountered over these years. I also thank Dr. Gang Li, Dr. Ziruo Hong, and Dr. Jingbi You for sharing many of their valuable experiences on solar cell research with me. I also enjoyed the collaboration with Dr. Jing Gao, Dr. Chun-Chao Chen, Dr. Yang (Michael)

Yang and Mr. Lei Meng, I thank them for helping me turn the materials into working devices and for their contribution in much of the data shown in this dissertation. In addition, thanks to Mr. Hongxiang Zhao and Mr. Eric Young for the help on the materials' synthesis, to Dr. Adam Sting for the instruction on the AFM measurement, to Dr. Ivo Atanasov for the support on the TEM measurement, to Dr. Wei Chen at Argonne National Laboratory for the GIWAXD characterizations, and to Dr. Blanton Martin and Prof. Kendal Houk for the helpful discussion on the calculation work, and to Mr. Nicholas De Macro and Mr. Onur Sahin for proofreading this dissertation. Moreover, I like to thank Dr. Wenbing Yang, Dr. Kitty Cha, Dr. Brion Bob, Dr. Wan-Ching Hsu, Dr. Hsin-Sheng Duan, Dr. Fei Wang, Dr. Steve Hawks, Ms. Cara Hsu, Dr. Tze-Bin Song, Mr. Zhenyi Wang, Mr. Jinhee Park, Dr. Shenglin Ye, Dr. Min Cai, Dr. Chenyang Jiang, Dr. Huanping Zhou, Dr. Qi Chen, Dr. You Seung Rim, Mr. Song Luo, Mr. Lei Meng, Mr. Huajun Chen, Mr. Yao-Tsung Hsieh, Mr. Penyu Sun, Mr. Sanghoon Bae, Mr. Sheng-Yung Chang, Ms. Shiqi Dong, and Mr. Zhanlue Yang for all the fruitful discussions and moment in the lab.

Besides the members at UCLA, I would also like to thank Dr. Ming-Ren Tarng, Ms. Anh Pham, Dr. Joshua Jiang, Dr. Greg Williams, Ms. Lan Liang, Mr. Truc Huynh and Dr. James Thomas for having me as a R&D intern at BEHR Process Corporation. Thank you for showing me how polymer chemistry is used in the coating industry. I was really excited that my knowledge could be applied to form a product that meets the customers' needs.

Specially, I like to show my appreciation to all my previous mentors/supervisors, Dr. Yuan-Chang Huang, Dr. Yuung-Ching Sheen, Prof. Yu-Jane Sheng, Prof. Wen-Chang Chen, and Prof. Cheng-Liang Liu, for cultivating my interest in scientific research. I also like to thank Dr.

Yu Chen and Ms. Szunung Ho for their endless advice/support, which greatly helped me move forward in the US.

Finally, I would like to thank my dearest parents, my brother and all other family members in Taiwan for their tremendous support and for giving me the chance to pursue my Ph.D. degree without hesitation. My appreciation to them can hardly be put into words. I also thank my wife, Ya-Ting Yeh and my son, Artus Chang; they make everything I did meaningful and I thank them for going through all these years with me. I would never be able to reach this step of my life without my family, for which I thank my family again deeply from my heart.

VITA

2007	Bachelor of Science, Chemical Engineering, National Tsing-Hua University (NTHU), Hsinchu, Taiwan
2006-2008	Intern Research Assistant, Industrial Technology Research Institute (ITRI), Hsinchu, Taiwan
2010	Master of Science, Polymer Science and Engineering, National Taiwan University (NTU), Taipei, Taiwan
2011	Project Research Assistant, Faculty of Engineering, Yamagata University (YU), Yamagata, Japan
2015	Research and Development Intern, BEHR Process Corporation, California, USA
2011-2015	Graduate Student Researcher, Department of Materials Science and Engineering, University of California, Los Angeles (UCLA), California, USA

PUBLICATIONS

1. Yongsheng Liu, Ziruo Hong, Qi Chen, Huajun Chen, Wei-Hsuan Chang, Yang (Michael) Yang, Tze-Bin Song and Yang Yang, "Perovskite Solar Cells Employing Dopant-Free Organic Hole Transport Materials with Tunable Energy Levels", *Adv. Mater*., Advance Article (2015)

2. Jingbi You, Lei Meng, Tze-Bin Song, Tzung-Fang Guo, Yang (Michael) Yang, Wei-Hsuan Chang, Ziruo Hong, Huajun Chen, Huanping Zhou, Qi Chen, Yongsheng Liu, Nicholas De Marco and Yang Yang, "Improved air stability of perovskite solar cells via solution-processed metal oxide transport layers", *Nature Nanotechnology* (2015)

3. Xiaobao Xu, Qi Chen, Ziruo Hong, Huanping Zhou, Zonghao Liu, Wei-Hsuan Chang, Pengyu Sun, Huajun Chen, Nicholas De Marco, Mingkui Wang and Yang Yang, "Working Mechanism for Flexible Perovskite Solar Cells with Simplified Architecture", *Nano Lett*., 15 (10), pp 6514–6520 (2015).

4. Wei-Hsuan Chang, Lei Meng, Letian Dou, Jingbi You, Chun-Chao Chen, Yang Yang, Eric Patrick Young, Gang Li, Yang Yang, "A Selenophene Containing Benzodithiophene-alt-thienothiophene Polymer for Additive-Free High Performance Solar Cell", *Macromolecules*, 48 (3), pp 562–568 (2015).

5. Yang (Michael) Yang, Wei Chen, Letian Dou, Wei-Hsuan Chang, Hsin-Sheng Duan, Brion Bob, Gang Li, Yang Yang, "High-performance multiple-donor bulk heterojunction solar cells", *Nature Photonics* 9, 190–198 (2015).

6. Chun-Chao Chen, Sang-Hoon Bae, Wei-Hsuan Chang, Ziruo Hong, Gang Li, Qi Chen, Huanping Zhou, Yang Yang, "Perovskite/polymer monolithic hybrid tandem solar cells utilizing a low-temperature, full solution process", *Mater. Horiz.*, 2, 203-211 (2015).

7. Yongsheng Liu, Ziruo Hong, Qi Chen, Weihsuan Chang, Huanping Zhou, Tze-Bin Song, Eric Young, Yang Yang, Jingbi You, Gang Li, Yang Yang, "Integrated Perovskite/Bulk-Heterojunction toward Efficient Solar Cells", *Nano Lett*., 15 (1), pp 662–668 (2015).

8. Letian Dou, Yang Micheal Yang, Jingbi You, Ziruo Hong, Wei-Hsuan Chang, Gang Li, Yang Yang, "Solution-processed hybrid perovskite photodetectors with high detectivity", *Nature Communications* 5:5404 (2014).

9. Jingbi You, Yang Michael Yang, Ziruo Hong, Tze-Bin Song, Lei Meng, Yongsheng Liu, Chengyang Jiang, Huanping Zhou, Wei-Hsuan Chang, Gang Li, Yang Yang, "Moisture assisted perovskite film growth for high performance solar cells", *Appl. Phys. Lett*. 105, 183902 (2014).

10. Chun-Chao Chen, Wei-Hsuan Chang, Ken Yoshimura, Kenichiro Ohya, Jingbi You, Jing Gao, Zirou Hong, Yang Yang, "An Efficient Triple-Junction Polymer Solar Cell Having a Power Conversion Efficiency Exceeding 11%", *Adv. Mater*. 26, 5670 (2014).

11. Jing Gao, Wei Chen, Letian Dou, Chun- Chao Chen, Wei- Hsuan Chang, Yongsheng Liu, Gang Li, Yang Yang, "Elucidating Double Aggregation Mechanisms in the Morphology Optimization of Diketopyrrolopyrrole-Based Narrow Bandgap Polymer Solar Cells", *Adv. Mater*., 26, 3142 (2014).

12. Wei-Hsuan Chang, Jing Gao, Letian Dou, Chun-Chao Chen, Yongsheng Liu, Yang Yang, "Side-Chain Tunability via Triple Component Random Copolymerization for Better Photovoltaic Polymers", *Adv. Energy Mater*. 4, 1300864 (2014).

13. Jing Gao, Letian Dou, Wei Chen, Chun- Chao Chen, Xuanrong Guo, Jingbi You, Brion Bob, Wei- Hsuan Chang, Joseph Strzalka, Cheng Wang, Gang Li, Yang Yang, "Improving Structural Order for a High-Performance Diketopyrrolopyrrole-Based Polymer Solar Cell with a Thick Active Layer", *Adv. Energy Mater*. 4, 1300739 (2013).

14. Chun-Chao Chen, Jingbi You, Letian Dou, Jing Gao, Wei-Hsuan Chang, Shenglin Ye, Brion Bob, Gang Li, and Yang Yang, "High Performance Transparent and Grayscale Polymer Solar Cells via Tandem Structures", *Energy Environ. Sci*. 6, 2714 (2013).

15. Letian Dou, Chun-Chao Chen, Ken Yoshimura, Kenichiro Ohya, Wei-Hsuan Chang, Jing Gao, Yongsheng Liu, Eric Richard, and Yang, Yang, "Synthesis of 5H-dithieno[3,2-b:2',3'-d]pyran as an Electron-rich Building Block for Donor-Acceptor Type Low-bandgap Polymers", *Macromolecules* 46, 3384 (2013).

16. Wei-Hsuan Chang, Letian Dou, Jing Gao, Chun-Chao Chen, Jingbi You, and Yang Yang, "A Selenium-substituted Low-Bandgap Polymer with Versatile Photovoltaic Applications", *Adv. Mater.* 25, 825 (2013).

17. Wei-Hsuan Chang, Shih-Hao Chou, Jiang-Jen Lin, Wen-Chang Chen, and Yu-Jane Sheng, "Thin film morphologies of π-conjugated rod-coil block copolymers with thermoresponsive property: A combined experimental and molecular simulation study", *J. Chem. Phys.* 132, 214901 (2010).

18. Kuan-Kai Huang, Yi-Kai Fang, Jung-Ching Hsu, Chi-Ching Kuo, Wei-Hsuan Chang, and Wen-Chang Chen, “Synthesis, Micellar Structures, and Multifunctional Sensory Properties of Poly(3-hexylthiophene)-b- poly(2-(dimethylamino)ethyl methacrylate) Rod-Coil Diblock Copolymers”, *J. Polym Sci. Part A: Polym. Chem*.; DOI: 10.1002/pola.24429 (2010).

19. Yuung-Ching Sheen, Wei-Hsuan Chang, Wen-Chang Chen, Yih-Her Chang, Yuan-Chang Huang, Feng-Chih Chang, “Non-fluorinated superamphiphobic surfaces throughsol–gel processing of methyltriethoxysilaneand tetraethoxysilane”, *Materials Chemistry and Physics*, 114, 63 (2009).

CHAPTER 1

General Introduction

Photovoltaic (PV) or solar cell technology is known to be a key solution to the increasingly prominent energy crisis. Presently, the solar market is dominated by inorganic-based materials, such as silicon (Si), III-V semiconductors, CdTe, CIGS, etc.[1] However, electricity that comes from sunlight is still low compared to the total grid-based energy (in the US, for example, solar energy only accounts for about 0.4% of total energy generation), which is partially due to the high production cost of these conventional PV technologies.[2] Consequently, there is a need for affordable solar cell technology. Among all emerging PV technologies, organic photovoltaics (OPVs) show a great potential in achieving this cost-effective goal, as they are mainly made of earth-abundant materials, such as carbon, hydrogen, and oxygen, etc. In addition, a solution processing approach is feasible for organic solar cells, making them processable by a range of printing techniques. Furthermore, due to organic materials' unique properties, these kinds of solar cells may feature many attractive properties such as being flexible, lightweight, or even visibly transparent. Due to these benefits, the OPV research field has drawn tremendous attention over the past decades.[3] In this chapter, a brief introduction to organic semiconductors and their application to solar cells is given.

1.1 Organic semiconductors

Organic semiconductors are discrete molecules. There is no bonding between each molecule, and it can be though of as a quasi-1D semiconductor.[4] As shown in Figure 1-1a, the structure of such materials (ethylene as an example) is created by σ bonds forming between carbons' sp^2 orbitals and the parallel overlapping of leftover carbons' p_z orbitals forming π bonds. For a small molecule like ethylene or 1,3-butadiene (Figure 1-1b), the splitting between the π bonding (π) and π anti-bonding (π^*) is quite large. Thus, the energy required to cause electronic transition is far into the UV range.

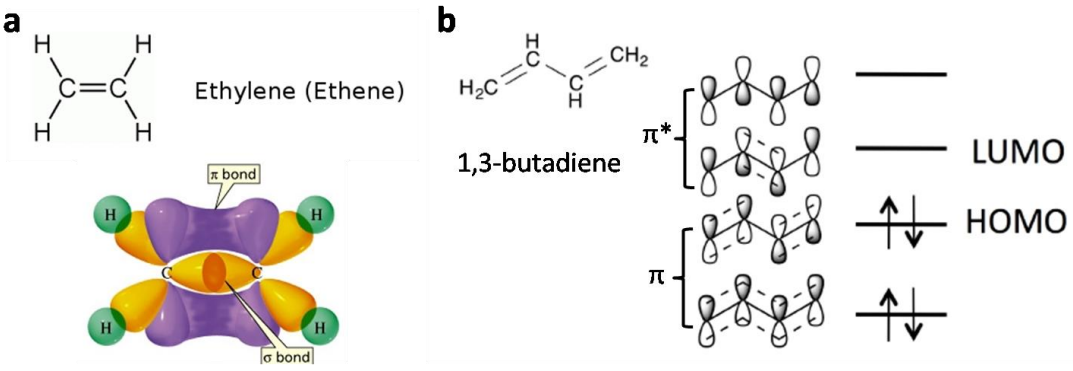

Figure 1-1. (a) Bonding in ethylene, and (b) bonding in 1,3-butadiene. (adopted and modified from reference [5] and [6])

As the overlapping of the carbons' p_z orbitals increases (for example, through polymerization of ethylene molecules), the π bondings further spread out into π-bands (Figure 1-2). The topmost π-band is referred to as the highest occupied molecular orbital (HOMO) and the lowest π* band is referred to as the lowest un-occupied molecular orbital (LUMO). The energy difference between the HOMO and LUMO thus determines the band gap (E_g) of the resulting molecule/polymer. Once the repeating unit is large enough, the splitting of the orbitals can thus

bring the HOMO and LUMO closer to each other. Once the E_g is close to the energy of UV or visible light, the material is considered to be a semiconductor.

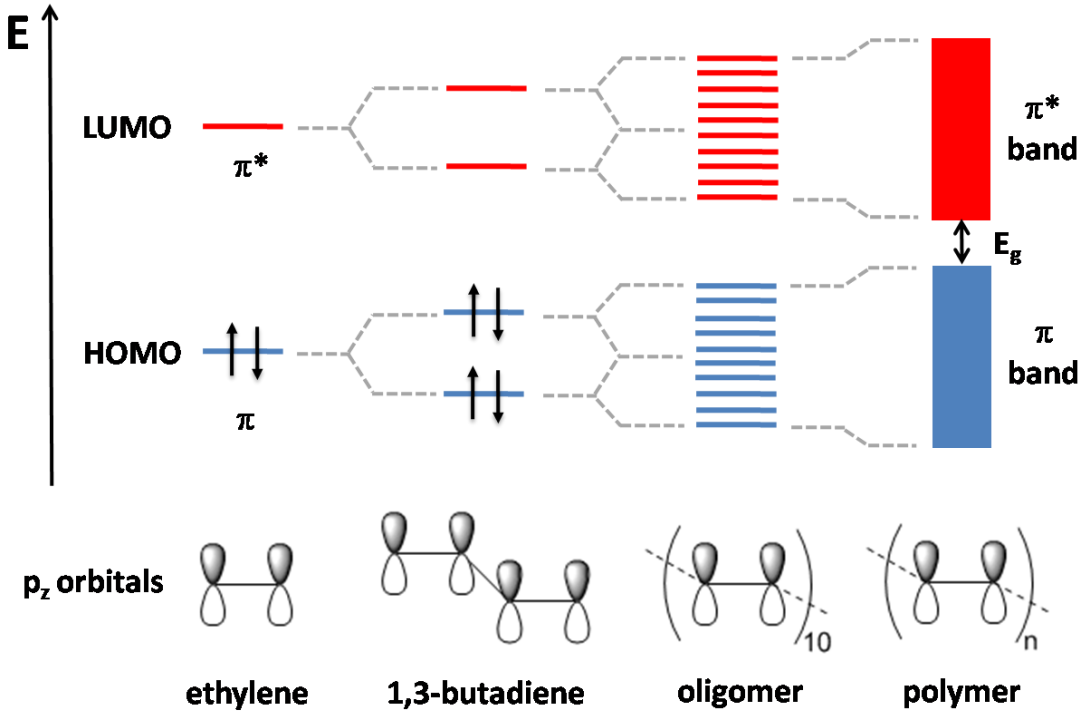

Figure 1-2. The relation between E_g and the number of overlapping p_z orbitals.

1.2 Properties of organic semiconductors

Unlike inorganic semiconductors, such as Si, where the atoms are covalently bonded in a 3-dimentional structure, the organic semiconductor has a link in only one dimension; and the intermolecular interaction can only form through weaker van der Waals and π-π interactions. Therefore, the electrons do not travel through the materials freely like in inorganic semiconductors; rather, they travel through a hopping mechanism.[7] As a result, the organic semiconductor charge carrier mobility is several orders lower than that of inorganic semiconductor charge carriers'. This further limits the diffusion length of carriers in organic semiconductors.

Other than carrier transportation, another major difference between these two types of semiconductors is the state of electron-hole pairs formed after optical or thermal excitation. In crystalline-Si, the take-up of photons that have enough energy generates freely moving electrons and holes. However, due to the lower dielectric constant (ε = 2-4) typical of organic semiconductors, the photoexcitation creates Frenkel excitons, with a binding energy of 0.3-1 eV, which can not dissociate under room temperature.

1.3 Background of organic photovoltaics

The first successful organic photovoltaic device was demonstrated by Tang *et al.* in 1986 [8] (note that the patent first appeared in 1979) with a reported power conversion efficiency (PCE) of ~1%. It was a bilayer device created through the evaporation of copper phthalocyanine (CuPc) and a subsequent o-phenylenediamine adduct of perylene tertracaboxylate. These two materials formed a heterojunction with a CuPc and perylene derivative as the p-type and n-type layer, respectively; and the charge-separation at this interface was found to be very efficient.

In the early 90s, ultrafast charge transfers (~ 50 fs) from polymer (MEH-PPV) to fullerene (C_{60}) were found to provide an efficient way of dissociating excitons formed in p-type polymers.[9] Furthermore, in order to overcome the short exciton diffusion length (~ 10 nm) issue in OPVs, the bulkheterojunciton (BHJ) structure, a mixed layer of p- and n-type organic semiconductors, was introduced, and the power conversion efficiency (PCE) was improved dramatically. This approach was first reported by Hiramoto *et. al.* for evaporation-processed small molecules in 1991[10] and in solution-processed MEH-PPV:C60 photodetectors by Heeger *et al.*[11] and Friend *et al.*[12] in 1994. Both discoveries mentioned above have together led to a great progression in the OPV field over the past decades.

1.4 Working mechanism of organic solar cells

Solar cells are devices that can generate voltage upon light absorption, and provide a power output if current flow is allowed. A typical graph to describe solar cell efficiency can be found in Figure 1-3, which is known as a current density – voltage (J-V or I-V) curve. As shown in the graph, the parameters used to evaluate a solar cell are open-circuit voltage (V_{OC}), short-circuit current (J_{SC}) and fill factor (FF%). This is because a solar cell's PCE can be calculated through the following equation: $PCE = V_{OC} \times J_{SC} \times FF/Pin$, where P_{in} is the input power.

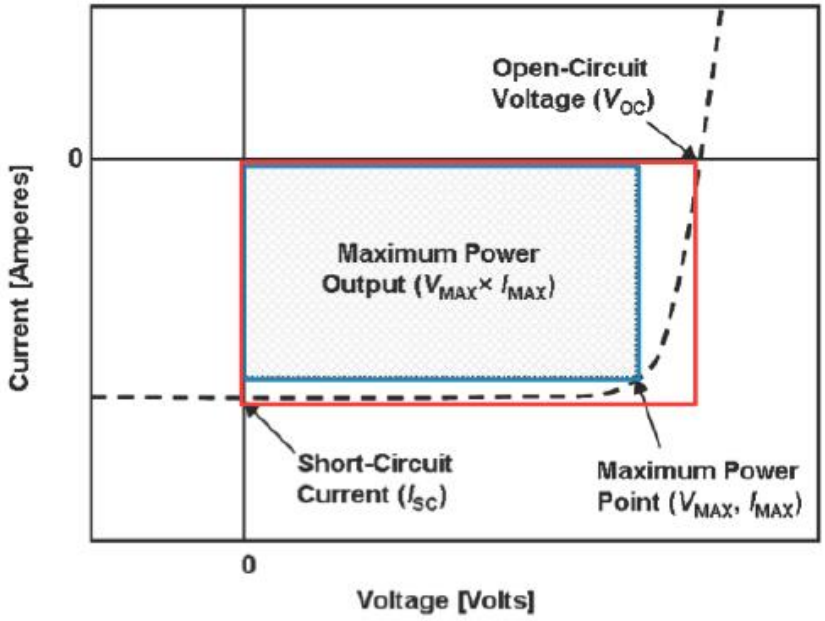

Figure 1-3. Typical J-V characterization curve for a solar cell. (adopted and modified from reference [13])

In OPVs, the basic process from light absorption to electron-hole generation can be broken down into four steps: 1) exciton generation, 2) exciton diffusion, 3) charge-separation, 4) charge diffusion and collection (Figure 1-4). The first step involves exciton generation, which is caused by incoming photon energies greater than the materials' E_g. The generated excitons then

diffuse to the p and n-type interface; this diffusion is believed to be a random walk process. Due to the limitation of exciton lifetime (~ ps), the distance that exciton can travel is only about 10-20 nm. The BHJ structure solves this issue by essentially providing interfaces everywhere in the active layer. Once the exciton reaches this interface, it will form a charge-transfer state (CT state), followed by electrons moving to the LUMO of n-type materials and holes staying at the HOMO of p-type materials. The whole process is now known to be photoinduced charge-transfer as mentioned above. Note that the LUMO-LUMO offset between the p-type and n-type is very important as it provides the necessary energy to dissociate the CT state. Once the CT state is separated, the electrons and holes are now free to move. The final step is the collection of these separated charges, which is done by selective contacts.

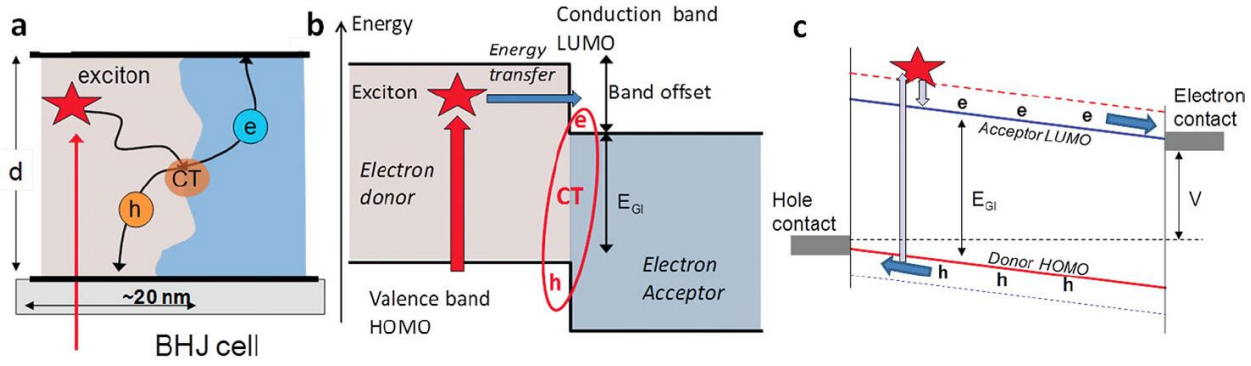

Figure 1-4. Basic geometry and electronic stricture of the BHJ OPV. (a) The nanoscale phase-separated domain morphology showing exciton absorption leading to the charge transfer state that separates into mobile electrons and holes, (b) The same process illustrated in an energy diagram showing the band offset between the donor (p-type) and acceptor (n-type) materials, and (c) Schematic of solar cell current flow at voltage bias V. (Adopted from reference [3])

In OPVs, the V_{OC} is closely related to the difference between HOMO and LUMO energy levels of p-type polymers and n-type materials, respectively. The J_{SC} is essentially determined by

the E_g of the p-type material and its light-absorbing capability (i.e. absorption coefficient). The FF% depends on charge separation and transportation properties within the device, and is largely influenced by the BHJ morphology, in which a nanoscale phase-separation is required.

Over the years, researchers have been putting effort into improving the PCE of lab scale OPV devices. At the time of writing this dissertation, the PCE of OPVs has increased to over 10% for single junction cells[14] and over 11% for multijunction stacking cells.[15] This is achieved through fundamentally understanding the material and morphology, designing and synthesizing novel materials, and optimizing the organic/electrode interfaces by researchers all over the field. This dissertation contributes to the research field from a polymer chemist's standpoint. We aim to resolve the shortcomings of several state-of-the-art "donor-acceptor" p-type polymers by re-designing the materials at the molecular scale, i.e. molecular engineering. Such modifications are achieved by carrying out innovative organic synthetic approaches, which will be detailed in the later chapters. Note that the donor-acceptor type polymers have been referred to as 3rd generation semiconducting polymers[4], and I will start with introducing these types of polymers in the following chapter.

References:

[1] Barkhouse D. A. R. *et al. Prog. Photovoltaics Res. Appl.* **2012**, *20*, 6–11.

[2] url: http://instituteforenergyresearch.org/topics/encyclopedia/solar/

[3] Dou, L. *et al. Adv. Mater.* **2013**, *25*, 6642–6671.

[4] Heeger, A. J. *Chem. Soc. Rev.* **2010**, *39*, 2354.

[5] http://andromeda.rutgers.edu/~huskey/images/ethylene_bonding.jpg

[6] Richard, E. T. *Design and Synthesis of Conjugated Polymers and Small Molecules Based on Thiophene-Substituted Isoindigo, 5-acetyl-4Hcyclopenta[ ]thiophene-4,6(5H)-dione, and Diketopyrrolopyrrole Electron-Deficient Units*, Ph.D. Thesis, University of California, Los Angeles, 2014.

[7] Bässler, H.; Köhler, A. *Top. Curr. Chem.* **2012**, *312*, 1–65.

[8] Tang, C. W. *Appl. Phys. Lett.* **1986**, *48*, 183.

[9] Sariciftci, N. S. e*t al. Science* **1992**, *258*, 1474–1476.

[10] Hiramoto, M. *et al. Appl. Phys. Lett.* **1991**, *58*, 1062–1064.

[11] Yu, G. *et al. Science* **1995**, *270*, 1789–1791.

[12] Halls, J. J. M. *et al. Nature* **1995**, *276*, 498-500.

[13] Dou, L. *Achieving High Performance Polymer Tandem Solar Cells via Novel Materials Design*, Ph.D. Thesis, University of California, Los Angeles, 2014.

[14] Liu, Y. *et al. Nat. Commun.* **2014**, *5*, 1–8.

[15] Chen, C. C. *et al. Adv. Mater.* **2014**, 5670–5677.

CHAPTER 2

Introduction to Donor-Acceptor Type Conjugated Polymers for Solar Cell Applications

The main focus of the present dissertation is the design and synthesis of p-type polymer semiconductors, concentrating on so-called "donor-acceptor" type conjugated polymers, for solar cell applications. We note that [6,6]-phenyl-C_{71}-butyric acid methyl ester ($PC_{71}BM$) is used as the n-type material throughout the entire study. The purpose of this chapter is to provide a background overview of this type of polymer, its application to organic solar cells, and its current status.

2.1 Background of donor-acceptor type conjugated polymers

Donor-acceptor polymers consist of at least two alternating moieties along their polymer backbone, one being electron-rich (i.e. the donor) and another being electron-deficient (i.e. the acceptor). This type of polymer is commonly referred to as a "D-A" type conjugated polymer (or D-A polymer), and it is now the most widely used semiconducting polymer in organic electronics.

In the early 1990s, Yamamoto *et al.* first observed intramolecular charge transfer behavior in a polymer consisting of thiophene and pyridine units.[1] In their work, thiophene was used as the donor moiety and pyridine as the acceptor moiety. The resulting D-A polymer's absorption/fluorescence spectra red-shifted relative to that observed in either thiophene or

pyridine homopolymers, indicating that the interaction of these two units formed a lower bandgap (E_g). Using this concept, Havinga *et al.* further demonstrated in 1993 a semiconducting polymer with a very low E_g of less than 0.5 eV.[2,3] This led to the emergence of using low band gap D-A polymers for spectral engineering. [4,5]

There are two different ways to elucidate the underlying mechanism behind why D-A polymers have a lower bandgap: delocalization of electrons along the polymer backbone and hybridization of frontier orbitals. First, using this structure facilitates the delocalization of electrons along the conjugated backbone. This helps stabilize the quinoid structure over the backbone, leading to a smaller energy gap.[6]

Second, hybridization of frontier orbitals can also explain the energy gap reduction.[7] As shown in Figure 2-1, as two moieties become closer to each other by chemical bonding, both highest occupied molecular orbitals (HOMOs) and lowest unoccupied molecular orbitals (LUMOs) of the donor and the acceptor start to interact with each other. As a result, new orbitals are formed. Once the electrons are redistributed, a new set of HOMO and LUMO levels of the bonded compound is produced, which results in a smaller bandgap. This concept also explains the fact that for the D-A polymer, the resulting HOMO level is largely affected by the donor, and the LUMO is largely affected by the acceptor.[8] Although these two concepts seem to be dissimilar, recent studies suggest that they are closely related and could be beneficial to each other.[9]

2.2 Synthesis of D-A polymers

Constructing D-A polymers starts by forming a C-C bond between two functionalized moieties. Transition metal catalyzed cross-coupling reactions, such as Sonogashira, Heck,

Suzuki–Miyaura, Stille or direct arylation couplings are used to form such bonding. Desired D-A polymer can be obtained through a controlled coupling reaction. [10, 12] Comprehensive reviews on these polymerization methodologies and their mechanisms can be found in previous review by Luh *et al*.[11] and Hsu *et al*.[8]

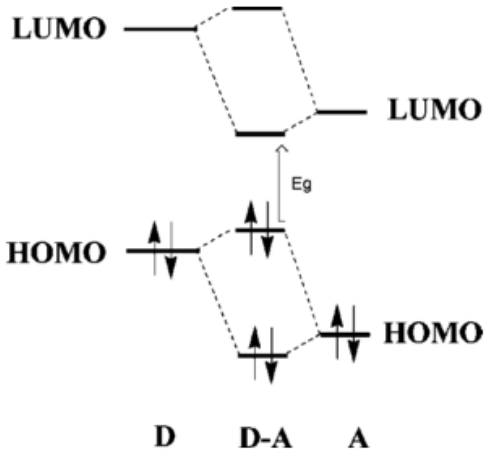

Figure 2-1. Orbital interactions of D and A units, which results in a smaller bandgap in D-A polymer. (Adopt from reference [8])

2.3 Design strategy of D-A polymers for solar cell applications

When designing a photovoltaic polymer, the first consideration is its resulting bandgap. This is because the bandgap of a polymer controls the amount of photons that can be absorbed; photons having energy larger than the bandgap are absorbed and photons having energy smaller than the bandgap pass through the polymer, resulting in wasted energy. Therefore, it is very important to design a polymer with a suitable bandgap. In D-A polymers, as mentioned above, the bandgap depends largely on the strength of electron-pushing (and withdrawing) ability of the donor (and acceptor). This provides material scientists a rather easier way (compared to inorganic semiconductors) to find the most suitable bandgap of their interest. Through combinations of different moieties, a wide range of bandgaps have been demonstrated.[8]

Second, it is also important to consider polymer's HOMO and LUMO energy levels. As discussed in the previous chapter, V_{OC} in organic photovoltaic (OPV) devices is closely related to the difference of HOMO and LUMO levels of p-type and n-type materials, respectively. In addition, charge-separation efficiency of OPV devices is highly related to the LUMO-LUMO offset of p-type and n-type materials. As a result, the rule of thumb when designing a p-type photovoltaic polymer is to down-shift the HOMO level while keeping the LUMO level above that of n-type material (for example, when utilizing [6,6]-phenyl-C_{61}-butyric acid methyl ester [PCBM] as n-type material, the LUMO level of the p-type material has to be at least higher than -3.7 eV in order to maintain a good charge separation).[13] Using this strategy, a maximum V_{OC} can be achieved without sacrificing the current generation.

Since solution-process is one of the key competences in OPVs, the third consideration of a polymer is to have a good solubility in common organic solvents. Solubility of polymers can be affected by a variety of factors, such as the molecular weight, the type of polymer side-chains, the rigidity of polymer backbone, and the strength of polymers' intermolecular interaction. In general, the easier the polymer to get aggregated, the harder it is to dissolve the polymer. Therefore, finding a great balance between solubility and short-range ordering of the polymers in the solid state is one of the major difficulties in OPV research. Often times, solving this issue, at this stage, evolves with many try-and-error experiments since the resulting solubility is hard to predict.[14]

2.4 Development of D-A polymers for solar cell applications

OPV research has sky rocketed since the success of P3HT-based devices (Figure 2-1a shows a P3HT structure). In the past decade this has resulted in solar cell power conversion efficiency (PCE) improvements as well as a better understanding of the underlying device

mechanisms.[13,15] One of the main contributions to the field's progression is materials development. Searching for materials that overcome the constraint of P3HT continues driving researchers around the world to synthesize new materials. To date, hundreds of D-A polymers have been made for solar cell applications. It is worth noting that the performance of OPV devices, as a rather complex system, is not only related to the polymer's intrinsic electronic property, but also dependent on the polymer ordering, as well as the nano- to micro-scale phase separation between the n-type materials, such as $PC_{71}BM$.

In the following sessions, several representative p-type D-A polymers for polymer solar cell (PSC) applications are reviewed and discussed. To simplify such a large amount of literature from the past ten years, polymers introduced here are being categorized by their bandgaps: 1) large Eg (>1.8 eV), 2) medium Eg (1.5-1.8 eV), and 3) small Eg (<1.5 eV).

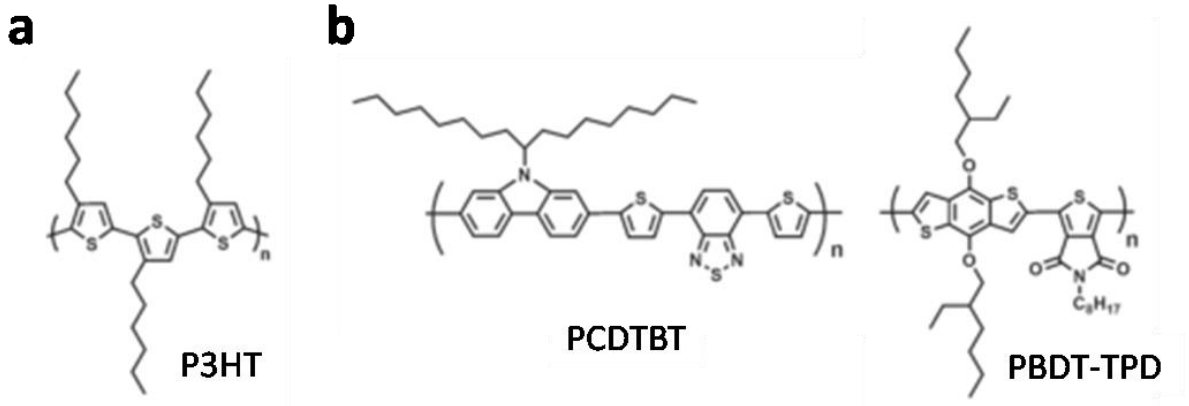

Figure 2-2. (a) P3HT, and (b) examples of large bandgap D-A polymers. (Adopted and modified from reference [13])

2.4.1 Large bandgap D-A polymers

One of the first successful large Eg p-type polymer is PCDTBT, reported by Leclerc *et al.*[16] They used carbazole as the donor and benzothiadiazole as the acceptor in this polymer.

As a result, this polymer has an optical bandgap of 1.88 eV. Combined with PCBM, it produced an initial PCE of 3.6% with a very high V_{OC} due to its low-lying HOMO level (-5.50 eV). The solar cell performance of this polymer later improved through different device engineering techniques, leading to a 6-7% PCE.[17,18] Another large bandgap polymer worth mentioning is PBDT-TPD, made by Leclerc, Frechet, and Jen groups independently.[19,20,21] Due to a relatively weak donor and acceptor, this polymer appeared to have an optical bandap of 1.81 eV with a very low HOMO value of -5.57 eV. The best device result was achieved by Frechet *et al*., giving a V_{OC} of 0.85 eV, a J_{SC} of 11.5 mA/cm^2, a FF of 68% and a PCE of 6.8%.[20] Note that this polymer consists of two monomers that are easily acquired, which is a great advantage when considering mass production.

2.4.2 Medium bandgap D-A polymers

Brabec *et al*.[22] and Yang *et al*.[24] further carried out different molecular modification approaches on PCDTBT to lower its bandgap. In Brabec' work, the carbazole (CDT) unit was replaced by cyclopenta[2,1-b;3,4-b']dithiophene (CPDT), which has a more electron-rich character than that of CDT. Due to a stronger donor-acceptor interaction, the new PCPDTBT polymer showed a smaller bandgap of ~1.5eV, and the initial device performance was around 3%. Interestingly, the PCE of PCPDTBT-based devices can be further improved to 5.5 % through adding a small amount of solvent additives (3 %, v/v), such as diiodoocatane (DIO), during device fabrication.[23] This is mainly due to a better nanoscale morphology formed in the PCPDTBT:$PC_{71}BM$ blend.

In Yang's work, the CPDT unit of the polymer is replaced by a silicon substituted analogue, dithieno[3,2-b:2',3'-d]silole (DTS). The bandgap and solar cell performance of the resulting polymer, PSBTBT, are similar to that of PCPDTBT-based devices but without using

any solvent additives. They attributed this observation to the fact that the C-Si bond is longer than the C-C bond. As a consequence, the side-chains on the PSBTBT are further pushed away from the backbone, resulting in a better stacking of the polymers. These two polymers, PCPDTBT and PSBTBT, successfully demonstrated the potential of utilizing near-infrared (NIR) photons in OPV devices at an early stage.

Tao *et al.* further combined DTS with TPD resulting in a polymer, PDTS-TPD, with a bandgap of 1.73 eV.[25] Compared to the PBDT-TPD series, PDTS-TPD has a higher photocurrent due to its lower Eg, and a recorded device PCE of 7.3%. Note that the device's active area was 1 cm^2, which is larger than the commonly reported OPV lab-cell value (~ 0.1 cm^2). So and Reynold *et al.* further optimized this structure by substituting silicon atom in the DTS unit with germanium. The resulting polymer, PDTG-TPD, achieved a 8.1 % PCE when blended with $PC_{71}BM$.[26]

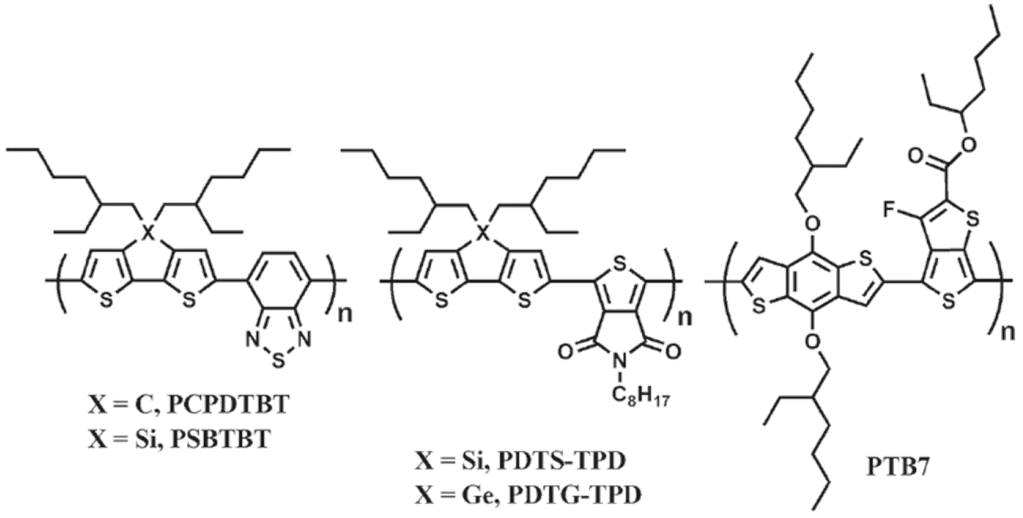

Figure 2-3. Examples of medium bandgap D-A polymers. (Adopted and modified from reference [13])

Based on the above progress, Yu *et al*. introduced the TT unit as a relatively stronger acceptor in 2009.[27] When the TT unit copolymerizes with the BDT unit, the resulting polymer, PTB7, has a bandgap of ~ 1.6 eV. The solar cell based on PTB7:$PC_{71}BM$ blend with assistance from DIO as a solvent additive shows an excellent PCE of 7.4 %. The appearance of PTB7 sets a milestone in the research of polymer solar cells. It has revolutionized the field repeatedly through different chemistry modifications (such as PBDT-TT-CF, PTB7-Th, etc) and device optimization.[28,29] Currently, PTB series polymers are able to reach ~ 10 % PCE, which is a tremendous achievement in this field.[30]

At the time of writing this dissertation, Yan *et al.* reported a series of thiophene and 5,6-difluoro-2,1,3-benzothiadiazole (DFBT) based polymers (Eg ~ 1.65 eV) with a maximum PCE of over 10%.[31] These polymers have very rigid backbones, and thus require a relatively high temperature fabrication process. Nevertheless, they also mark a significant milestone for single junction polymer solar cells.

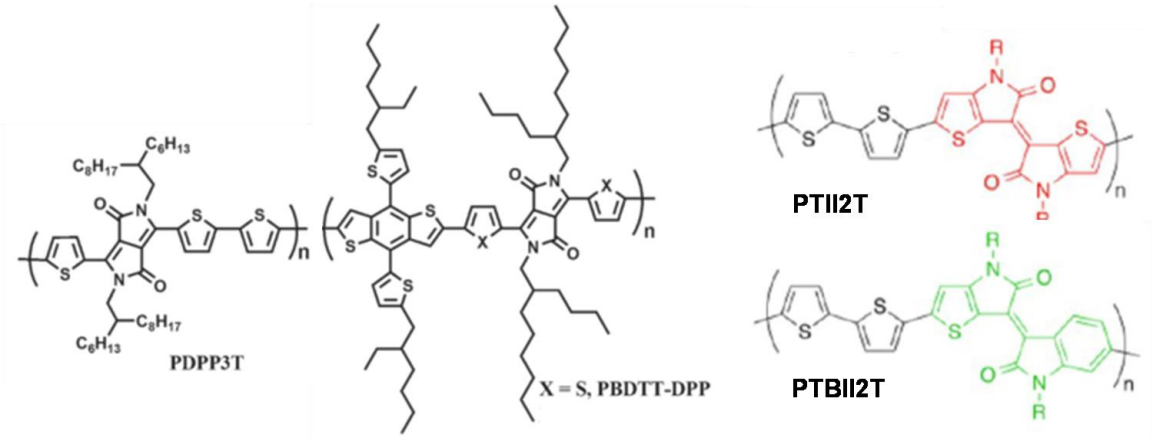

Figure 2-4. Examples of small bandgap D-A polymers. (Adopted and modified from reference [13] and [36])

2.4.3 Small bandgap D-A polymers

Interest in tandem OPVs drove the development of small bandgap polymer in the 2010s.[32] Currently, this bandgap category is dominated by polymers with strong electron-deficient moieties such as diketopyrrolopyrrole (DPP) or isoindigo. The first DPP-based polymer, PDPP3T, was introduced by Janssen *et al*.[33] This polymer exhibited a bandgap of 1.31 eV, which allows the material to extend photon absorption to 930 nm. When combined with $PC_{71}BM$, a solar cell with 4.7 % PCE was demonstrated. Through optimizing the molecular weight, the same group further improved its PCE to ~ 6%.[34] Later on, Yang *et al.* combined DPP with thienyl substituted BDT (BDTT) to afford a polymer, PBDTT-DPP, with a bandgap of 1.46 eV. This polymer has a PCE of ~6.2 % when blending with $PC_{71}BM$. Most importantly, it produces one of the first successful tandem OPV devices by working with P3HT in 2012.[35]

Another small bandgap polymer family is based on isoindigos. Due to its internal lactam ring, isoindigo has a very strong electron-withdrawing property. Frechet *et al.* reported the first thienyl-derived isoindigo (TII)-based polymer.[36] They found that each thiophene substitution resulted in an ~ 0.2 eV reduction in bandgap. As a result, a 1.4 eV E_g polymer was produced using one benzene and one thiophene, and a 1.15 eV E_g polymer was achieved by using full thiophene replacing isoindigo (ie TII). Although these polymers have very good charge-carrier transport properties, the best PCE achieved (through PTBII2T) merely made 4% (for PTII2T polymer, the PCE drops to around 1%). This possibility is due to their low-lying LUMO levels, which affects the charge-separation efficiency in the device; the LUMO-LUMO offset is not large enough. Later on, Seki *et al*. further copolymerized TII with different donor groups such as BDT, CPDT and fluorene.[37] The bandgap was successfully lowered to around 1.0 eV.

However, the solar cell performance of these polymer are not attracting as they still suffered from the low current generation issue.

In the present dissertation, we aim to improve the medium and small bandgap polymers as they have shown a great potential in achieving high performance applications in tandem and transparent cells. Throughout my study, different synthetic strategies, ranging from backbone to side chain modifications, were used to improve these polymers, which will be detailed in the following chapters.

References:

[1] Zhou, Z.-H. *et al. Chem. Soc. Chem. Commun.* **1991**, *1460*, 1210.

[2] Havinga, E. E. *et al. Synth. Met.* **1993**, *55*, 299–306.

[3] Hyon, S. *et al. Polym. Bull.* **1987**, *29*, 119–126.

[4] Kitamura, C. *et al. Chem. Mater.* **1996**, *8*, 570–578.

[5] Yamamoto, T. *et al. J. Am. Chem. Soc.* **1996**, *118*, 10389–10399.

[6] Brédas, J. L. *J. Chem. Phys.* **1985**, *82*, 3808.

[7] Brocks, G. *et al. J. Phys. Chem.* **1996**, *100*, 1838–1846.

[8] Cheng, Y.-J. *et al. Chem. Rev.* **2009**, *109*, 5868–5923.

[9] Gibson, G. L. *et al. J. Am. Chem. Soc.* **2012**, *134*, 539–547.

[10] Yuen, J. D. *et al. Energy Environ. Sci.* **2013**, *6*, 392–406.

[11] Cheng, Y. J. *et al. J. Organomet. Chem.* **2004**, *689*, 4137–4148.

[12] Mercier, L. G. *et al. Acc. Chem. Res.* **2013**, *46*, 1597–1605.

[13] Dou, L. *et al. Adv. Mater.* **2013**, *25*, 6642–6671.

[14] Dou, L. *et al. Chem. R*ev., **2015**, 115, 12633–12665.

[15] Heeger, A. J. *Adv. Mater.* **2014**, *26*, 10–28.

[16] Blouin, N. *et al. Adv. Mater.* **2007**, *19*, 2295–2300.

[17] Park, S. H. *et al. Nat. Photonics* **2009**, *3*, 297–302.

[18] Beiley, Z. M. *et al. Adv. Energy Mater.* **2011**, *1*, 954–962.

[19] Zou, Y. *et al. J. Am. Chem. Soc.* **2010**, *132*, 5330–5331.

[20] Piliego, C. *et al. J. Am. Chem. Soc.* **2010**, *132*, 7595–7597.

[21] Zhang, Y. *et al. Chem. Mater.* **2010**, *22*, 2696–2698.

[22] Zhu, Z. *et al. Macromolecules* **2007**, *40*, 1981–1986.

[23] Peet, J. *et al. Nat. Mater.* **2007**, *6*, 497–500.

[24] Hou, J. *et al. J. Am. Chem. Soc.* **2008**, 16144–16145.

[25] Chu, T.-Y. *et al. J. Am. Chem. Soc.* **2011**, *133*, 4250–4253.

[26] He, Z. *et al. Nat. Photonics* **2012**, *6*, 593–597.

[27] Liang, Y. *et al. Adv. Mater.* **2010**, *22*, 135–138.

[28] Hou, J. *et al. J. Am. Chem. Soc.* **2009**, *131*, 15586–15587.

[29] Liao, S.-H. *et al. Adv. Mater.* **2013**, *25*, 4766–4771.

[30] Lu, L. *et al. Adv. Mater.* **2014**, *26*, 4413–4430.

[31] Liu, Y. *et al. Nat. Commun.* **2014**, *5*, 1–8.

[32] You, J. *et al. Prog. Polym. Sci.* **2013**, *38*, 1909–1928.

[33] Bijleveld, J. C. *et al. J. Am. Chem. Soc.* **2009**, 131, 16616–16617.

[34] Hendriks, K. H. *et al. Angew. Chemie. Int. Ed.* **2013**, *52*, 8341–8344.

[35] Dou, L. *et al. Nat. Photonics* **2012**, *6*, 180–185.

[36] Chen, M. S. *et al. Chem. Mater.* **2013**, *25*, 4088–4096.

[37] Koizumi, Y. *et al. Polym. Chem.* **2013**, *4*, 484.

CHAPTER 3

Bandgap Engineering of PBDTT-DPP Photovoltaic Polymer Through Main-Chain Selenium Substitution

(This chapter is based on the following publication: *Adv. Mater.*, **2013**, *25*, 825-831.)

In chapters 1 and 2, the importance of OPV technology, the background of D-A polymers, and the development of polymers in OPV applications have been briefly reviewed. Starting with this chapter, we are going to show how different molecular engineering techniques can be successfully applied to make existing photovoltaic D-A polymers perform better. Here in chapter 3, we aim to improve the performance of the solar cell based on the PBDTT-DPP:$PC_{71}BM$ blend by attempting to capture more photons out of the same solar spectrum. To realize this goal, we choose to further narrow the bandgap of the p-type material, PBDTT-DPP, as this can allow us to utilize near-infrared photons, while the n-type material remains fixed. To fulfill this concept, we carefully re-design the polymer structure by substituting part of the sulfur atoms along the polymer main-chain with selenium atoms. Using selenium in the polymer main-chain narrows the energy gap by changing the molecular orbitals' energy levels. The newly synthesized polymer, PBDTT-SeDPP, shows a bandgap of 1.38 eV, which is lower than that of PBDTT-DPP (E_g = 1.46 eV). Combined with enhanced charge transportation properties, which is thought to be due

to the enhanced short-range ordering caused by strong selenium-selenium interactions, a high solar cell power conversion efficiency of 7.2 % was demonstrated.

3.1 Introduction

To harvest a greater part of the solar spectrum, lowering the energy bandgap (E_g) of the active material is a major task for materials scientists. The design and synthesis of small bandgap conjugated polymers for use as electron donor materials for bulk heterojuction (BHJ) polymer solar cell (PSC) applications have attracted remarkable attention during the last decade.[1, 2] The reasons for pursuing such polymers include: 1) the Shockley-Quiesser equation indicates a bandgap of around 1.4 eV is ideal for a single junction solar cell device[3]; 2) tandem PSCs require an active material with a bandgap less than 1.5 eV together with a large bandgap material having a bandgap around 1.9 eV[4]; 3) some specific applications such as visibly-transparent PSCs need an active material to be more absorbing of near-infrared (NIR) and ultra-violet (UV) light and less absorbing of visible light.[5] In order to realize these goals, several synthetic strategies have been proven to be very effective in terms of narrowing the bandgap of organic polymeric materials.[2] However, a small bandgap doesn't directly guarantee high power conversion efficiency (PCE) of the solar cell devices. Proper alignment of the highest occupied molecular orbital (HOMO) and lowest unoccupied molecular orbital (LUMO) energy levels are also critical for efficient charge transfer to the electron acceptor material (for example, [6,6]-phenyl-C_{71}-butyric acid methyl ester [$PC_{71}BM$]) and to ensure a large open circuit voltage (V_{OC}) of the device; High charge carrier mobility as well as favorable morphology when blended with the acceptor material are required as well to enhance device's short circuit current (J_{SC}) and fill factor (FF).[1,2] So far, PCEs of over 7% for single junction devices have been achieved using carefully-designed active materials with bandgaps of 1.8 to 1.6 eV (note: medium bandgap

polymer).[6] Regardless of great efforts having been made, there is still a lack of high performance polymers with bandgaps less than 1.5 eV that can compete with the state-of-art medium bandgap polymers such as the thionothiophene (TT) and benzodithiophene (BDT) based PTB7 and PBDTTT-CF (E_g = 1.6 eV).[6a,6b,7]

Recently, we have demonstrated a series of small bandgap polymers (E_g < 1.5 eV) based on alternating diketopyrrolopyrrole (DPP) and thienylbenzodithiophene (BDTT) units. When the BDTT unit is copolymerized with the furan-containing DPP unit (FDPP), the resulting polymer (PBDTT-FDPP, E_g = 1.51 eV) gives a PCE ~ 5% in a single junction solar cell.[8] By switching the furan to a thiophene moiety, PBDTT-DPP (E_g = 1.46 eV) shows increased J_{SC} and FF, and this resulted in a higher PCE of 6.5%.[4g,8] The successful application of PBDTT-DPP in tandem PSCs has led to a National Renewable Energy Laboratory certified PCE of 8.6% and its application in visibly-transparent PSCs has lead to ~4% PCE with over 60% transparency in the visible region.[4g,5f] Nevertheless, the efficiencies were limited mainly by the relatively narrow absorption range (up to 850 nm) and low external quantum efficiency (EQE, <50%) in the NIR region. Further lowering the bandgap to harvest more photons in the NIR part of the solar radiation, as well as increasing the charge carrier mobility of the small bandgap polymers is desired to reach higher efficiency in both types of devices. Very recently, it has been found that changing the sulfur atom on the thiophene moiety of the DPP unit to a selenium atom to form the selenophene-based DPP (SeDPP) unit in the conjugated polymer backbone can decrease the bandgap and enhance the charge transport properties in organic field effect transistor (FET) devices.[9,10] However, the photovoltaic performance of the SeDPP-based small bandgap polymer (PSeDPPDTT) was lower than its thiophene counterpart mainly due to its higher HOMO level and thus lower V_{OC} of the device.[10a] Similarly, early effort on changing the

sulfur atoms on poly(3-hexylthiophene) (P3HT) to selenium atoms to form poly(3-hexylselenophene) (P3HS) gave lower bandgap and lower PCE.[10b,10c] On the other hand, Yu *et al.* recently reported a Se-substituted PTB8 polymer based on TT and BDT units, which showed similar V_{OC}, FF, higher J_{SC}, and thus higher PCE than its thiophene counterpart.[11] Based on the above contradictory results, more investigation of the effects of Se-substitution is definitely needed.

In the present chapter, we show that the reduction of the bandgap and the enhancement of the charge transport properties of a small bandgap polymer (PBDTT-DPP) can be accomplished simultaneously by substituting the sulfur atoms on the DPP unit with selenium atoms. The newly designed polymer, poly{2,6′-4,8-di(5-ethylhexylthienyl)benzo[1,2-b;3,4-b]dithiophene-alt-2,5-bis(2-butyloctyl)-3,6-bis(selenophene-2-yl)pyrrolo[3,4-c]pyrrole-1,4-dione} (PBDTT-SeDPP, E_g = 1.38 eV), shows excellent photovoltaic performance in single junction devices with PCEs over 7% and photo-response up to 900 nm. Tandem polymer solar cells and visibly-transparent solar cells based on PBDTT-SeDPP are also demonstrated with a 9.5% and 4.5% PCE, which are more than 10% enhancement over those based on PBDTT-DPP.

3.2 Experimental method

3.2.1 Synthetic procedures

Materials: 2,6-Bis(trimethyltin)-4,8-bis(5-ethylhexyl-2-thienyl)-benzo[1,2-b:4,5-b']dithiophene (BDTT), 2,5-Diethylhexyl-3,6-bis(5-bromofuran-2-yl)pyrrolo[3,4-c]-pyrrole-1,4-dione (FDPP), 2,5-Dibutyloctyl-3,6-bis(5-bromothiophen-2-yl)pyrrolo[3,4-c]-pyrrole-1,4-dione (DPP), Selenophene-2-carbonitrile (1), 2-ethylhexylthiophene and Indene-C_{60}bisadduct (ICBA) were synthesized according to the procedures reported in the literature.[6e, 8, 9c] Poly(3-

hexylthiophene) (P3HT) was purchased from Rieke Metals. [6,6]-phenyl-C_{71}-butyric acid methyl ester ($PC_{71}BM$) was purchased from Nano-C. Diisopropyl succinate was purchased from TCI. Unless otherwise stated, all of the chemicals were purchased from Aldrich and used as received. A summarize of synthetic routes is shown in Scheme 3-1.

Synthesis of 3,6-bis-(selenophenyl)-1,4-diketopyrrolo[3,4*c*]pyrrole (2): Sodium (1.54 g, 67.2 mmol) was added to a two-neck round bottom flask with nitrogen protection. 2-methyl-2-butanol (38 mL) was subsequently added, and followed by heating up the solution to 110 ºC until the sodium was totally consumed. After cooled down the solution to 65 ºC, the compound **1** (7.0 g, 44.9 mmol) was injected in one portion. The mixture was stirred for another 20 min, and then diisopropyl succinate (3.94 g, 19.5 mmol) was slowly dropped in 1 h. The reaction temperature was gradually increased to 70 ºC and kept for about 1 h. Then the solution was further heated to 80 ºC and stirred for an additional 11 h. Finally, the mixture was cooled to 0 ºC, diluted with 20 mL methanol, and neutralized by stirring with acetic acid. After 2h, the suspension was filtered, and the black filter cake was washed with methanol and water twice and dried in vacuum to obtain a dark purple crude product that could be used directly without further purification (6.2 g, yield 81%).

Synthesis of 2,5-di(2-butyloctyl)-3,6-bis-(selenophenyl)-1,4-diketopyrrolo[3,4*c*]pyrrole (3)**:** Compound 2 (2.9 g, 7.4 mmol), 18-crown-6 (~20 mg), and anhydrous potassium carbonate (4.57 g, 33.1 mmol) were dissolved into N,N-dimethylformamide (50 ml) in a two-neck round flask under nitrogen protection. 2-butyloctyl bromide (7.3 g, 29.4 mmol) was injected in one portion by syringe, and gradually heated to 120 °C. After 4 h, the reaction was further heated to 135 °C with stirring for another 8 h. The reaction mixture was the cooled to room temperature, poured into 100 mL of ice water and extracted with dichloromethane. The combined extracts

were washed with water several times, and the solvent was then removed under reduced pressure. After drying, the crude product was purified by silica gel chromatography using a dichloromethane and hexane mixture as the eluent to obtain a purple-red solid (1.1 g, 20%). ^{1}H NMR ($CDCl_3$, 400MHz) δ: 8.79 (dd, J = 4.1, 1.0 Hz, 2H), 8.37 (dd, J = 5.6, 1.0 Hz, 2H), 7.47 (dd, J = 5.6, 4.1 Hz, 2H), 3.96 (d, J = 7.8 Hz, 4H), 1.91 (br, 2H), 1.55-0.84 (br, 44H) ppm.

Scheme 3-1. Synthesis of monomers and polymers.

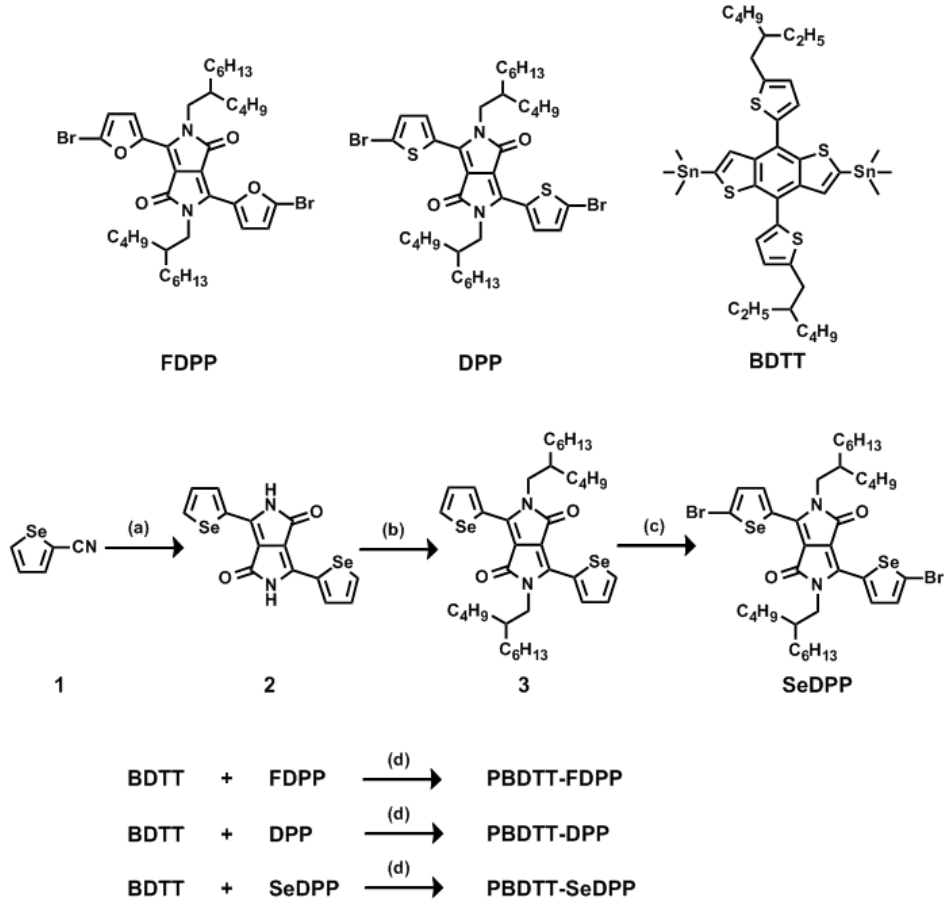

(a) Sodium, 2-methyl-2-butanol, Diisopropyl succinate, 80 °C, (b) 2-butyloctyl bromide, K_2CO_3, DMF, 135°C, (c) NBS, $CHCl_3$, RT, and (d) $Pd(PPh_3)_4$, Toluene/DMF, 115 °C.

Synthesis of 2,5-di(2-butyloctyl)-3,6-bis-(5-bromoselenophenyl)-1,4-diketopyrrolo[3,4*c*]pyrrole (SeDPP): Compound 3 (0.74 g, 1.0 mmol) and N-bromosuccinimide

(0.38 g, 2.1 mmol) were dissolved into chloroform (20 mL) in a two-neck round bottom flask under nitrogen protection, then the reaction mixture was protected from light and stirred at room temperature overnight. The mixture was then poured into methanol (100 mL) and then filtered. The filtered cake was washed with hot water and methanol twice. After drying in a vacuum, the pure product was obtained as dark-purple solid (0.7 g, 78 %). ^{1}H NMR ($CDCl_3$, 400 MHz) δ: 8.38 (d, J = 4.4 Hz, 2H), 7.39 (d, J = 4.4 Hz, 2H), 3.86 (d, J = 7.8 Hz, 4H), 1.89 (br, 2H), 1.40-0.80 (br, 44H) ppm.

Polymerization of PBDTT-SeDPP: SeDPP (0.1760g, 0.1981 mmol) and compound BDTT (0.1810g, 0.2001 mmol) were dissolved into 10 mL toluene and 1 mL DMF in a flask protected by argon. The solution was flushed with argon for 10 minutes, then 10 mg of $Pd(PPh_3)_4$ was added into the flask. The solution was flushed with argon again for another 10 minutes. The oil bath was heated to 115 ºC gradually, and the reaction mixture was stirred for 8 hours at 115 ºC under argon atmosphere. Then, the mixture was cooled down to room temperature and the polymer was precipitated in 100 ml methanol and the precipitated solid was collected and purified by silica gel chromatography using chloroform as eluent. The polymer was obtained as dark green-purple solid, yield 56%. The polymer can be readily dissolved into chloroform, chlorobenzene or dichlorobenzene, etc**.** Mn=38.0 k; polydispersity=2.1.

Polymerization of PBDTT-FDPP: PBDTT-FDPP was prepared using the same procedure as PBDTT-SeDPP. Mn=35.2 k; polydispersity=2.2.

Polymerization of PBDTT-DPP: PBDTT-DPP was prepared using the same procedure as PBDTT-SeDPP. Mn=40.3 k; polydispersity=2.2.

3.2.2 Molecular simulation

The geometry of all three compounds was subjected to density functional theory (DFT) optimizations by Gaussian 03 software package. Hybrid three-parameter B3LYP functional combined with 6-31G(d) basis set was used. The HOMO as well as LUMO energy levels were analyzed using minimized singlet geometries to approximate the ground state.

3.2.3 Materials characterization

Instrumentation: ^{1}H spectra were measured on a Bruker ARX-400 spectrometer. Absorption spectra were taken on a Varian Cary 50 ultraviolet-visible spectrometer. Gel permeation chromatographic analysis (GPC) was performed on a Varian Star Chromatography Workstation (column: MIXED-C from Polymer Laboratories) connected with one UV-Vis detector from Varian (ProStar 340). All GPC analyses were performed on polymer/chloroform solution at the flow rate of 1 ml/min at 40 ^{o}C and calibrated with polystyrene. The electrochemical cyclic voltammetry (CV) was conducted with Pt disk, Pt plate, and Ag/AgCl electrode as working electrode, counter electrode, and reference electrode, respectively, in a 0.1 mol/L tetrabutylammoniumhexafluorophosphate (Bu_4NPF_6) acetonitrile solution. The polymer films for electrochemical measurements were coated from a polymer chloroform solution, ca. 5 mg/mL. For calibration, the redox potential of ferrocene/ferrocenium (Fc/Fc^+) was measured under the same conditions, and it is located at 0.39 V vs. the Ag/AgCl electrode. It is assumed that the redox potential of Fc/Fc^+ has an absolute energy level of -4.80 eV to vacuum. The energy levels of the highest (HOMO) and lowest unoccupied molecular orbital (LUMO) were then calculated according to the following equations,

$$E_{HOMO} = -(\varphi_{ox} + 4.41)\ (eV)$$

$$E_{LUMO} = -(\varphi_{re} + 4.41)\ (eV)$$

where φ_{ox} is the onset oxidation potential vs Ag/AgCl and φ_{re} is the onset reduction potential vs Ag/AgCl.

3.2.4 Device fabrication and measurement

Single junction solar cell (regular): PBDTT-FDPP, PBDTT-DPP or PBDTP-SeDPP was co-dissolved with $PC_{71}BM$ in 1,2-dichlorobenzene (DCB) with a weight ratio of 1:2 with a polymer concentration of 8 mg/mL. ITO-coated glass substrates ($15\Omega/cm^2$) were cleaned stepwise in detergent, water, acetone, and isopropyl alcohol under ultrasonication for 15 min each and subsequently dried in an oven for 5 h. A thin layer (~30 nm) of PEDOT:PSS (Baytron P VP A1 4083) was spin-coated onto the ITO surface which was pretreated by ultraviolet ozone for 15 min. Low-conductivity PEDOT:PSS was chosen to minimize measurement error from device area due to lateral conductivity of PEDOT:PSS. After being baked at 120 ºC for ~ 20 min, the substrates were transferred into a nitrogen-filled glove box (<0.1 ppm O_2 and H_2O). A polymer/$PC_{71}BM$ composite layer (ca.100 nm thick) was then spin-cast from the blend solutions at 2500 rpm on the ITO/PEDOT:PSS substrate without any annealing or other special treatments. Then the film was transferred into a thermal evaporator that is located in the same glovebox. A Ca layer (20 nm) and an Al layer (100 nm) were deposited in sequence under a vacuum of 2×10^{-6} torr. The effective area of the device was measured to be 0.10 cm^2.

Tandem solar cell (Inverted): The device architecture of the tandem solar cell is shown in Figure S7. The pre-cleaned ITO substrates were treated with UV-ozone. The P3HT:ICBA at a 1:1 weight ratio in DCB with a 18 mg/mL polymer concentration was spin-casted at 800 rpm for 30 s on top of a layer of ZnO. The Films were annealed at 150ºC for 10 min. PEDOT:PSS was

spin-coated on the first active layer, and annealed at 150 ^{o}C for 10min. After that, a thin layer of ZnO film was spin-cast, followed by thermal annealing at 150 ^{o}C for 10 min. Polymer:$PC_{71}BM$ at a 1:2 weight ratio in DCB with a 8 mg/mL polymer concentration was then spin-coated without any subsequent processing. The device fabrication was completed by thermal evaporation of 15 nm MoO_3 and 100 nm Ag as the anode under vacuum at a base pressure of 2×10^{-6} torr. The effective area of the device was measured to be 0.10 cm^2.

Visibly-transparent (or transparent) solar cells: Visibly transparent polymer solar cells were fabricated on patterned ITO-coated glass substrates. The PEDOT:PSS layer was spin-cast at 4000 rpm for 60 s and annealed at 120 ^{o}C for 15 min in air. The PBDTT-SeDPP:PCBM at a weight ratio of 1:2 in DCB with a 8 mg/mL polymer concentration was spin-cast at 2500 rpm for 80 s on top of the PEDOT:PSS layer to form a ~100 nm thick active layer. A TiO_2 sol-gel solution was then spin-coated onto the active layer at 2500 rpm for 30 s and annealed at 100 ^{o}C for 1 min to form the n-type interface layer. For the deposition of the AgNW-based composite electrode, the silver nanowire dispersion in isopropyl alcohol was spin-coated (2 mg/mL dispersion, 2500 rpm, 10 drops) onto the TiO_2 layer to form AgNW conducting networks. The fusing process of the silver nano-wire network was then carried out by applying diluted TiO_2 sol-gel solution in ethanol at 3000 rpm and baking at 100 ^{o}C for 10 s. The ITO nanoparticle dispersion (10 wt %) was used as transparent conductive filler and was spin-coated onto the fused AgNW matrix to form the composite electrode. Mild heating at 80 ^{o}C for 1 min removed the residual solvent. The thickness of the transparent composite electrode is around 400 nm. The device electrode fingers were formed by cutting the films with a blade and blowing the devices with N_2 to avoid possible short circuits between the top AgNWs and the bottom ITO substrate.

The active area is 0.10 cm^2, which is defined by the overlap between bottom ITO substrate and the top fingers.

Current-voltage measurement: The fabricated device was encapsulated in a nitrogen-filled glovebox by UV cured epoxy and a cover glass. The current density-voltage (J-V) curves were measured using a Keithley 2400 source-measurement unit. The photocurrent was measured under AM 1.5 G illumination at 100 mW/cm^2 under a Newport Thermal Oriel 91192 1000W solar simulator. The light intensity was determined by a Si photodiode as a reference cell, followed by the calculation of spectral mismatch factor and then short circuit current correction. External quantum efficiencies were measured using a lock-in amplifier (SR830, Stanford Research Systems) with current preamplifier (SR570, Stanford ResearchSystems) under short-circuit conditions. The devices were illuminated by monochromatic light from a xenon lamp passing through a monochromator (SpectraPro-2150i, Acton Research Corporation) with a typical intensity of 10 μW. The photocurrent signal is then amplified by an SR570 and detected with an SR830. A calibrated monosilicon diode with known spectral response is used as a reference.

Hole mobility: Hole mobility was measured using the space charge limited current model (SCLC), using a diode configuration of ITO/ PEDOT:PSS/polymer:$PC_{71}BM$/Au and taking current-voltage measurements in the range of 0-10 V and fitting the results to a space charge limited form, where the SCLC is described by

$$J = (8/9)\varepsilon_r\varepsilon_0\mu_e(V^2/L^3)$$

where ε_0 is the permittivity of free space, ε_r is the dielectric constant of the polymer, μ is the hole mobility, V is the voltage drop across the device ($V = V_{appl} - V_r - V_{bi}$, where V_{appl} is the applied

voltage to the device, V_r is the voltage drop due to contact resistance and series resistance across the electrodes, and V_{bi} is the built-in voltage due to the difference in work function of the two electrodes), L is the polymer thickness. The dielectric constant ε_r is assumed to be 3, which is a typical value for conjugated polymers. The thickness of the polymer films is measured by using a Dektak profilometer.

Transmission electron microscopy measurements: Transmission electron microscopy was conducted with a JEOL 2010F electron microscope.

3.3 Result and discussion

3.3.1 Polymer design, synthesis and characterization

The SeDPP monomer was synthesized using a reported method with slight modification.[9c] After adding the carbonitrile group onto the 2-position of selenophene, the SeDPP core unit was formed by condensation reaction with selenophene-2-carbonnitrile and diisopropylsuccinate in a basic environment. It should be noted that decreasing the reaction temperature (from 120 °C to 80 °C) and increasing the reaction time (from 2 hours to 12 hours) can enhance the yield of this step significantly, possibly due to the poor stability of the selenothiophene-2-carbonnitrile at high temperature. Then, 2-butyloctyl chains were attached onto the DPP core to ensure good solubility, and finally the bromination was performed by N-bromosuccinimide (NBS) under Argon protection. To fully investigate the effect of the Se-substitution on the DPP unit, the furan and thiophene counterparts (PBDTT-FDPP and PBDTT-DPP) were also synthesized and characterized for comparison, and their chemical structures are shown in Figure 3-1a. The polymers PBDT-FDPP, PBDTT-DPP, and PBDTT-SeDPP were then obtained via Stille-coupling polymerization.

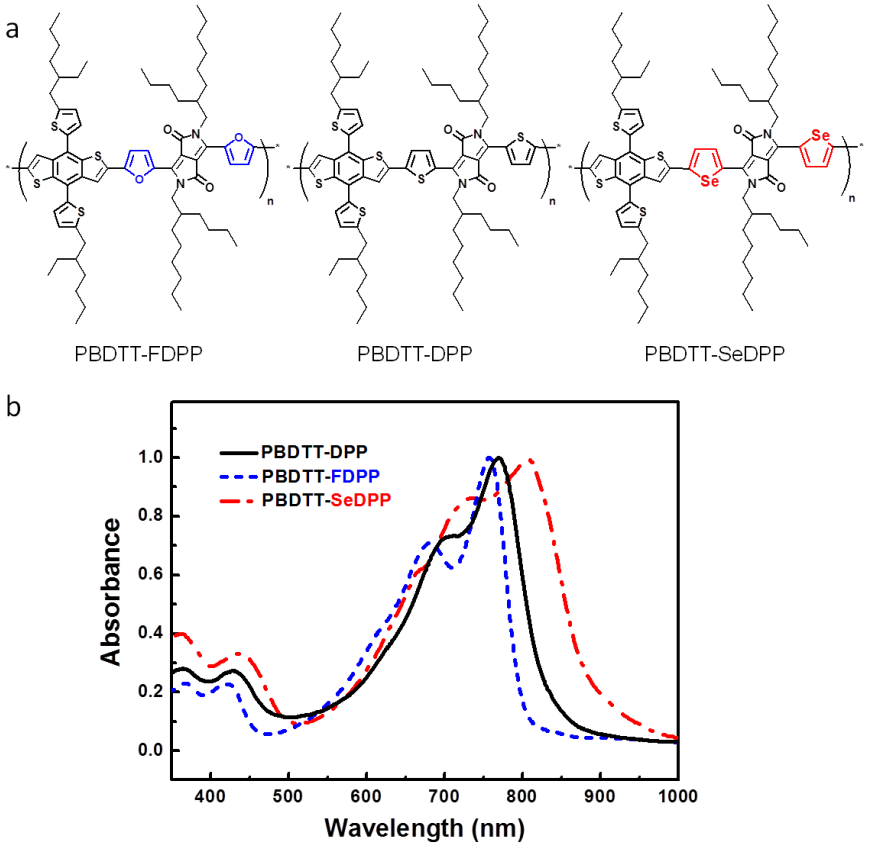

Figure 3-1. (a) Chemical structures of PBDTT-FDPP, PBDTT-DPP and PBDTT-SeDPP, and (b) Absorption spectra of PBDTT-FDPP, PBDTT-DPP and PBDTT-SeDPP in thin films.

The gel permeation chromatography (GPC) measurements show similar average molecular weights (M_n) of 35.2 kDa, 40.7 kDa, and 38.4 kDa for PBDTT-FDPP, PBDTT-DPP, and PBDTT-SeDPP, respectively. It should be noted that higher M_n batches of PBDTT-DPP and PBDTT-SeDPP showed very poor solubility and cannot be used for solution processing. And higher M_n batches of PBDTT-FDPP showed similar or even lower performance. For the consistency of the report, polymers with similar M_n values are used here. The polydispersity index of these three polymers was also determined by GPC to be around 2.1. These polymers can be dissolved in chloroform (CF), chlorobenzene (CB), and dichlorobenzene (DCB).

Figure 3-1b shows the comparison of the ultraviolet/visible (UV/Vis) absorption spectra of the polymer thin films. All three polymers have a main absorption range starting from ~550, and the absorption edges are from 810 nm to 900 nm. The absorption shapes are similar to each other, which indicate the characteristics of the BDTT-DPP backbone system. The new PBDTT-SeDPP polymer displays a clear red-shift of the absorption onset as well as the maximum peak value (nearly 50 nm) as compared to PBDTT-DPP. According to the onset of the film absorption spectra, the optical band gap of PBDT-FDPP, PBDTT-DPP, and PBDTT-SeDPP are calculated to be 1.51, 1.46, and 1.38eV, respectively. The relatively low absorptivity in the visible region (400 – 650 nm) and high absorptivity in the NIR (650 – 900 nm) and UV (<400 nm) region of PBDTT-SeDPP make it a very promising candidate for high performance tandem PSCs and visibly-transparent PSC applications.

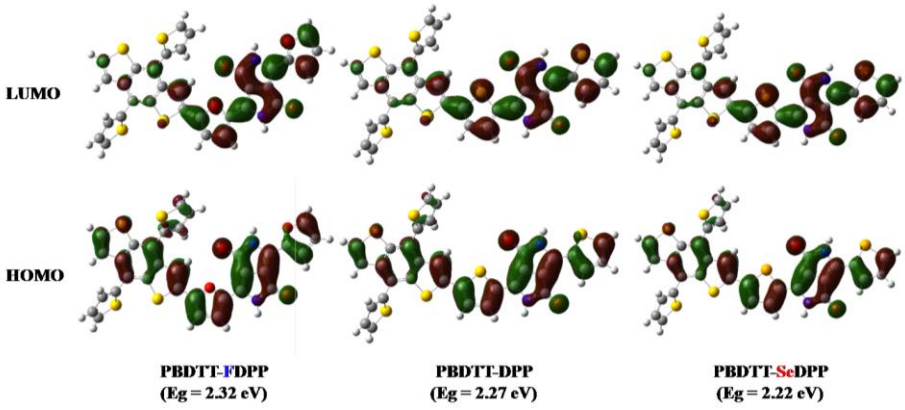

Figure 3-2. Calculated HOMOs and LUMOs of PBDTT-FDPP, PBDTT-DPP, and PBDTT-SeDPP.

To study the energy levels of this series of polymers, density functional theory (DFT) calculation was performed on one repeating unit (BDTT-FDPP. BDTT-DPP and BDTT-SeDPP) of the three polymers firstly and the calculated HOMO/LUMO are shown in Figure 3.2. The

result shows that by substituting the sulfur atoms with selenium atoms, the HOMO level increases slightly, and meanwhile the LUMO level drops a little. The narrowing of the bandgap is mainly due to the electron stabilizing effect of selenophene moieties, since selenium is more polarizable than either sulfur or oxygen.[9] The actual HOMO and LUMO energy levels of polymers are then determined by cyclic voltammetry (CV) measurement (Figure 3.3). The HOMO/LUMO levels of PBDTT-FDPP, PBDTT-DPP, and PBDTT-SeDPP are measured to be -5.26/-3.64 eV, -5.30/-3.63 eV, and -5.25/-3.70 eV, respectively. The bandgap of PBDTT-FDPP turns out to be the smallest based on the CV testing, which conflicts with the optical bandgap; a similar phenomenon has also been observed in other FDPP based polymer systems.[7d] Overall, the UV/Vis absorption spectra, DFT calculations, and the CV measurements are in good agreement.

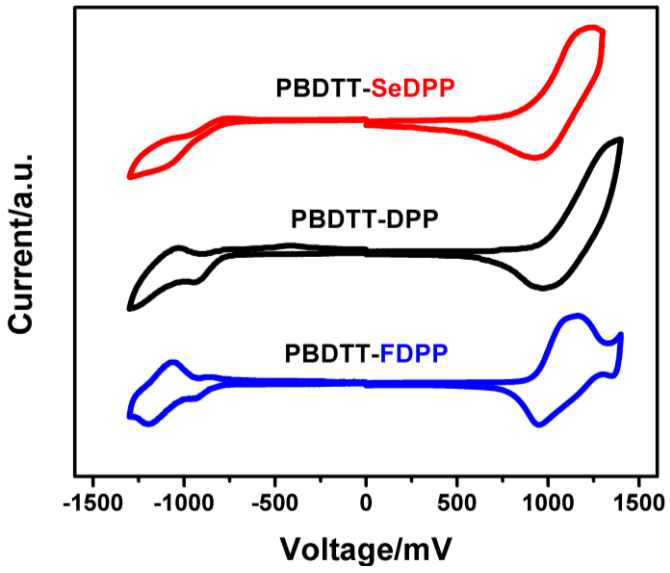

Figure 3-3. Cyclic voltammograms of polymer thin films.

3.3.2 Single junction solar cell performance

Single junction BHJ solar cell performance of these polymers were preliminarily investigated with the regular structure of ITO/PEDOT:PSS (30 nm)/polymer:$PC_{71}BM$ (100 nm)/Ca/Al under AM1.5G illumination (100 mW/cm^2). These three polymers were spin-coated onto the PEDOT:PSS coated indium-doped tin oxide (ITO) glass substrate from DCB solution, followed by the evaporation of Ca/Al as top electrode. It should be noted that neither solvent nor thermal annealing was performed on all devices presented here, since no significant difference in the photovoltaic performance was observed for the annealed devices. The optimized polymer:$PC_{71}BM$ ratio was found to be 1:2 by weight.

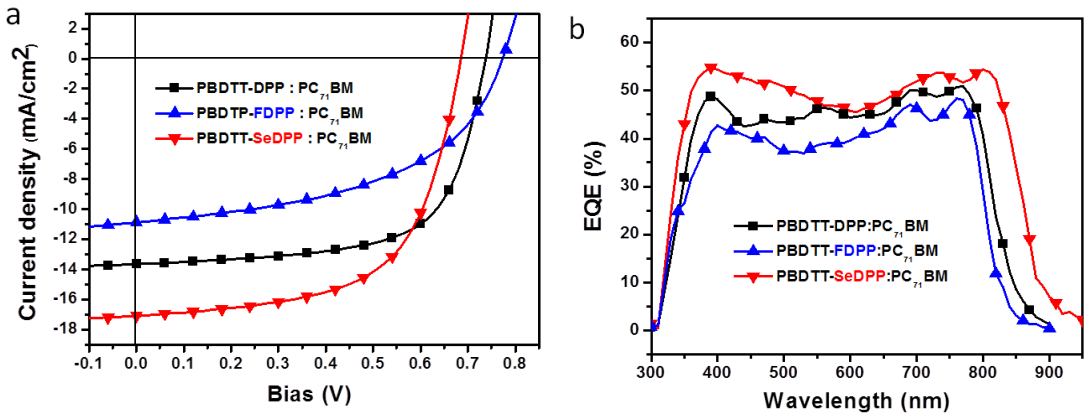

Figure 3-4. (a) Current density-voltage characteristics of polymer/$PC_{71}BM$ single junction solar cellsunder AM1.5G illumination (100 mW/cm^2), and (b) EQEs of the corresponding devices.

Typical current density-voltage (J-V) curvesare shown in Figure 3-4a, the corresponding EQE curvesare presented in Figure 3-4b and the results are summarized in Table 3-1. As we can see, the V_{OC} of the polymer solar cell drops from PBDTT-FDPP to PBDTT-DPP to PBDTT-SeDPP (from 0.77 to 0.73 to 0.69 V). The PBDTT-SeDPP based device turns out to have the lowest V_{OC}, and it is mainly due to a relatively high HOMO energy level. The J_{SC}, in contrast,

increases from PBDTT-FDPP to PBDTT-DPP to PBDTT-SeDPP based devices. A high J_{SC} of 16.8 mA/cm^2 was observed in PBDTT-SeDPP based devices, which is 52% and 23% higher than PBDTT-FDPP (10.9 mA/cm^2) and PBDTT-DPP (13.7 mA/cm^2) based devices. With an FF of around 62%, the PBDTT-SeDPP based device shows a maximum efficiency of 7.2% (the averaged PCE from ~40 devices is 7.0%), whereas the PBDTT-FDPP and PBDTT-DPP based devices show max/average PCEs of 4.7/4.5% and 6.5/6.4%, respectively. From the external quantum efficiency (EQE) results (Figure 3-4b), a broader coverage of PBDT-SeDPP from 300 nm to 900 nm is clearly seen. Also, the average values (note: estimated from numerical values between the two peaks at ~350 and ~800 nm) are around 42%, 47% and 53 % for PBDTT-FDPP, PBDTT-DPP, and PBDTT-SeDPP based single-layer devices, respectively. The highest averaged EQE of the PBDTT-SeDPP based device is probably due to a slightly higher hole mobility of PBDTT-SeDPP (6.9×10^{-4} cm^2/V·s) as compared to that of PBDTT-DPP (2.5×10^{-4} cm^2/V·s) and PBDTT-FDPP (2.2×10^{-4} cm^2/V·s) in the blend film, which are determined by space charge limited current (SCLC) model. It worthy to note the maximum EQE for the small bandgap polymers (~50%) are still lower than the state-of-art MBG polymers such as PTB7 (~60%).[6] One possible reason provided by Janssen is that the relatively low-lying LUMO levels of the small bandgap polymers led to poor charge separation and thus low internal quantum efficiency (IQE) of the devices.[7g] Here the IQE of PBDTT-SeDPP beased devices was around 60%, indicating there is still significant energy loss during the photon-to-electron conversion process. Further optimizing the energy levels of the materials as well photo-physics study to understand the mechanism are currently underway.

Table 3-1. Photovoltaic properties of single layer BHJ solar cells

	V_{OC} (V)	J_{SC} (mA/cm^2)	FF (%)	$PCE_{max}/_{aver}$ (%)
P1	0.77	10.9	56	4.7/4.5
P2	0.73	13.7	65	6.5/6.4
P3	0.69	16.8	62	7.2/7.0

P1: PBDTT-FDPP. P2: PBDTT-DPP. P3: PBDTT-SeDPP.

3.3.3 Thin film morphology study

The morphology of the blend films, which is believed to be critical for the efficient charge transport in the polymer domains and charge separation at the polymer/fullerene interfaces,[1,7] was examined by transmission electron microscopy (TEM) and the results are shown in **Figure 3-5**. It is found that both PBDTT-DPP:$PC_{71}BM$ and PBDTT-SeDPP:$PC_{71}BM$ blend films show fine features of phase separation and plausibly bi-continuous networks (Figure 3-5b, 3-5c) whereas the PBDTT-FDPP:$PC_{71}BM$ blend film shows slightly weaker phase separation (Figure 3-5a). The more favorable morphology of PBDTT-DPP:$PC_{71}BM$ and PBDTT-SeDPP:$PC_{71}BM$ blend films may contribute to the high performance of these two polymers. It should be pointed out that these morphology features were developed spotaneously since as-cast films were used during the processing. In addition, previous research on the morphology optimization of PBDTT-FDPP has led to slightly enhanced PCE (up to 5.8%) by using 1,8-diiodooctane (DIO) as additive during device processing. However, no improvement of the performance of PBDTT-DPP was observed using DIO as additive and similar results are obtained here for the new polymer PBDTT-SeDPP. The broader absorption range and higher EQE in the whole region of PBDTT-SeDPP compared to its furan or thiophene counterparts lead to the significant enhancement of J_{SC} of PBDTT-SeDPP based devices. Further studies on the structural order and molecular packing will be carried out to fully understand this enhancement.

Although the devices containing the Se-substituted polymer show a slightly lower V_{OC} due to its higher HOMO level, the overall performance was improved due to the significant enhancement of the J_{SC}.

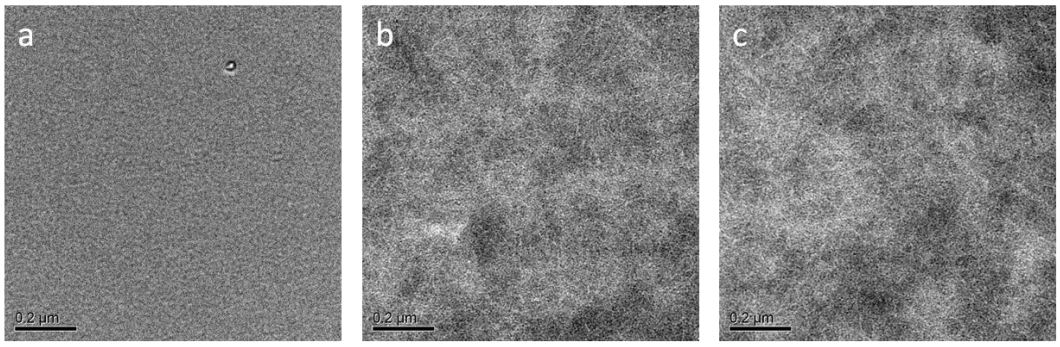

Figure 3-5. TEM images of (a) PBDTT-FDPP:$PC_{71}BM$, (b) PBDTT-DPP:$PC_{71}BM$, and (c) PBDTT-SeDPP:$PC_{71}BM$ blend films processed in DCB.

3.3.4 Tandem solar cell performance

The versatile photovoltaic applications of PBDTT-SeDPP are featured by tandem and visibly-transparent PSCs. The tandem solar cell architecture, which consists of a front cell with a wide-bandgap material, an interconnecting layer (ICL), and a rear cell with a small bandgap material, is an effective way to harvest a broader part of the solar spectrum and make more efficient use of the photonic energy than the single junction structure.[4] Tandem PSCs with inverted configuration[4d,12] were fabricated using PBDTT-SeDPP as the rear cell donor material. P3HT (E_g ~1.9 eV) was used as the front cell donor material and indene-C_{60}bisadduct ($IC_{60}BA$)[13] was used as the front cell acceptor material. The device structure is ITO/ZnO(30 nm)/P3HT:$IC_{60}BA$(160 nm)/PEDOT:PSS(30 nm)/ZnO (30 nm)/PBDTT-SeDPP:$PC_{71}BM$ (100 nm)/MoO_3(5 nm)/Ag (shown in Figure 3-6a). Figure 3-6b shows the J-V characteristics of a typical inverted single junction front cell device, rear cell device, and the inverted tandem device.

The averaged PCE from 20 tandem devices is 9.5% with a V_{OC} of 1.52 V, a J_{SC} of 9.44 mA/cm^2, and a FF of 66.3%. The V_{OC} of the tandem device is almost the sum of two sub-cells (0.84 V and 0.69 V), indicating the effectiveness of the highly performing ICL. The FF of the tandem device is around the average of the two sub-cells (70% for the front cell and 62% for the rear cell). The major improvement compared to previously reported tandem cells based on PBDTT-DPP is the J_{SC} (from ~8.3 A/cm^2 to 9.4 A/cm^2). To further confirm the high J_{SC} achieved here, EQE of the two sub-cells in the tandem device was measured using a reported method.[4g,14] As shown in Figure 3.6c, the front cell had a photo-response from 300 to 650 nm, showed an EQE as high as 67% at 530 nm, and its integrated J_{SC} was 9.3 mA/cm^2. The rear cell had a broad photo-response from 300 to 900 nm, showed a maximum EQE of 51% at 810 nm, and a balanced integrated J_{SC} of 9.2 mA/cm^2 was achieved. The high J_{SC} obtained from the rear cell is due to the ability of PBDTT-SeDPP to use the NIR light very efficiently.

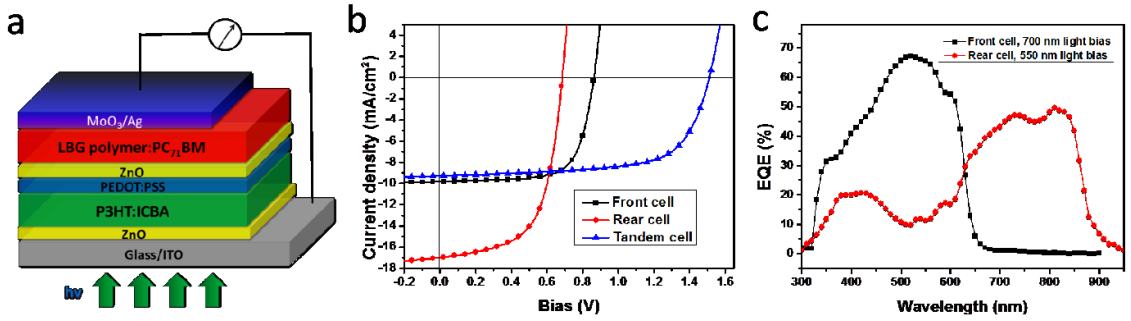

Figure 3-6. (a) Device structure of the inverted tandem solar cell, (b) Current density-voltage characteristics of the single junction front cell, single junction rear cell, and inverted tandem cell under AM1.5G illumination (100 mW/cm^2), and (c) EQE of the P3HT:ICBA based front cell, PBDTT-SeDPP:$PC_{71}BM$ based rear cell in a typical tandem device.

3.3.5 Transparent solar cell performance

The visibly-transparent PSC, which enables part of the visible light (400 – 700 nm) passing through the device, has high potential in many photovoltaic applications, such as building-integrated photovoltaics (BIPV) or integrated photovoltaic-chargers for portable electronics.[5,12] Previous studies showed ether low transmittance in the visible region or low efficiencies due to the lack of a proper small bandgap polymer that can use the NIR light very efficiently while transmit most of the visible light.[5a-5e,12] Recently, we have demonstrated a visibly-transparent PSC with PCE of 4% and transmittance ~ 60% by using PBDTT-DPP as the active material.[5f] The performance was limited mainly by the relatively narrow absorption range (up to 850 nm) and low external quantum efficiency (<50%) in the NIR region. Here, a highly efficient visibly-transparent PSC is demonstrated with the device structure of ITO/PEDOT:PSS(30 nm)/PBDTT-SeDPP:$PC_{61}BM$ (100 nm)/TiO_2/AgNW (AgNW: silver nano-wire) and a schematic structure is shown in Figure 3-7a. It should be noted that the high-performance AgNW-based composite transparent electrode plays an important role and the detailed preparation and characterization of it can be found in reference 5f. Figure 3-7b shows the transmission spectrum and a photograph of the complete device. It can be found that an average light transmission of 58% within the 400 to 700 nm range and a maximum transmission of 66% at ~550 nm are achieved. From the real device image, the UCLA logo with different colors can be seen clearly. Figure 3-7b demonstrates the J-V curves of the visibly-transparent PSC. The device performance was measured with illumination from either the ITO substrate side or the top AgNW-composite transparent conductor side. When illuminated from the ITO substrate side, a PCE of 4.5% was achieved with Voc = 0.72 V, Jsc = 11.5 $mA \cdot cm^{-2}$, and FF = 55%. Ref. 5f showed PBDTT-DPP based visibly-transparent OPV with PCE of 3.9%. The

transmission spectrum in the visible region is similar in the two visibly transparent OPV devices. The 15% improvement in efficiency clearly shows that harvesting NIR photons by the new polymer is more effective in the visibly-transparent solar cells. When the device test was performed with illumination from the top AgNW composite electrode side, similar performance was obtained: Voc = 0.71 V, Jsc = 11.2 mA·cm^{-2}, FF = 54%, and PCE = 4.3%. The difference of the J_{SC} is due to the slightly lower transparency of the AgNW-based composite electrode films as compared to the commercial ITO substrates.[5f] These results show that with effective NIR photon harvesting and proper energy levels, PBDTT-SeDPP is a good candidate for visibly-transparent PSCs with real world applications.

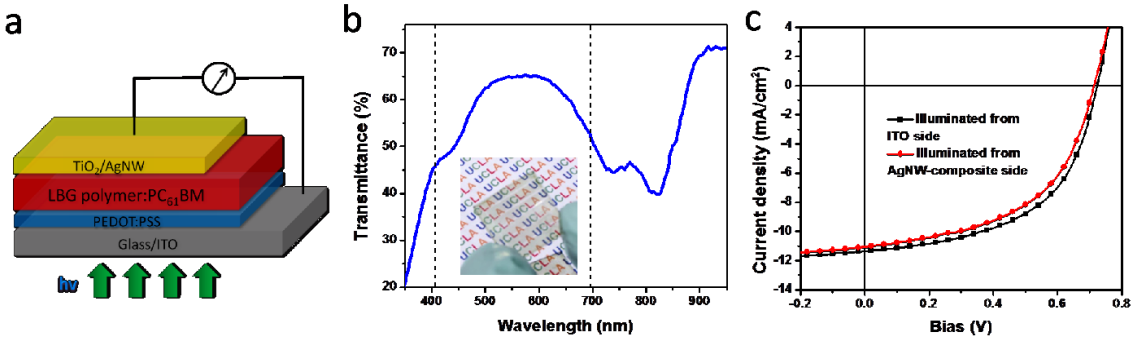

Figure 3-7. (a) Device structure of the visibly-transparent polymer solar cell, (b) Transmission spectrum and a photograph, and (c) Current density-voltage characterization (illuminated from ITO side or AgNW composite electrode side) of the visibly-transparent polymer solar cell with the device structure of ITO/PEDOT:PSS/PBDTT-SeDPP:$PC_{61}BM$/TiO_2/AgNW.

3.4 Summary and outlook

In summary, we have demonstrated the design, synthesis, and characterization of a selenium-substituted low bandgap polymer PBDTT-SeDPP. The substitution of the O or S by Se atoms on the DPP unit led to a reduced bandgap and enhanced hole mobility of the polymers.

High photo-current of 16.8 mA/cm^2 and PCE of 7.2% were obtained in a single junction PSC device, which showed significant improvement compared to its counterparts PBDTT-FDPP and PBDTT-DPP. Even more importantly, the new polymer significantly enhanced the tandem and visibly-transparent PSCs performance, with PCEs as high as 9.5% and 4.5%, respectively. Our result is an excellent example of the selenium-substitution approach to improve the photovoltaic performance of small bandgap polymers. This study emphasizes again that the research on small bandgap polymers (Eg < 1.5 eV) is a critical direction in the PSC field not only because of efficiency enhancement, but also because it enables a variety of new types of photovoltaic devices and thus applications.

References:

[1] a) Yu, G. *et al. Science* **1995,** *270*, 1789; b) Li, G. *et al. Nat. Mater.* **2005**, *4*, 864; c) Krebs, F. C. *Sol. Energy Mater. Sol. Cells* **2009**, *93*, 394; d) Brabec, J. *et al. Adv. Funct. Mater.* **2011,** *11*, 15; e) Li, G. *et al. Nat. Photon.* **2012**, *6*, 153.

[2] a) Thompson, B. C. *et al. Angew. Chem. Int. Ed.* **2008**, *47*, 58; b) Cheng, Y. J. *et al. Chem. Rev.* **2009**, *109*, 5868; c) Boudreault, P. L. T. *et al. Chem. Mater.* **2011**, *23*, 456; d) Beaujuge, P. M. *et al. J. Am. Chem. Soc.* **2011**, *133*, 20009.

[3] Shockley, W. *et al. J. Appl. Phys.* **1961**, *32*, 510.

[4] a) Hadipour, A. *et al. Adv. Funct. Mater.* **2006**, *16*, 1897; b) Kim, J. Y. *et al. Science* **2007**, *317*, 222; c) Sista, S. *et al. Adv. Mater.* **2010**, *22*, 380; d) Chou, C. H. *et al. Adv. Mater.* **2011**, *23*, 1282; e) Yang, J. *et al. Adv. Mater.* **2011**, *23*, 3465; f) Gevaerts, V. S. *et al. Adv. Mater.* **2012**, *24*, 2130; g) Dou, L. *et al. Nat. Photon.* **2012**, *6*, 180.

[5] a) Bailey-Salzman, R. F. *et al. Appl. Phys. Lett.* **2006**, *88*, 233502; b) Ng, G. M. *et al. Appl. Phys. Lett.* **2007**, *90*, 103505; c) Huang, J. *et al. Adv. Mater.* **2008**, *20*, 415-419; d) Gaynor, W. *et al. ACS Nano* **2010**, *4*, 30-34; e) Meiss, J. *et al. Appl. Phys. Lett.* **2011**, *99*, 193307; f) Chen, C.-C. *et al. ACS Nano* **2012**, *6*, 7185.

[6] a) Chen, H.-Y. *et al. Nat. Photon.* **2009,** *3*, 649; b) Liang, Y. *et al. Adv. Mater.* **2010,** *22*, E135; c) He, Z. C. *et al. Adv. Mater.* **2011,** *23*, 4636; d) Amb, C. M. *et al. J. Am. Chem. Soc.* **2011**, *133*, 10062; e) Chu, T. Y. *et al. J. Am. Chem. Soc.* **2011**, *133*, 4250; f) Huo, L. *et al. Angew. Chem. Int. Ed.* **2011**,*50*, 1.

[7] a) Peet, J. *et al. Nat. Mater.* **2007**, *6*, 497; b) Hou, J. *et al. J. Am. Chem. Soc.* **2008**, *130*, 16144; c) Bijleveld, J. C. *et al. J. Am. Chem. Soc.* **2009,** *131*, 16616; d) Woo, C. H. *et al. J. Am. Chem. Soc.* **2010,** *132*, 15547; e) Huo, L. *et al. Macromolecules* **2009,** *42*, 6564; f)

Zhou, E. *et al. Macromolecules* **2010,** *43*, 821; g) Li, W. *et al. J. Am. Chem. Soc.* **2012**, *134*, 13787.

[8] Dou, L. *et al. J. Am. Chem. Soc.* **2012**, *134*, 10071.

[9] a) Kronemeijier, A. J. *et al. Adv. Mater.* **2012,** *24*, 1558; b) Ha, J. S. *et al. J. Am. Chem. Soc.* **2011**, *133*, 10364; c) Shahid, M. *et al. Chem. Sci.* **2012**, *3*, 181.

[10] a) Shahid, M. *et al. J. Mater. Chem.* **2012**, *22*, 12817; b) Ballantyne, A. M. *et al. Adv. Mater.* **2007,** *19*, 4544; c) Klein, M. F. G. *et al. J. Polym. Sci. Part B:Polym. Phys.* **1993**, *31*, 735.

[11] Saadeh, H. A. *et al. ACS Macro Lett.* **2012**, *1*, 361.

[12] Li, G. *et al. Appl. Phys. Lett.* **2006**, *88*, 253503.

[13] He, Y. *et al. J. Am. Chem. Soc.* **2010**, *132*, 1377.

[14] a) Burdick. J. *et al. Solar Cells* **1986**, *18*, 301; b) Meusel, M. *et al. Prog. Photovolt. Res.* **2003**, *11*, 499.

CHAPTER 4

Short-Range Ordering Control of PBDTT-DPP Photovoltaic Polymer Through Side-Chain Engineering

(This chapter is based on the following publication: *Adv. Energy Mater.*, **2014**, *4*, 1300864.)

In chapter 3, an improvement of the small bandgap polymer, PBDTT-DPP is made by main-chain selenium substitutions. Such methodology results in a red-shifted absorption spectrum and better charge transportation property, both of which contribute to enhanced solar cell performance. In this chapter, a different approach is adopted to improve the same polymer. The goal herein is to optimize the short-range ordering of the polymer as well as the polymer:$PC_{71}BM$ phase separation morphology without changing the backbone. With such optimization, the charge transportation within the bulk heterojunction layer should be improved and a higher solar cell performance is expected. To achieve this goal, we introduce an easy-to-crystalize molecule, triethylene glycol, to the polymer as the side-chain. We anticipate these stack-induced side-chains can lead to a more pronounced polymer aggregation. Furthermore, through a triple component random copolymerization approach, the amount of triethylene glycol side-chains can be introduced precisely into PBDTT-DPP, which allows us to balance between the polymer aggregation and solubility. We demonstrated that this strategy can result in a more

favorable morphology in the PBDTT-DPP:$PC_{71}BM$ blend, which brings an overall 10% improvement in power conversion efficiency while nearly maintaining V_{OC}.

4.1 Introduction

As mentioned in previous chapters, the power conversion efficiency (PCE) of single junction organic polymer solar cells (PSCs) has improved significantly and gradually approached its 10% milestone over the past decade.[1] From the material standpoint, these improvements are mainly based on tailoring the bandgap (E_g) of conjugated polymers, where the easiness of doing so is offered by constructing an electron donor-acceptor alternating copolymer.[2] Through bandgap lowering, more photons are absorbed and thus higher short-circuit current (J_{SC}) can be achieved. Simultaneously, a careful control over the energy level alignment between highest occupied molecular orbital (HOMO) and lowest unoccupied molecular orbital (LUMO) of p-type and n-type material, respectively, can help in realizing a large open-circuit voltage (V_{OC}).[2] Within these strategies, several successful medium or small bandgap polymers (E_g of 1.8-1.4 eV) were made and demonstrated to have 5-9% PCE, such as PTB7, PBDTTT-CF, PBDTTPD, PDTS(G)TPD, PMDPP3T, PBDTTSeDPP, and etc.[3-4]

These state-of-the-art polymers all exist at a proper energy level that can collaborate with $PC_{61}BM$ or $PC_{71}BM$. Nevertheless, the PCEs being reported to date are still much lower than the theoretical limit (largely limited by low J_{SC} and fill factor, FF%) and obviously, there is still a plenty of room for improvement within their given bandgap.[5] In past few years, regardless of the vast variety of newly designed conjugated building blocks, few investigations, however, have focused on side-chain modification. Side-chains are known to affect solution-processed PSC extensively. To ensure a good solubility in common organic solvent (ex. chlorobenzene (CB), chloroform (CF), and etc.), long or bulky aliphatic groups are usually attached onto the

conjugated moieties. These groups, on the contrary, act as a blocking layer toward a good packing between the polymers and therefore can affect the thin film morphology and their resulting performance in electronic devices. Previous efforts on trying to optimize side-chains' size and shape often lead to bad solubility or poor solar cell performance; only few examples have been done successfully.[3f, 4c, 6] In an early work done by Yang *et al.*, a more balanced charge transport in PFDTBT based solar cells was achieved by substitution of an unbulky side-chain.[6a] Frechet *et al.* found that a longer but less bulkier side-chain would increase the ordering in PBDTTPD:fullerene blend thin film and thus, a better cell was obtained.[3f] Later, the same group had applied similar strategy on diketopyrrolopyrrolo (DPP) based polymers, and a comparable improvement was seen.[4c] Bao *et al.* had tried functionalizing the isoindigo unit by a more soluble siloxane group with the branched point reside away from the polymer backbone. Consequently, charge transport in organic field-effect transistors (OFET) was improved, but the photovoltaic performance was not as good as expected because of the morphology issue when blended with $PC_{71}BM$.[6c-d] Therefore, modifying the side-chains indeed impart us a chance to acquire a more optimized molecular structure but doing so without giving-up the material's original property is still being recognized as a difficult topic.

Recently, triethylene glycol (TEG) side-chain has been found to effectively induce self-assembly of organic semiconductors while still maintaining a good solubility.[7-8] For example, P3HT with TEG substituted for hexyl groups showed a better crystallinity.[7b-c] TEG functionalized DPP based conjugated molecule and polymer both showed a better molecule stacking and thereby a higher charge carrier mobility in OFET devices.[8] Inspired by these earlier results, we suggest that the strong self-assembling effect awarded by TEG side-chain could potentially be helpful to improve the photovoltaic performance in a given polymer system.

To realize the goal, we propose that the amount of the TEG group should be controlled very carefully to reach the most optimized condition since the morphology and photovoltaic performance are usually affected by a subtle change in the chemical structure of the materials.[1g, 2] Herein, we report a successful and easy way of introducing a certain amount of straight TEGs as side-chains into conjugated polymers via a tri-component copolymerization approach. The concept of triple component random copolymerization has recently been adapted as an effective way to adjust the bandgap and energy levels of the conjugated polymers.[9] However, side-chain modification through this kind of approach has not been realized so far. A small bandgap conjugated polymer (PBDTT-DPP, or PBD) based on alternating thienylbenzodithiophene (BDTT) and DPP units was chosen as a model compound in this study.[4h-k] TEG functionalized DPP (TEGDPP) was copolymerized with BDTT and DPP using different TEGDPP/DPP ratio to alter the structure. Interestingly, our results indicate that 10% TEGDPP modified polymer performs at an over 10% enhancement in solar cell's PCE (6.2% to 7.0%) as compared to non-modified control analogue, mainly due to the improved thin film morphology and enhanced structural ordering.

4.2 Experimental method

4.2.1 Synthetic procedures

Materials: 2,6-Bis(trimethyltin)-4,8-bis(5-ethylhexyl-2-thienyl)-benzo[1,2-b:4,5b']dithiophene (BDTT) was purchased from SunaTech Inc. 3,6-Dithiophen-2-yl-2,5-dihydropyrrolo[3,4-c]pyrrole-1,4-dione (1), 2,5-Dibutyloctyl-3,6-bis(5-bromothiophen-2-yl)pyrrolo[3,4-c]-pyrrole-1,4-dione (DPP), and 2-(2-(2-methoxyethoxy)ethoxy)ethyl 4-methylbenzenesulfonate were synthesized according to the literature.[4h, 7-8] [6,6]-phenyl-C_{71}-butyric acid methyl ester ($PC_{71}BM$) was purchased from Nano-C. Unless otherwise stated, all of

the chemicals were purchased from Aldrich and used as received. A summarize of synthetic routes is shown in Scheme 4-1.

Synthesis of *N*,*N*'-Bis-(10-(3,6,9-trioxadecyl)-3,6-di(5-thienyl)-1,4-diketo-pyrrolo[3,4-c]pyrrole (2): Compound 1 (2 g, 6.7 mmol), 2-(2-(2-methoxyethoxy)ethoxy)ethyl 4-methylbenzenesulfonate (8.1 g, 25.5 mmol), tetrabutylammonium bromide (0.22 g, 0.7 mmol) and anhydrous potassium carbonate (4.6 g, 33.1 mmol) were dissolved into N,N-dimethylformamide (65 ml) in a three-neck round flask under nitrogen protection, and then gradually heated to 120 °C. After 24 h, the reaction mixture was cooled to room temperature, pour into 100 mL of icewater and extract with dichloromethane. The combined extracts were washed with water several times, and the solvent was then removed under reduced pressure. After drying, the crude product was purified by silica gel chromatography using dichloromethane and acetone mixture as the eluent to obtain a purple-red solid (0.8 g, 20%). ^{1}H NMR ($CDCl_3$, 400MHz) δ: 8.75 (dd, J = 3.9, 1.1 Hz, 2H), 7.62 (dd, J = 5.0, 1.1 Hz, 2H), 7.24 (m, 2H), 4.26 (t, J = 6.3 Hz, 4H), 3.79 (t, J = 6.2 Hz, 4H), 3.64-3.48 (br, 16H), 3.34 (s, 6H) ppm.

Synthesis of *N*,*N*'-Bis-(10-(3,6,9-trioxadecyl)-3,6-di(5-bromothienyl)-1,4-diketo-pyrrolo[3,4-c]pyrrole (TEGDPP): Compound 2 (0.39 g, 0.65 mmol) and N-bromosuccinimide (0.24 g, 1.35 mmol) were dissolved into chloroform (30 mL) in a two-neck round bottom flask under nitrogen protection, then the reaction mixture was prevented from light and stirred at room temperature overnight. The mixture was then poured into methanol (100 mL) and then filtered. The filtered cake was washed with hot water and methanol twice. After drying in the vacuum, the pure product was obtained as dark-purple solid (0.42 g, 85 %). ^{1}H NMR ($CDCl_3$, 400MHz) δ: 8.49 (d, J = 4.2 Hz, 2H), 7.21 (d, J = 4.2 Hz, 2H), 4.18 (t, J = 6.0 Hz, 4H), 3.78 (t, J = 5.9 Hz, 4H), 3.63-3.47 (br, 16H), 3.34 (s, 6H) ppm.

Polymerization for PBD: BDTT (0.1809 g, 0.2000 mmol), and DPP (0.1590 g, 0.20 00 mmol) were dissolved into 10 mL toluene and 1 mL DMF in a flask protected by argon. The solution was flushed with argon for 10 minutes, then 10 mg of $Pd(PPh_3)_4$ was added into the flask. The solution was flushed with argon again for another 10 minutes. The oil bath was heated to 115 ºC gradually, and the reaction mixture was stirred for 10 hours at 115 ºC under argon atmosphere. Then, the mixture was cooled down to room temperature and the polymer was precipitated in ~100 ml methanol and the precipitated solid was collected and purified by silica gel chromatography using chloroform as eluent. The polymer was obtained as dark purple-black solid, yield 30%. The polymer can be readily dissolved into chloroform, chlorobenzene or dichlorobenzene, etc. Mn = 29.8 k; polydispersity = 2.1.

Polymerization for PBDTEG5: BDTT (0.1809 g, 0.2000 mmol), DPP (0.1510 g, 0.1900 mmol) and TEGDPP (0.0075g, 0.0100 mmol) were dissolved into 10 mL toluene and 1 mL DMF in a flask protected by argon. The solution was flushed with argon for 10 minutes, then 10 mg of $Pd(PPh_3)_4$ was added into the flask. The solution was flushed with argon again for another 10 minutes. The oil bath was heated to 115 ºC gradually, and the reaction mixture was stirred for 10 hours at 115 ºC under argon atmosphere. Then, the mixture was cooled down to room temperature and the polymer was precipitated in ~100 ml methanol and the precipitated solid was collected and purified by silica gel chromatography using chloroform as eluent. The polymer was obtained as dark purple-black solid, yield 30%. The polymer can be readily dissolved into chloroform, chlorobenzene or dichlorobenzene, etc. Mn = 29.0 k; polydispersity = 2.2.

Polymerization for PBDTEG10: PBDTTEG10 was prepared using the same procedure as PBDTTEG5 with monomer molar ratio of BDTT:DPP:TEGDPP = 0.2000:0.1800:0.0200 mmol. Mn = 29.2 k; polydispersity = 2.2.

Scheme 4-1. Synthesis of monomers and polymers.

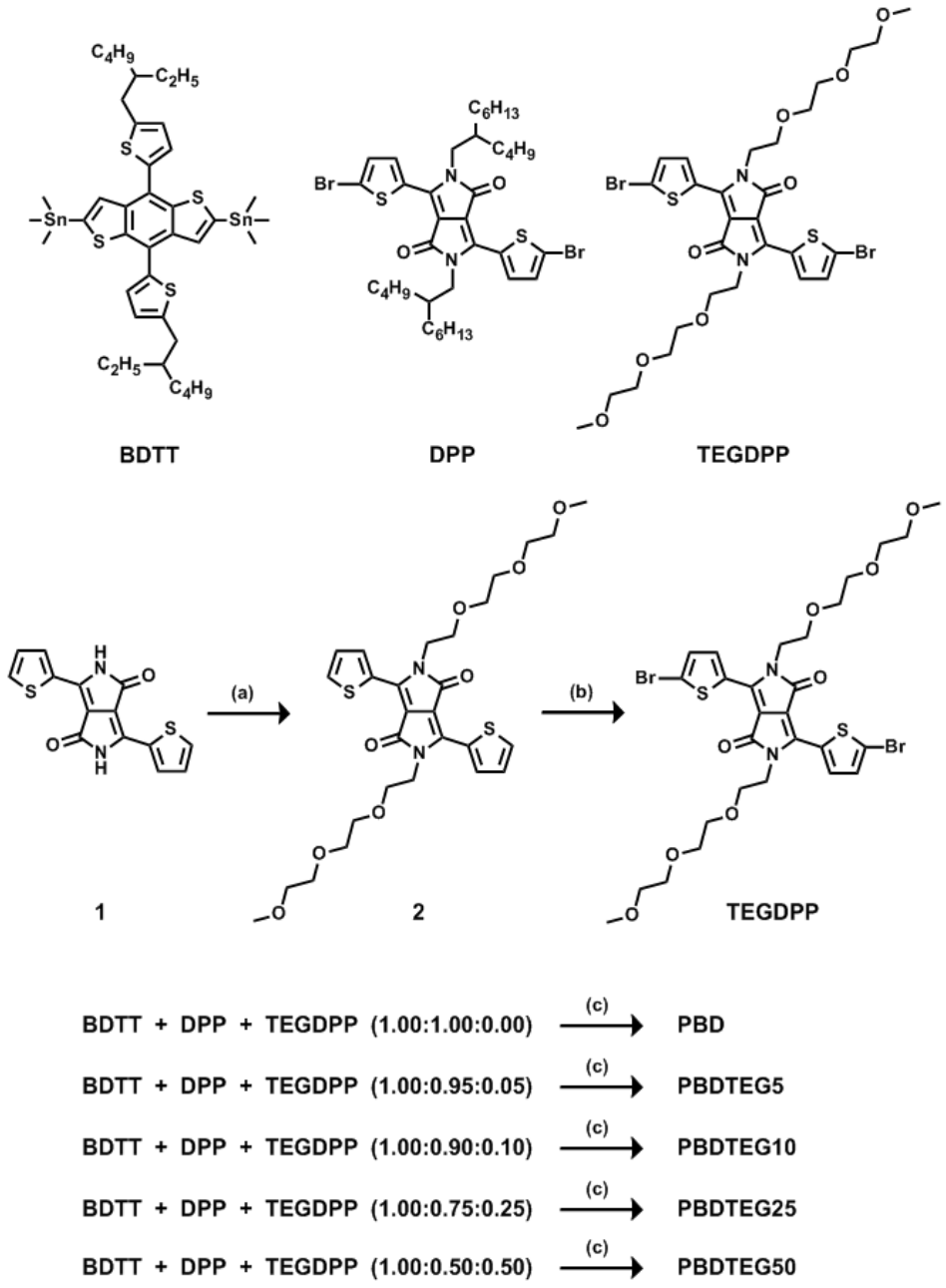

(a) 2-(2-(2-methoxyethoxy)ethoxy)ethyl 4-methylbenzenesulfonate, Bu_4NBr, K_2CO_3, DMF, 120°C, (b) NBS, $CHCl_3$, RT, and (c) $Pd(PPh_3)_4$, Toluene/DMF, 115 °C.

Polymerization for PBDTEG25: PBDTTEG25 was prepared using the same procedure as PBDTTEG5 with monomer molar ratio of BDTT:DPP:TEGDPP = 0.2000:0.1500:0.0500 mmol. Mn = 28.9 k; polydispersity = 2.1.

Polymerization for PBDTEG50: PBDTTEG50 was prepared using the same procedure as PBDTTEG5 with monomer molar ratio of BDTT:DPP:TEGDPP = 0.2000:0.1000:0.1000 mmol. Mn = 20.2 k; polydispersity = 2.1.

4.2.2 Molecular simulation

The geometry of all three compounds was subjected to density functional theory (DFT) optimizations by Gaussian 03 software package. Hybrid three-parameter B3LYP functional combined with 6-31G(d) basis set was used. The HOMO as well as LUMO energy levels were analyzed using minimized singlet geometries to approximate the ground state. Note that due to limited computational source, one donor-acceptor repeat unit with shorter alkyl and ethylene glycol side chains was carried out as representative.

4.2.3 Materials characterization

Instrumentation: ^{1}H NMR spectra were measured on a Bruker ARX-400 spectrometer. Absorption spectra were taken on a Varian Cary 50 ultraviolet-visible spectrometer. The molecular weight of the polymers was measured by the GPC method, and polystyrene was used as a standard and chloroform was used as eluent. The electrochemical cyclic voltammetry (CV) was conducted with Pt disk, Pt plate, and Ag/AgCl electrode as working electrode, counter electrode, and reference electrode, respectively, in a 0.1 mol/L tetrabutylammoniumhexafluorophosphate (Bu_4NPF_6) acetonitrile solution. For calibration, the redox potential of ferrocene/ferrocenium (Fc/Fc^{+}) was measured under the same conditions, and

it is located at 0.39 V vs. the Ag/AgCl electrode. It is assumed that the redox potential of Fc/Fc^+ has an absolute energy level of -4.80 eV to vacuum. The energy levels of the highest (HOMO) and lowest unoccupied molecular orbital (LUMO) were then calculated according to the following equations,

$$E_{HOMO} = -(\varphi_{ox} + 4.34)\ (eV)$$

$$E_{LUMO} = -(\varphi_{re} + 4.34)\ (eV)$$

whereφ_{ox} is the onset oxidation potential vs Ag/AgCl and φ_{re} is the onset reduction potential vs Ag/AgCl. X-ray diffraction (XRD) experiments were carried out using a PANalytical X'Pert Pro X-ray Powder Diffractometer using Cu-K radiation (λ=1.54050Å). The polymer films for XRD measurements were spin-coated from a polymer chloroform solution, ~ 8 mg/mL on silicon substrates. Transmission electron microscopy (TEM) measurements was conducted with a JEOL 2010F electron microscope.

4.2.4 Device fabrication and measurement

Single junction solar cell (regular): PBD, PBDTEG5, PBDTEG10, PBDTEG25 or PBDTEG50 was co-dissolved with $PC_{71}BM$ in 1,2-dichlorobenzene (DCB) with a weight ratio of 1:3 with a concentration of 8 mg/mL. ITO-coated glass substrates ($15\Omega/cm^2$) were cleaned stepwise in detergent, water, acetone, and isopropyl alcohol under ultrasonication for 15 min each and subsequently dried in an oven for 5 h. A thin layer (~30 nm) of PEDOT:PSS (Baytron P VP A1 4083) was spin-coated onto the ITO surface which was pretreated by ultraviolet ozone for 15 min. Low-conductivity PEDOT:PSS was chosen to minimize measurement error from device area due to lateral conductivity of PEDOT:PSS. After being baked at 120 ºC for ~ 20 min, the substrates were transferred into a nitrogen-filled glove box (<0.1 ppm O_2 and H_2O). A

polymer:$PC_{71}BM$ composite layer (ca.100 nm thick) was then spin-coated from the blend solutions at ~1500 rpm on the ITO/PEDOT:PSS substrate without further special treatments. Different polymer:$PC_{71}BM$ blend ratios were carried out based on PBDTEG10 in order to find out the optimal ratio as 1:3 by weight. Then the film was transferred into a thermal evaporator that is located in the same glovebox. A Ca layer (20 nm) and an Al layer (100 nm) were deposited in sequence under a vacuum of 2×10^{-6} torr. The effective area of the device was measured to be 0.10 cm^2. Note that we have also added 3% (v/v, DIO/DCB) DIO as additive and performed methanol post-treatment separately on the PBDTEG10 based devices. However, none of them showed improvement in device performance.

Current-voltage measurement: The fabricated device was encapsulated in a nitrogen-filled glovebox by UV cured epoxy and a cover glass. The current density-voltage (J-V) curves were measured using a Keithley 2400 source-measurement unit. The photocurrent was measured under AM 1.5 G illumination at 100 mW/cm^2 under a Newport Thermal Oriel 91192 1000W solar simulator. The light intensity was determined by a KG-5 filter diode (traceable to NREL calibration) as a reference cell, followed by the calculation of spectral mismatch factor and then short circuit current correction. External quantum efficiencies were measured using a lock-in amplifier (SR830, Stanford Research Systems) with current preamplifier (SR570, Stanford ResearchSystems) under short-circuit conditions. The devices were illuminated by monochromatic light from a xenon lamp passing through a monochromator (SpectraPro-2150i, Acton Research Corporation) with a typical intensity of 10 μW. The photocurrent signal is then amplified by an SR570 and detected with an SR830. A calibrated monosilicon diode with known spectral response is used as a reference.

Hole mobility: Hole mobility was measured using the space charge limited current model (SCLC), using a diode configuration of ITO/ PEDOT:PSS/polymer:$PC_{71}BM$/Au and taking current-voltage measurements in the range of 0-10 V and fitting the results to a space charge limited form, where the SCLC is described by

$$J = (8/9)\varepsilon_r\varepsilon_0\mu_e(V^2/L^3)$$

where ε_0 is the permittivity of free space, ε_r is the dielectric constant of the polymer, μ is the hole mobility, V is the voltage drop across the device ($V = V_{appl} - V_r - V_{bi}$, where V_{appl} is the applied voltage to the device, V_r is the voltage drop due to contact resistance and series resistance across the electrodes, and V_{bi} is the built-in voltage due to the difference in work function of the two electrodes), L is the polymer thickness. The dielectric constant ε_r is assumed to be 3, which is a typical value for conjugated polymers. The thickness of the polymer films is measured by using a Dektak profilometer.

4.3 Result and discussion

4.3.1 Polymer design, synthesis and characterization

The BDTT unit was purchased from SunaTech Inc. and the DPP unit were synthesized according to the reported method.[4h] The TEGDPP unit was synthesized through a S_N2 reaction of TEG tosylate with DPP core unit under a basic environment and followed by bromination with N-bromosuccinimide (NBS) under Argon protection.[8] To fully investigate the influence of the TEG side- chain's amount on PSC's performance, a series of tri-component conjugated polymer based on BDT, DPP, and TEGDPP unit were synthesized via Stille polycondensation, namely PBD, PBDTEG5, PBDTEG10, PBDTEG25, and PBDTEG50, which correspond to 0%, 5%, 10%, 25%, and 50% of TEGDPP respectively (Figure 4-1a).

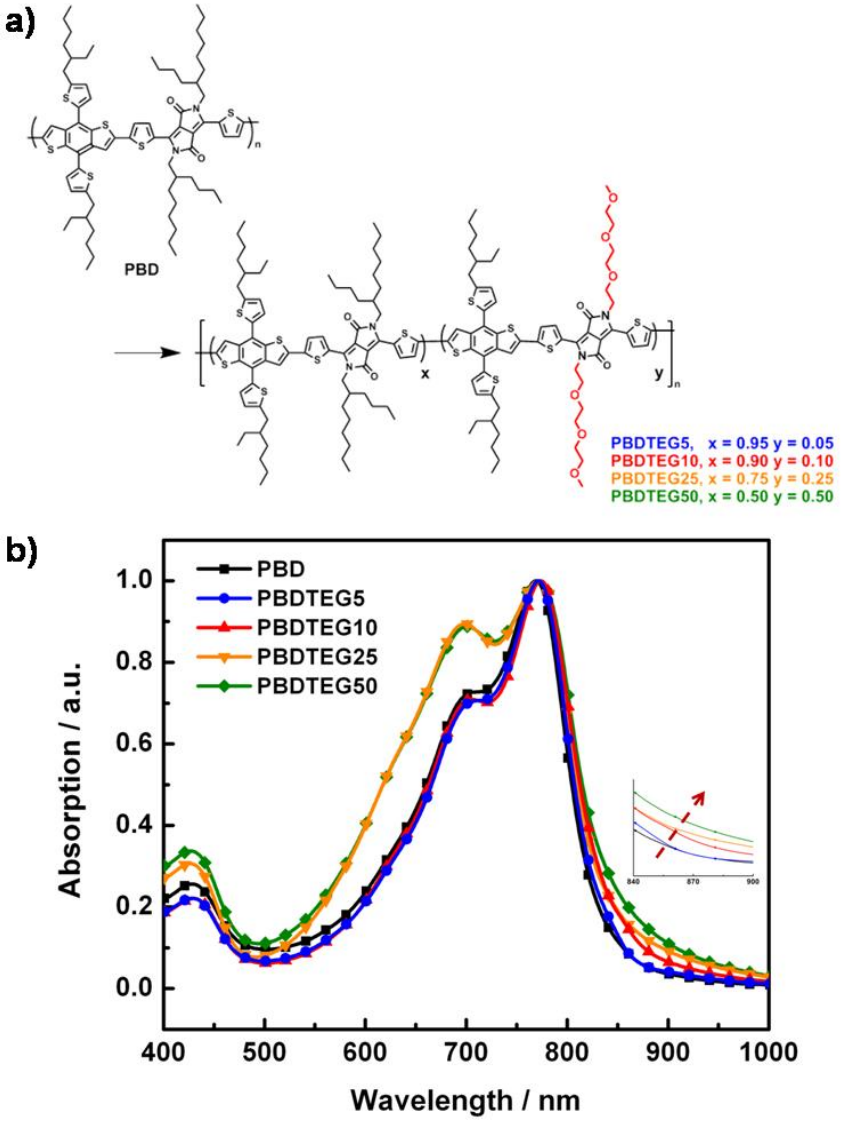

Figure 4-1. (a) Molecular structure of PBD, PBDTEG5, PBDTEG10, PBDTEG25, and PBDTEG50, and (b) Normalized UV/Vis absorption of PBD, PBDTEG5, PBDTEG10, PBDTEG25, and PBDTEG50 in thin films.

The gel permeation chromatography (GPC) measurement shows an average molecular weight of 29.8 kDa, 29.0 kDa, 29.2 kDa, 28.9 kDa, and 20.2 kDa for PBD, PBDTEG5, PBDTEG10, PBDTEG25, and PBDTEG50, respectively. The polydispersity index (PDI) of these polymers was determined as around 2.1. The increasing ratio of TEG group to alkyl group

has also been confirmed by ^{1}H NMR spectrum of polymers from PBD to PBDTEG50 (please see Figure 4-2 and 4-3 as examples). All polymers can be dissolved in CF, CB, and DCB at room temperature. It is worth noting that our experiment indicates that the solubility of polymers in CF, DCB, or hot toluene increases as the percentage of TEGDPP becomes higher, which seems to be benefited from TEG side-chains.[8a]

Figure 4-1b shows the comparison of the ultraviolet/visible (UV/Vis) absorption spectra of the polymer in thin films. All five polymers reveal a main absorption ranging from 650 to 850 nm. From PBD, PBDTEG5, PBDTEG10, and PBDTEG25 to PBDTEG50, a gradually red-shifted absorption peak is found, and moreover, the shoulder around 830-900 nm broadens as TEGDPP percentage increases (see the intersection figure). Note that the shoulder signal did not appear in the solution state. These observations may reflect a formation of a larger aggregation or a better π–π staking between the polymers in the solid state, which is likely being induced by TEG side-chains.[10] According to the onset of thin film absorption spectra, the optical bandgap of PBD, PBDTEG5, PBDTEG10, PBDTEG25, and PBDTEG50 are calculated to be 1.49, 1.49, 1.47, 1.46, and 1.45 eV, respectively. Interestingly, a slight peak blue-shifting, however, was observed in solution absorption spectrum while the percentage of TEGDPP progresses (Figure 4-4). As mentioned above, this could be attributed to the increased solubility when the content of TEG side-chain is higher, which leads to a more disordering in polymer's structural conformation when dissolved in solvent.

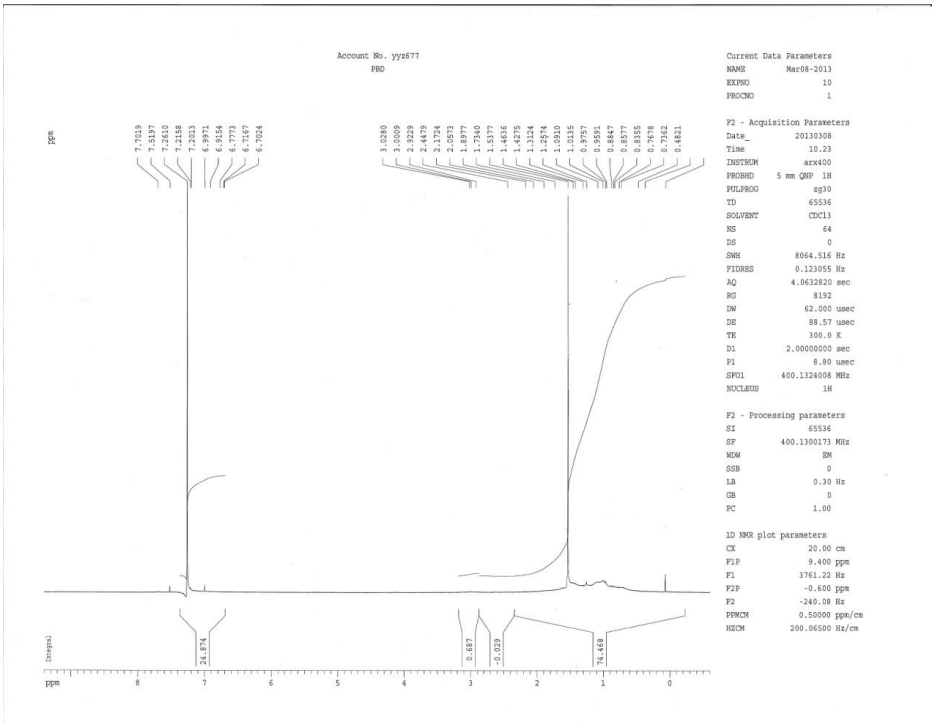

Figure 4-2. ^{1}H NMR spectrum of PBD at 298 K.

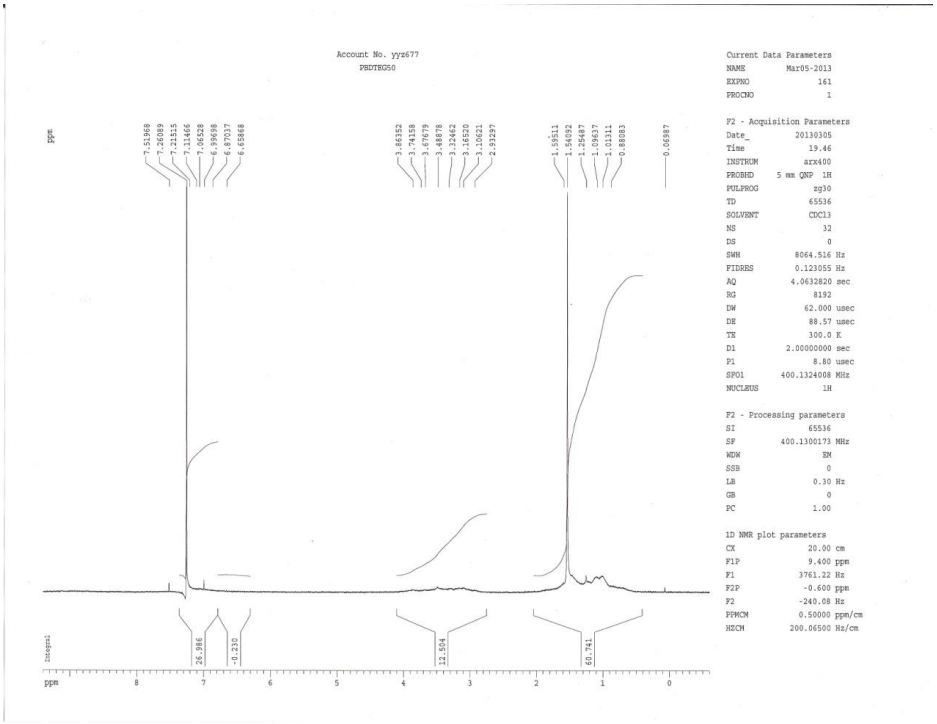

Figure 4-3. ^{1}H NMR spectrum of PBDTEG50 at 298 K.

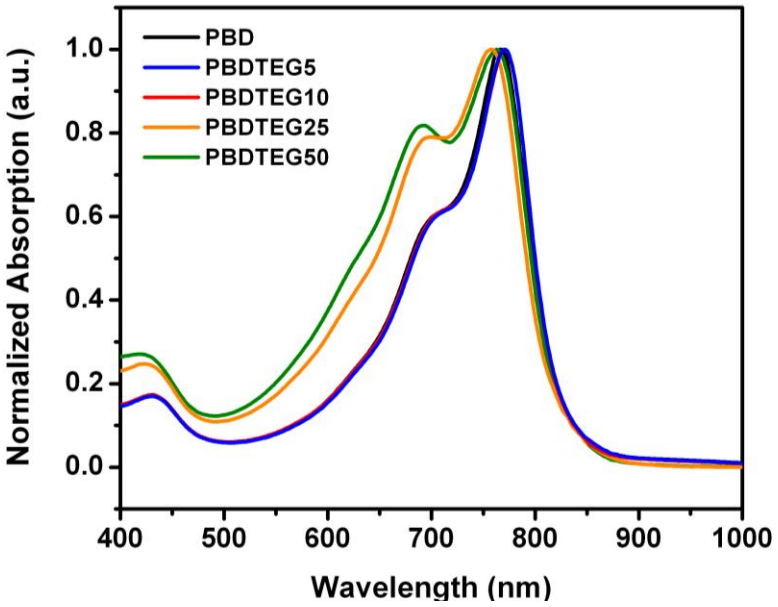

Figure 4-4. Normalized UV/Vis absorption of PBD, PBDTEG5, PBDTEG10, PBDTEG25, and PBDTEG50 in chloroform.

To study the energy level of the PBDTEG series polymer, electrochemical cyclicvoltammetry and theoretical calculations using density functional theory were carried out. From experimental CV data (Figure 4-5), the HOMO/LUMO levels are all located at around -5.30/-3.76 eV with a slight increase in HOMO level from PBD to PBDTEG50. This might be due to the weak electron-donating effect of the TEG side-chains to the polymer backbone. In addition, by performing the DFT calculation (Figure 4-6), there is also a small increase in HOMO and LUMO levels by swiching the side-chains on DPP unit from alkyl groups to methoxyalkyl groups (n-butyl versus 2-methoxyethyl in this study for computational easiness). Summarized from these results, applying TEG side-chain seems to have no major effect on the molecule's energy level. The absorption shift and the shoulders are possibly caused by increasing HOMO and additional polymer packing when TEGDPP is at present.

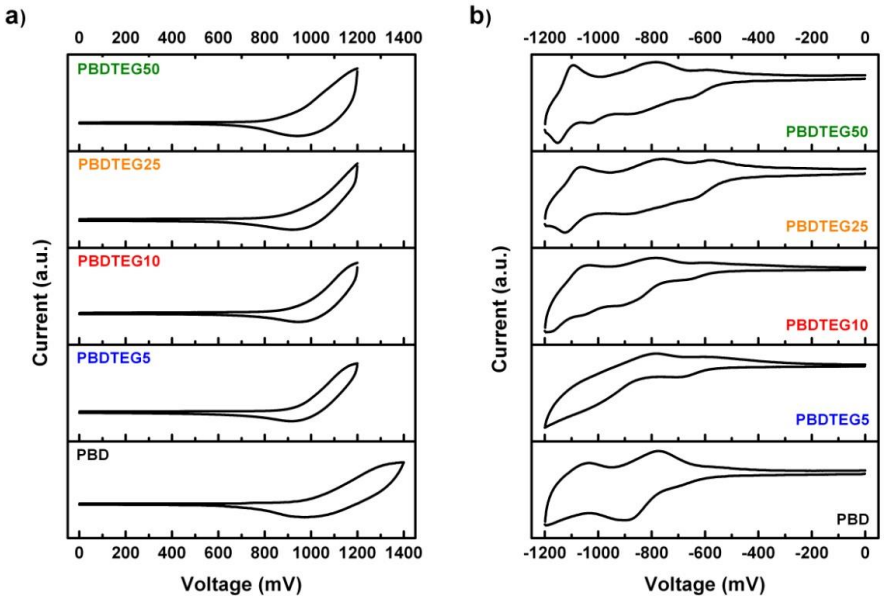

Figure 4-5. Cyclic voltammograms of PBD, PBDTEG5, PBDTEG10, PBDTEG25, and PBDTEG50 polymer thin films (a) oxidation, and (b) reduction.

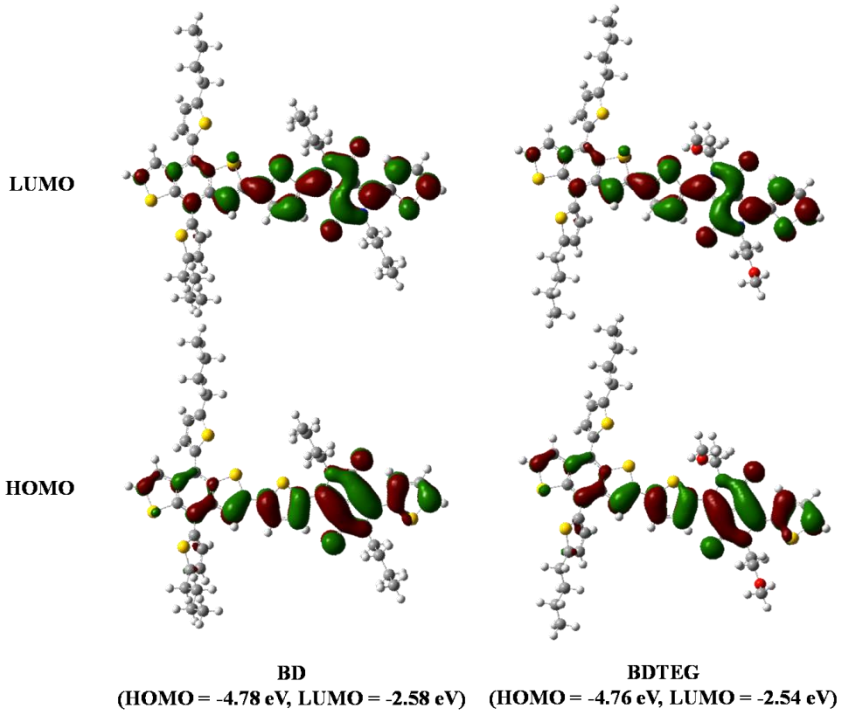

Figure 4-6. Calculated HOMOs and LUMOs of BD, and BDTEG.

4.3.2 Single junction solar cell performance

Single junction BHJ solar cell's performance of these polymers were preliminarily investigated with the regular structure of ITO/PEDOT:PSS/polymer:$PC_{71}BM$/Ca/Al under AM1.5G illumination (100 mW/cm^2). All polymer:$PC_{71}BM$ (ratio fixed as 1:3 by weight) were first spin-coated onto the PEDOT:PSS coated indium-doped tin oxide (ITO) glass substrate from DCB solutions. Without any additives or post-treatment, Ca/Al layer was then evaporated as the top electrode.

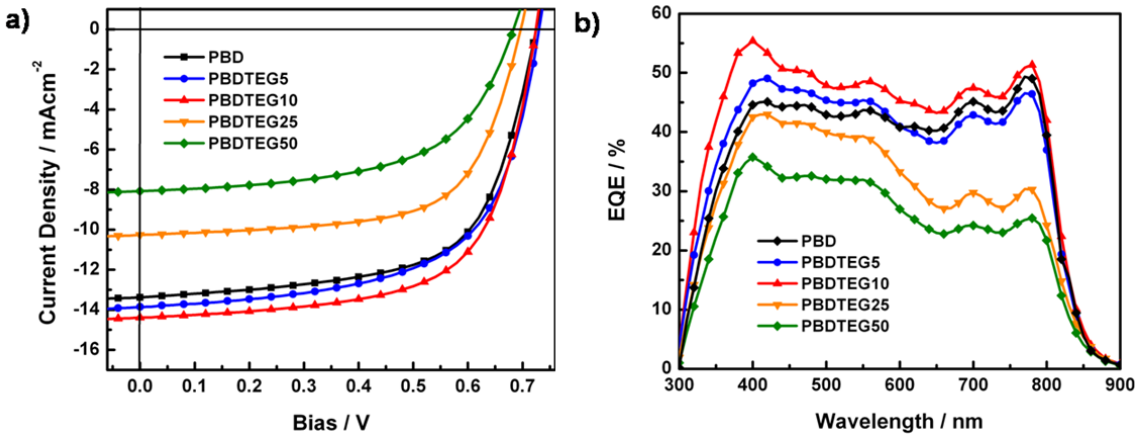

Figure 4-7. (a) Current density-voltage characteristics of polymer:$PC_{71}BM$ solar cells under AM1.5G illumination (100 mW/cm^2), and b) EQEs of the corresponding polymer:$PC_{71}BM$ devices.

Typical current density-voltage (J-V) curves are shown in Figure 4-7a, and the correspondence external quantum efficiency (EQE) data are presented in Figure 4-7b. All device data are summarized in Table 4-1. As shown in Figure 4-7a, the V_{OC} of the device drops from PBD, PBDTEG5, PBDTEG10, PBDTEG25, and PBDTEG50 slightly (from 0.73 to 0.68 V). This trend closely matches the HOMO level progression from PBD toward PBDTEG50, where a lifting HOMO energy could result in a smaller V_{OC}.[1g, 2a-b] The J_{SC} and FF%, on the contrary,

shows a peak value at PBDTEG10 based device. From PBD, PBDTEG5 to PBDTEG10, both J_{SC} and FF% increased from 13.4 to 14.3 mA/cm^2 and 63 to 68%, respectively. However, both numbers drop tremendously when TEGDPP's percentage goes beyond 10%. Similarly, EQE results clearly show the relatively highest value of PBDTEG10 based device. In average, this value is nearly 5% higher than the non-modified PBD control device (50% compared to 45%). Other than average EQE values, we found that the shoulder absorption around 830-900 nm does not contribute much to the current, showing that these π-stack induced excitations may not result in charge separation. The hole mobility of each device was further carried out by utilizing space charge limited current (SCLC) model to figure out the reason behind higher EQE in PBDTEG10 based cell; based on our experiments, mobilities of five devices were measured to be around 9.5×10^{-5} cm^2/V·s with a small variation. Therefore, it is likely that the improvement comes from other thin film properties, where we refer it to a morphology issue and is discussed below.

Table 4-1. Photovoltaic properties of single layer BHJ solar cells.

Polymer[a]	V_{OC} (V)	J_{SC} (mA/cm^2)	FF (%)	$PCE_{max/avg}$ (%)
PBD	0.73	13.4	63	6.2/6.1
PBDTEG5	0.73	13.8	63	6.3/6.1
PBDTEG10	0.72	14.3	68	7.0/6.8
PBDTEG25	0.70	10.3	65	4.7/4.6
PBDTEG50	0.68	8.1	58	3.2/3.1

[a] 0.8 wt% in 1,2-dichlorobenzene, Polymer:$PC_{71}BM$ = 1:3, ~1500 rpm.

4.3.3 Thin film morphology study

As TEG side-chains are expected to affect polymers' crystallinity and their miscibility with $PC_{71}BM$s, the thin film morphology could possibly be influenced during the film casting process. To gain more understanding of the thin film morphology, the XRD and TEM analysis were performed on PBD, PBDTEG10, and PBDTEG50 for further comparison.

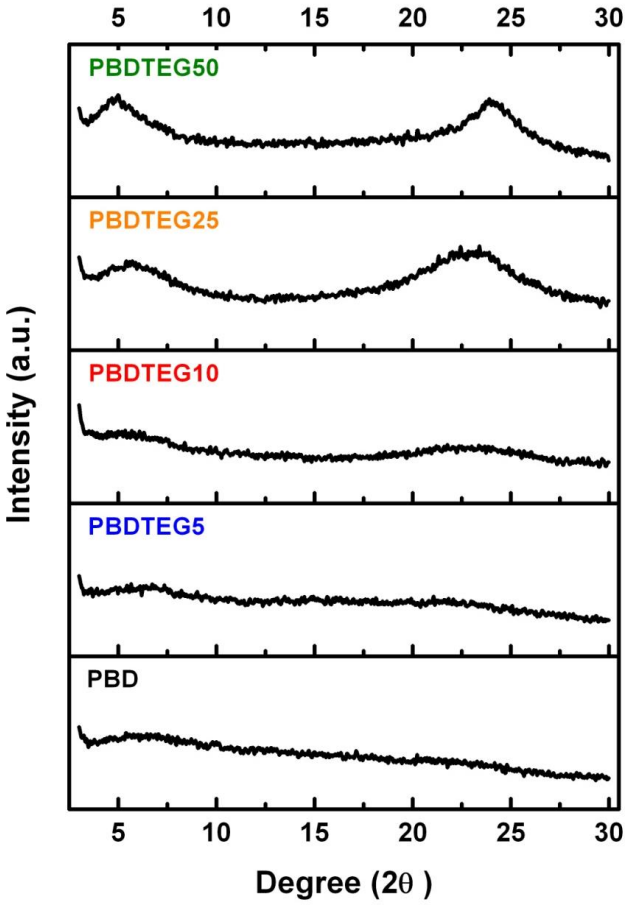

Figure 4-8. XRD spectrum of PBD, PBDTEG5, PBDTEG10, PBDTEG25, and PBDTEG50 polymer thin films.

From the XRD result of pure polymer thin films (Figure 4-8), an intensity enhancement along with TEGDPP percentage in both wider and lower angle region is found. The broad peak around $2\theta = 23^{o}$ (d = 3.86 Å) is probably correlated to π–π stacking of the polymer backbones.[11] These increments are consistent with the broadening of the shoulders obtained in UV-Vis absorption. The lower angle signal, on the other hand, is originally located at around $2\theta = 6.4^{o}$ (d = 13.8 Å) with nearly undistinguishable intensity and gradually moves to $2\theta = 5.4^{o}$ (d = 16.4 Å), and $2\theta = 4.8^{o}$ (d = 18.4 Å) with stronger intensity by PBDTEG10 and PBDTEG50, respectively. Observation above represents a larger and more regulated inter-chain spacing

between the polymer main-chains is presented, indicating a formation of a more ordered polymer domain when the content of TEGDPP becomes higher.[12] Based on the XRD result, we conclude that TEG side-chains could make polymers more prone to aggregate and have a more organized packing among each other. However, a better polymer packing itself does not link directly to a better BHJ photovoltaic device since the thin film morphology when blended with PC71BM is another important issue.[1d, 1g] Thus, TEM images were captured to find the polymer:PC71BM blend thin film morphology. From Figure 4-9, a slightly larger phase separation and fiber-like structure is observed at first in PBDTEG10:PC71BM blend as compared to PBD:PC71BM counterpart (Figure 4-9b to 4-9a). This morphology difference is assumed by us to be the reason for higher JSC and FF% in PSC device. That is, a more favorable morphology is formed with the assistance from a small amount of TEG side-chains and therefore, PBDTEG10 based cell outperforms that of PBD. However, when larger amount of TEGDPP is applied (beyond 10%), the resultant polymer's propensity to aggregate becomes too strong; and a large, detrimental phase separation occurs (the more bundle-like structure in Figure 4-9c). At this stage, the interfacial area between polymers and PC71BMs is significantly reduced and this leads to a drop in JSC and FF% because of inefficient exciton dissociation. This observation matches the previous work by other groups, which point out that a proper degree of phase separation between the polymers and the PC71BMs is essential for good exciton separation and charge transport.[1g, 13] Here, our result also reinforced the importance of a balanced phase separation. Furthermore, a fine-tuning of the blended thin film morphology by side-chain modification on the polymer can lead to a greatly improved device, as shown in our case.

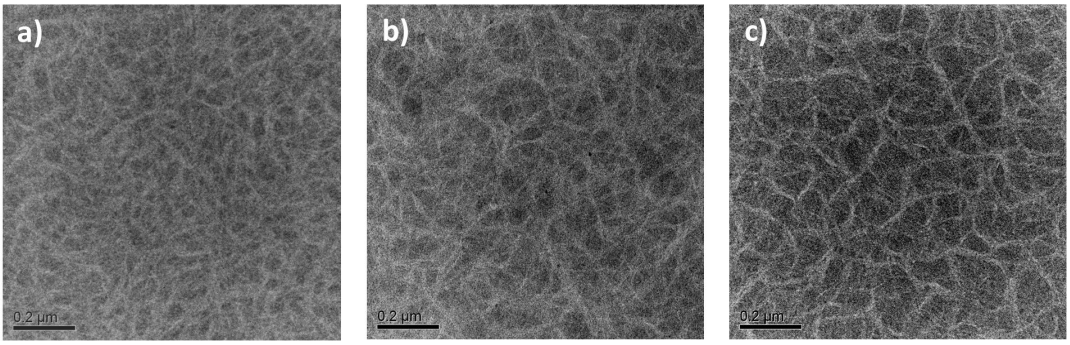

Figure 4-9. TEM image of a) PBD:$PC_{71}BM$, b) PBDTEG10:$PC_{71}BM$, and c) PBDTEG50:$PC_{71}BM$ blend thin film. (Scale bar: 200 nm)

4.4 Summary and outlook

In conclusion, we have successfully demonstrated a non-conventional TEG side-chain introduction into conjugated polymers for solar cell applications. Via a triple component random copolymerization approach, a material's electronic property can be fine-tuned. Based on the result of low-bandgap polymer consisting of BDTT and DPP moieties, this approach can bring us an over 10% improvement in PCE (from 6.2% to 7.0%) with 10% TEG modification. Furthermore, the boost in efficiency is caused by higher J_{SC} and FF% while V_{OC} is basically maintained. This enhancement is believed by us to be benefited from a more correct degree of phase separation between polymers and $PC_{71}BM$s with the aid of TEG groups, which act as a stack-inducing agent. That is, the TEGs, when attached onto the polymer backbone, are able to enhance the aggregation propensity of the polymers. As a result, the interfacial area between polymers and $PC_{71}BM$s can be maximized by a precise control over the amount of TEG groups. The evidence is shown by a combination of device characterization and morphological study, which point to a formation of better structural ordering in polymers and a more favorable morphology as a thin film. The present contribution provides a simple and effective method to

adjust the existing photovoltaic polymer's structure as well as the thin film morphology without losing its original advantages. We envision that this strategy should also be applicable for other material systems and new materials with even higher performance may be obtained in the near future.

References:

[1] a) Yu, G. *et al. Science* **1995,** *270,* 1789; b) Halls, J. J. M. *et al. Nature* **1995**, *376*, 498; c) Brabec, J. *et al. Ad*v. *Funct. Mater.* **2011,** *11,* 15; d) Li, G. *et al. Nat. Mater.* **2005**, *4*, 864; e) Ma, W. L. *et al. Adv. Funct. Mater.* **2005**, *15,* 1617; f) F. C. Krebs, *Sol. Energy Mater. Sol. Cells* **2009**, *93,* 394; g) Li, G. *et al. Nat. Photon.* **2012**, *6,* 153.

[2] a) Thompson, B. C. *et al. Angew. Chem. Int. Ed.* **2008**, *47*, 58; b) Cheng, Y. J. *et al. Chem. Rev.* **2009**, *109*, 5868; c) Boudreault, P. L. T. *et al. Chem. Mater.* **2011**, *23*, 456; d) Beaujuge, P. M. *et al. J. Am. Chem. Soc.* **2011**, *133*, 20009.

[3] a) Chen, H.-Y. *et al. Nat. Photon.* **2009,** *3,* 649; b) Liang, Y. *et al. Adv. Mater.* **2010,** *22,* E135; c) He, Z. C. *et al. Adv. Mater.* **2011,** *23,* 4636. d) Huo, L. *et al. Angew. Chem. Int. Ed.* **2011**, *50,* 1; e) Zou, Y. *et al. J. Am. Chem. Soc.* **2010**, *132*, 5330; f) Piliego, C. *et al. J. Am. Chem. Soc.* **2010**, *132*, 7595; g) Chu, T. Y. *et al. J. Am. Chem. Soc.* **2011**, *133,* 4250; h) Amb, C. M. *et al. J. Am. Chem. Soc.* **2011**, *133*, 10062; i) Xu, Y.-X. *et al. Adv. Mater.* **2012,** *24,* 6356.

[4] a) Peet, J. et al. Nat. Mater. **2007**, 6, 497; b) Hou, J. et al. J. Am. Chem. Soc. **2008**, 130, 16144; c) Yiu, A. T. et al. J. Am. Chem. Soc. **2012**, 134, 2180; d) Li, W. et al. J. Am. Chem. Soc. **2012**, 134, 13787; e) Ye, L. et al. Adv. Mater. **2012**, 24, 6335; f) Li, W. et al. Adv. Mater. **2013,** DOI: 10.1002/adma.201300017; g) Li, W. et al. J. Am. Chem. Soc. **2013,** 135, 5529; h) Dou, L. et al. J. Am. Chem. Soc. **2012,** 134, 10071; i) Zhang, S. et al. J. Phys. Chem. C, **2013**, 117, 9550; j) Dou, L. et al. Nat. Photon. **2012**, 6, 180; k) Chen, C.-C. et al. ACS Nano, **2012**, 6, 7185; l) Dou, L. et al. Adv. Mater. **2013,** 25, 825; m) Dou, L. et al. Macromolecules **2013,** 46, 3384.

[5] Bundgaard, E. et al. Sol. Energy Mater. Sol. Cells **2007**, 91, 954.

[6] a) Chen, M.-H. *et al. Adv. Mater.* **2009**, *21*, 4238; b) Liang, Y. *et al. J. Am. Chem. Soc.* **2009,** *131*, 7792; c) Mei, J. *et al. J. Am. Chem. Soc.* **2011**, *133*, 20130; d) Kim, D. H. *et al. Chem. Mater.* **2013**, *25*, 431; e) Lu, K. *et al. New J. Chem.* **2013**, 37, 1728.

[7] a) Feng, X. *et al. Nat. Mater.* **2009**, *8*, 421; b) Lee, E. *et al. J. Am. Chem. Soc.* **2011,** *133*, 10390; c) Song, I. Y. *et al. Macromolecules* **2012,** 45,5058.

[8] a) Mei, J. *et al. Chem. Mater.* **2011**, *23*, 2285; b) Kanimozhi, C. *et al. J. Am. Chem. Soc.* **2012**, *134*, 16532.

[9] a) Jiang, J.-M. *et al. Polym. Chem.* **2013**, DOI: 10.1039/c3py00132f; b) Zhou, J. *et al. Macromolecules* **2013**, 46, 3391.

[10] Balakrishnan, K. *et al. J. Am. Chem. Soc.* **2005**, *127*, 10496.

[11] Shahid, M. *et al. Chem. Sci.* **2012**, 3, 181.

[12] Salleo, A. *Adv. Mater.* **2010**, 22, 3812.

[13] Yang, X. *et al. Macromolecules* **2007,** 40, 1353.

CHAPTER 5

Removing the Need of Solvent-Additives: the Effect of Side Chain Selenophene Substitution on the PTB-based Photovoltaic Polymer

(This chapter is based on the following publication: *Macromolecules*, **2015**, 48, 562–568.)

In this chapter, I turn my focus to the state-of-the-art medium bandgap PTB polymer. As described in chapter 2, PTB7, one of the highest preforming photovoltaic polymers to this date, requires a solvent additive to reach the optimal morphology when blended with $PC_{71}BM$. However, the usage of solvent additive may decrease the device's thermal stability; and in addition, complicates the device fabrication process. In this chapter, we present a new PTB polymer, PBDTSe-TT, which contains a selenophene side-chain. The structure adjustment carried out by the alkylselenophene substitution on the BDT building block is shown to slightly affect the polymer's electronic properties. The observed result is an increase in open-circuit voltage. More importantly, the phase separation domain of the PBDTSe-TT:$PC_{71}BM$ blend is shown to have the optimal size, ~ 10 nm, for spin-casting from a single solvent. As a result, an efficient solar cell of 8.8% efficiency is achieved without using any solvent additive or special interfacial layer. Furthermore, the PBDTSe-TT based device is relatively stable under thermal stress, making it a good candidate for fabricating stacked cells. Finally, a ~ 10% efficient tandem device is demonstrated by using identical PBDTSe-TT:$PC_{71}BM$ sub-cells.

5.1 Introduction

The development of novel materials has a major contribution to the improvement of the performance of polymer solar cells (PSCs).[1] Among all the semiconducting polymers been reported, one of the most successful and commonly used structures is PTB7 (Poly[[4,8-bis[(2-ethylhexyl)oxy]benzo[1,2-b:4,5-b']dithiophene-2,6-diyl][3-fluoro-2-[(2-ethylhexyl)carbonyl]thieno[3,4-b]thiophenediyl]], bandgap (E_g) ~ 1.6 eV). Single junction PTB7 based PSC have exhibited power conversion efficiencies (PCE) exceeding 9% after years of efforts.[2] Due to morphological challenges, reported PTB7 based devices can only function well with fullerene derivatives when a high boiling point solvent additive, usually 1,8-diiodooctane (DIO), is added.[2a] However, incorporation of solvent additives intrinsically complicates device construction thus making large-area fabrication difficult to realize. In addition, evidence indicates that the kinetic controlled morphology obtained through DIO seems to be unstable towards thermal treatment.[3] This prohibits PTB7 from applying to all-solution processed tandem structure, as heat drying is usually needed during the inter-connecting layer processing.[4] Studies on the effect of DIO have been carried out extensively for several years. It is commonly believed that these low volatility additives (1) dissolves $PC_{71}BM$ aggregates selectively, thus allowing them to penetrate into polymer domains, and (2) retards the evaporation rate of solvent during the spin-coating, thus allowing mitigation of optimal thin-film morphology of the active layer.[2c,5] As this morphology is critical to the BHJ solar cells, reaching a so-called “bi-continuous” phase separation with correct domain size (typically 10-20 nm) can thus find a balance between charge separation (requires enough donor-acceptor interface) and transport (requires continuous percolation pathway), and therefore the maximum PCE of these PTB7 based devices can be achieved.[1d-e,1g-i,2a,2c]

Our group has been working towards developing new low Eg photovoltaic polymers and their versatile applications (E_g ~ 1.4 eV).[6] Interestingly, we found that the current state-of-the-art small bandgap polymers, such as PBDTT-DPP, PDPP3T, and PDTP-DFBT, usually do not require DIO to achieve moderate solar cell performance.[6,7] It is frequently observed that these polymers can form a good nanoscale bi-continuous phase separation with $PC_{71}BM$ spontaneously.[6,7b-c] As these small bandgap polymers are believed to possess a stronger inter-chain interaction, fibril-like polymeric nanostructure is often observed and thus appropriate bulk BHJ morphology can be formed during the spin-casting or perhaps as early as in the solution state. The necessity of DIO is thus avoided in the corresponding PSCs. Here, we propose that if the molecular interaction of the PTB7 based polymer can be carefully adjusted to increase its aggregation propensity, one might be able to get rid of additive while maintains a good photovoltaic performance.

Recently, Liao *et al.* reported an alkylthiophene substituted PTB7, PTB7-Th, with a PCE of 9% by utilizing cathode interface engineering.[8] The PTB7-Th also shows an enhanced V_{OC} compared to PTB7. Furthermore, recent studies also indicate that alkylselenophene substituded benzodithiophene (BDT) could be a good donor building block for photovoltaic molecules or polymers due to its suitable energy level and strong Se-Se interaction.[9] Based on these previous findings, herein, we report a newly synthesized conjugated polymer with selenium insertion on the side-groups of PTB7-Th, namely PBDTSe-TT. Besides commonly observed red-shifted spectrum, selenium substitution on organic molecules usually improves the carrier transportation in the resulting electronic devices.[6b,9-10] This improvement is believed to be a result of enhanced π-π interaction between molecules brought by selenium atoms. Taking these advantages into account, we anticipate that a stronger stacking between polymer chains could be

achieved through selenium substitution on the PTB7-based polymer, and thus the usage of solvent additives may not be necessary. Although the backbone selenium substitution on PTB7 has been previously reported, the polymer exhibits “too” strong of an inter-chain interaction thus the device performance is reduced as a result of improper phase separation.[11] Moreover, the synthesis of such molecules is rather complicated. As we will discuss below, side-chain selenium modification is shown to be an effective way to address morphological issue of PTB7 related polymers. PBDTSe-TT, as we proposed, can achieve high performance of 8.8% PCE without any additives, such as DIO or CN. Furthermore, it is shown that the newly synthesized polymer exhibits relatively good thermal stability. When taking a further step to fabricate tandem device through identical PBDTSe-TT:$PC_{71}BM$ sub-cells, an ~10 % PCE is demonstrated.

5.2 Experimental method

5.2.1 Synthetic procedures

Materials: 2,6-Bis(trimethyltin)-4,8-bis(5-ethylhexyl-2-thienyl)-benzo[1,2-b:4,5-b’]dithiophene (BDTT) was purchased from SunaTech Inc. 2-Ethylhexyl-4,6-dibromo-3-fluorothieno[3,4-b]thiophene-2-carboxylate (TT), and 2-(2-ethylhexyl)selenyl (1) were synthesized according to the literature.[2,9] [6,6]-phenyl-C_{71}-butyric acid methyl ester ($PC_{71}BM$) was purchased from Solarmer Energy Inc. Unless otherwise stated, all of the chemicals were purchased from Aldrich and used as received. A summarize of synthetic routes is shown in Scheme 5-1.

Scheme 5-1. Synthesis of monomers and polymers.

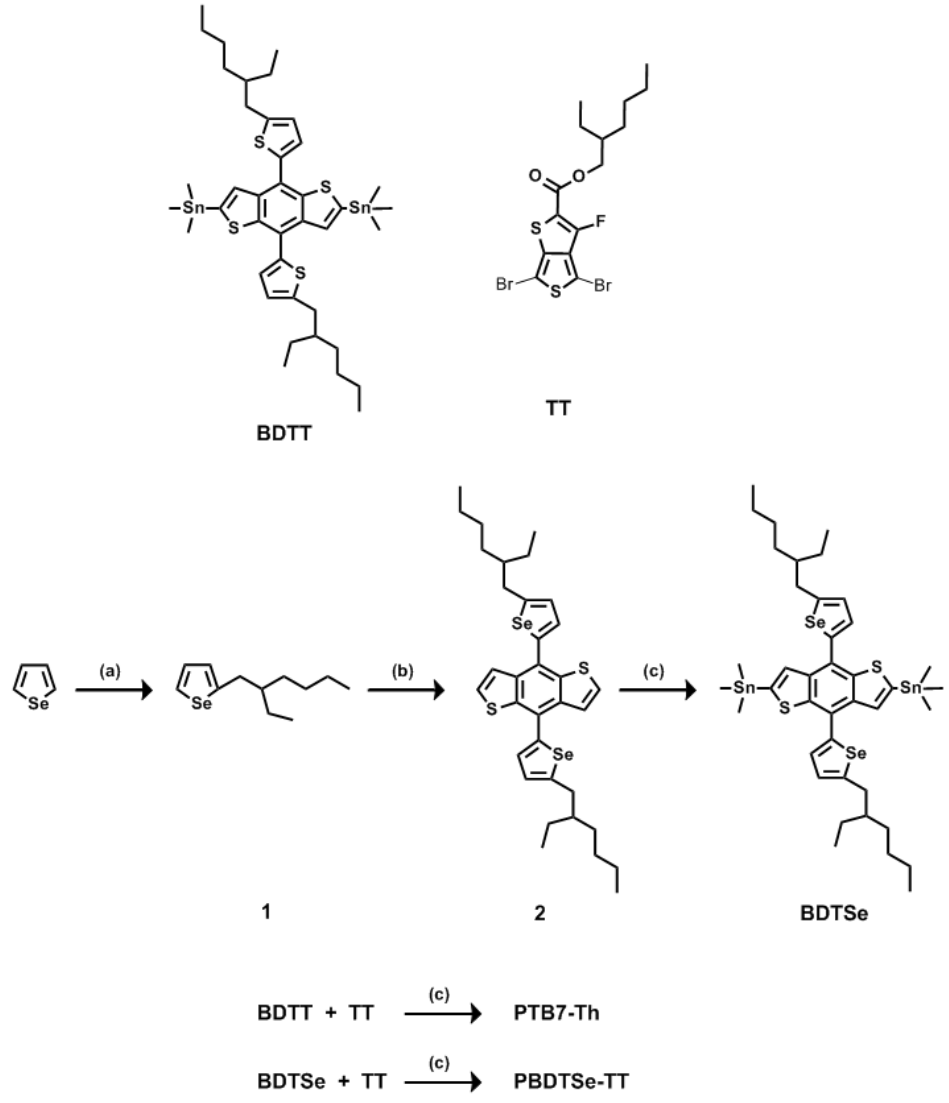

(a) n-butyllithium, THF, -78 °C, then 2-ethylhexyl bromide, 40 °C. (b) n-butyllithium, THF, -78 °C, then benzo[1,2-b:4,5-b']dithiophene-4,8-dione, room temperature, then $SnCl_2 \cdot 2H_2O$, 10% HCl, room temperature.(c) n-butyllithium, THF, -78 °C, then $SnMe_3Cl$, room temperature. (d) $Pd(PPh_3)_4$, Toluene/DMF, 105 °C.

4,8-bis(5-(2-ethylhexyl)selenophen-2-yl)benzo[1,2-b:4,5-b']dithiophene (2): Under the protection of argon, *n*-butyllithium solution (2.5 M, 11.1 mmol) was added dropwise to (1) (3.00

g, 12.3 mmol) in THF (16 mL) at -78 °C, and then the mixture was warmed up to RT and stirred for 4 h. Subsequently, 4,8-dehydrobenzo[l,2-b:4,5-b']dithiophene-4,8-dione(0.91 g, 4.1 mmol) was added. After stirring at RT overnight, $SnCl_2 \cdot 2H_2O$ (7.46 g, 60 mmol) in 10% HCl (13.3 mL) was added, and the mixture was stirred for another 1.5 h and poured into ice water. The mixture was extracted by hexane, and the combined extracts were washed by water for 3 times, dried over Na_2SO_4, and then concentrated under vacuum. Further purification was carried out by silica gel chromatography using hexane as eluent to obtain pure product as a light yellow solid (2.10 g, yield 80%). ^{1}H NMR ($CDCl_3$, 400MHz) δ: 7.64 (d, J = 5.6 Hz, 2H), 7.44 (d, J = 5.6 Hz, 2H), 7.40 (d, J = 3.6 Hz, 2H), 7.03 (d, J = 3.6 Hz, 2H), 2.92 (d, J = 6.4 Hz, 4H), 1.65 (m, 2H), 1.53-1.33 (m, 16H), 0.97-0.92 (m, 12H) ppm. MALDI-TOF, *m/z*: Calcd, 674.11; Found, 674.07 (M^+).

(4,8-bis(5-(2-ethylhexyl)selenophen-2-yl)benzo[1,2-b:4,5-b']dithiophene-2,6-diyl)bis(trimethylstannane) (BDTSe): Under protection of argon at -78 °C, *n*-butyllithium solution in hexanes (1.6 M, 6.63 mmol) was added dropwise to 4,8-bis(5-(2-ethylhexyl)selenophen-2-yl)benzo[1,2-b:4,5-b']dithiophene (1.92 g, 2.83 mmol) dissolved in 40 mL of anhydrous THF. The solution was warmed to RT for 1 h, and then trimethyltin chloride solution in THF (1.0 M, 8.48 mmol) was added and then stirred at RT for 1.5 h. The reaction mixture was poured into water (100 mL) and extracted with ether (50 mL). The combined extracts was dried over Na_2SO_4, concentrated under vacuum, and the crude product was recrystallized from 20 mL of acetone to afford the yellow compound (2.51 g, 74%). ^{1}H NMR ($CDCl_3$, 400MHz) δ: 7.6 (m, 2H), 7.41 (d, J = 3.6 Hz, 2H), 7.05 (d, J = 3.6 Hz, 2H), 2.92 (m, 4H), 1.69 (m, 2H), 1.54-1.27 (m, 16H), 0.98-0.88 (m, 12H), 0.39 (m, 18H) ppm. MALDI-TOF, *m/z*: Calcd, 998.04; Found, 997.83 (M^+).

Polymerization for PBT7-Th: BDTT (0.2255 g, 0.2493 mmol), TT (0.1177 g, 0.2492mmol) were dissolved into 7.5 mL anhydrous toluene and 1.5 mL anhydrous DMF in a flask protected by argon. The solution was flushed with argon for 10 minutes, then 14.6 mg of $Pd(PPh_3)_4$ was added into the flask. The solution was flushed with argon again for another 10 minutes before stirring for 10 hours at 105 ºC under argon atmosphere. Then, the mixture was cooled down to room temperature and the polymer was precipitated in ~100 mL methanol and the precipitated solid was collected. The crude polymer was subjected to soxhlet extraction by methanol (6h), hexane (12h), and acetone (6h). Finally, the polymer was purified by silica gel chromatography using chloroform as eluent and then slowly precipitated in ~75 ml acetone. The polymer was collected as dark green-black solid, yield 30%. The polymer can be readily dissolved into chloroform, chlorobenzene or dichlorobenzene, etc**.** GPC result: Mn ~ 20.4k; polydispersity = 4.1.

Polymerization for PBDTSe-TT**:** BDTSe (0.2496 g, 0.2504 mmol), TT (0.1185g, 0.2509 mmol) were dissolved into 7.5 mL anhydrous toluene and 1.5 mL anhydrous DMF in a flask protected by argon. The solution was flushed with argon for 10 minutes, then 14.5 mg of $Pd(PPh_3)_4$ was added into the flask. The solution was flushed with argon again for another 10 minutes before stirring for 10 hours at 105 ºC under argon atmosphere. Then, the mixture was cooled down to room temperature and the polymer was precipitated in ~100 mL methanol and the precipitated solid was collected. The crude polymer was subjected to soxhlet extraction by methanol (6h), hexane (12h), and acetone (6h). Finally, the polymer was purified by silica gel chromatography using chloroform as eluent and then slowly precipitated in ~75 ml acetone. The polymer was collected as dark green-black solid, yield 30%. The polymer can be readily

dissolved into chloroform, chlorobenzene or dichlorobenzene, etc**.** GPC result: Mn ~ 24.6 k; polydispersity = 4.4.

5.2.2 Materials Characterization

Instrumentation: ^{1}H NMR spectra were measured on a Bruker ARX-400 spectrometer. MALDI-TOF spectra were recorded on Applied Biosystems Voyager-DE STR using dihydroxybenzoic acid as matrix. Absorption spectra were taken on a Varian Cary 50 ultraviolet-visible spectrometer. The molecular weight and polydispersity of the polymers were determined by the gel permission chromatography (GPC) method through Agilent Infinity 1260 system. Polystyrene was used as standard and chloroform was used as eluent (flow rate: 1.0 mL/min; column temperature: 40 ºC). The electrochemical cyclic voltammetry (CV) was conducted with Pt disk, Pt plate, and Ag/AgCl electrode as working electrode, counter electrode, and reference electrode, respectively, in a 0.1 mol/L tetrabutylammoniumhexafluorophosphate (Bu_4NPF_6) acetonitrile solution. For calibration, the redox potential of ferrocene/ferrocenium (Fc/Fc^+) was measured under the same conditions, and it is located at 0.46 V vs. the Ag/AgCl electrode. It is assumed that the redox potential of Fc/Fc^+ has an absolute energy level of - 4.80 eV to vacuum. The energy levels of the highest (HOMO) and lowest unoccupied molecular orbital (LUMO) were then calculated according to the following equations,

$$E_{HOMO} = -(\varphi_{ox} + 4.34)\ (eV)$$

$$E_{LUMO} = -(\varphi_{re} + 4.34)\ (eV)$$

where φ_{ox} is the onset oxidation potential vs Ag/AgCl and φ_{re} is the onset reduction potential vs Ag/AgCl. Transmission electron microscopy (TEM) measurements were conducted with a T12 cryo-electron microscope.

5.2.3 Device fabrication and measurement

Single junction solar cell (inverted): PTB7-Th or PBDTSe-TT was co-dissolved with $PC_{71}BM$ in chlorobenzene (CB) with a weight ratio of 1:1:5 at a concentration of 1.2 mg/mL. Depends on the experimental condition, the weight ratio may be varied from 1:1 to 1:2, and 1,8-diiodooctane may be added as solvent additive (0% - 3%, v/v). ITO-coated glass substrates ($15\Omega/cm^2$) were cleaned stepwise in detergent, water, acetone, and isopropyl alcohol under ultrasonication for 15 min each and subsequently dried in an oven for 5 h. A thin layer (~30 nm) of ZnO was spin-coated onto the ITO surface. After being baked at 150 ºC for 15 min, the substrates were transferred into a nitrogen-filled glove box (<0.1 ppm O_2 and H_2O). A polymer/$PC_{71}BM$ composite layer (ca. 100 nm thick) was then spin-coated from the blend solutions at ~ 1500 rpm on the ITO/ZnO substrate without further special treatments. Note that for the thermal stability experiment, the whole substrate with polymer/$PC_{71}BM$ composite layer was annealed at 100 ºC for 1-10 min. The device fabrication was completed by thermal evaporation of 15 nm MoO_3 and 100 nm Ag as the anode under vacuum at a base pressure of 2×10^{-6} torr. The effective area of the device was measured to be 0.10 cm^2.

Inverted structure tandem cell with identical sub-cells: The front cell was made according to the single cell procedure as mentioned above, and then the sample was transferred into the evaporation chamber for MoO_3 layer deposition, the thickness of MoO_3 is around 15 nm. Then modified PEDOT:PSS (m-PEDOT:PSS) was spin-casted on MoO_3 surface, the details of m-PEDOT:PSS can be found elsewhere, the only difference is that PEDOT:PSS (Al 4083) was used here to avoid parasitic current.[S1] And then the rear cell was fabricated as the front cell; the thicknesses of the active layer were controlled by the spin coating speed. Finally, the samples

were transferred into the evaporation chamber for fabricating the MoO_3/Ag electrode. The effective area of the device was measured to be 0.10 cm^2.

Current-voltage measurement: The fabricated device was encapsulated in a nitrogen-filled glovebox by UV cured epoxy and a cover glass. The current density-voltage (J-V) curves were measured using a Keithley 2400 source-measurement unit. The photocurrent was measured under AM 1.5 G illumination at 100 mW/cm^2 under a Newport Thermal Oriel 91192 1000W solar simulator. The light intensity was determined by a KG-5 filter diode (traceable to NREL calibration) as a reference cell, followed by the calculation of spectral mismatch factor and then short circuit current correction. External quantum efficiencies were measured using a lock-in amplifier (SR830, Stanford Research Systems) with current preamplifier (SR570, Stanford ResearchSystems) under short-circuit conditions. The devices were illuminated by monochromatic light from a xenon lamp passing through a monochromator (SpectraPro-2150i, Acton Research Corporation) with a typical intensity of 10 μW. The photocurrent signal is then amplified by an SR570 and detected with an SR830. A calibrated monosilicon diode with known spectral response is used as a reference.

Photo-induced charge carrier extraction in a linearly increasing voltages (Photo-CELIV) measurement: To measure the mobility of the polymer:$PC_{71}BM$ blend system, Photo-CELIV measurement was used to determine the charge carrier mobility in bulk heterojunction solar cells.[S2] The device structure is ITO/ZnO/Polymer:$PC_{71}BM$/MoO_3/Ag, where the active layer thicknesses are around 100 nm. A 590-nm dye (Rhodamine Chloride 590) laser pumped by a nitrogen laser (LSI VSL-337ND-S) was used as the excitation source, the pulse energy and pulse width being about 0.02 μJcm^{-2} and 4 ns, respectively. The current of the photodiode was recorded using a digital oscilloscope (Tektronix DPO 4104), the mobilities of PTB7-

Th:$PC_{71}BM$, PTB7-Th:$PC_{71}BM$ with 3% DIO, PBDTSe-TT:$PC_{71}BM$, and PBDTSe-TT:$PC_{71}BM$ with 3% DIO based devices are calculated to be 1.71×10^{-4}, 3.00×10^{-4}, 7.59×10^{-4} and 6.94×10^{-4} $cm^2V^{-1}s^{-1}$, respectively, based on the following equation,

$$\mu = \frac{2d^2}{3At_{max}^2\left[1+0.36\frac{\Delta j}{j(0)}\right]} \quad \text{if } \Delta j \leq j(0)$$

where μ is the mobility, d is the thickness of the active layer, t_{max} is the time when the extraction current is reached, A is the voltage rise speed $A = dU/dt$. In this measurement, the applied maximum voltage is 0.25 V, and U_{offset} is chosen to be near the corresponding open-circuit voltage but without any forward injection current, the time t for voltage increase from U_{offset} to maximum voltage is 30 μs, and $j(0)$ is the capacitive displacement current.

5.3 Result and discussion

5.3.1 Polymer design, synthesis and characterization

The BDTT unit and PBT7-Th polymer was synthesized according to the reported procedure.[6a,8] For the BDTSe unit, benzo[1,2-b:4,5-b']dithiophene-4,8-dione (BDT) was firstly reacted with lithiated 2-(2-ethylhexyl)selenophene, and then encapsulated with trimethyltinchloride ($SnMe_3Cl$) to obtain the BDTSe monomer.[9b-d] The polymerization was carried out by Stille coupling reaction. The chemical structure of PBT7-Th and PBDTSe-TT is drawn in Figure 5-1a. The newly synthesized PBDTSe-TT can be readily dissolved in common organic solvents, such as chloroform (CF), chlorobenzene (CB), or dichlorobenzene (DCB). From the GPC result (Figure 5-2), both PTB7-Th and PBDTSe-TT shows approximately same retention time; and we can therefore exclude the effect of molecular weight in the comparison of

the device performance in the later section (note that oligomer residuals are still existed after purification, which leads to broad GPC peaks for both polymers).

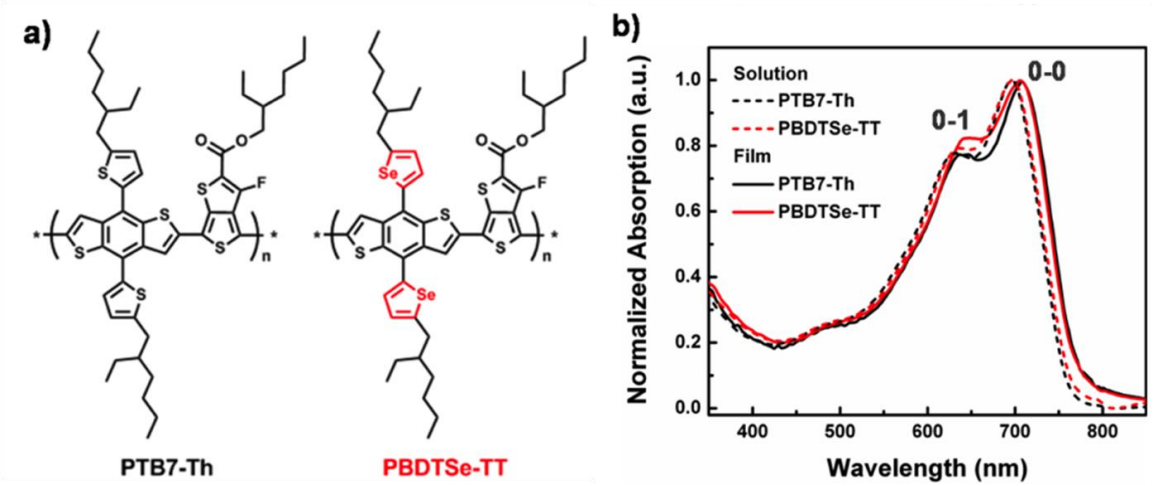

Figure 5-1. (a) Structure of PTB7-Th and PBDTSe-TT, and (b) UV-Vis spectrum of PTB7-Th and PBDTSe-TT in chloroform and thin film.

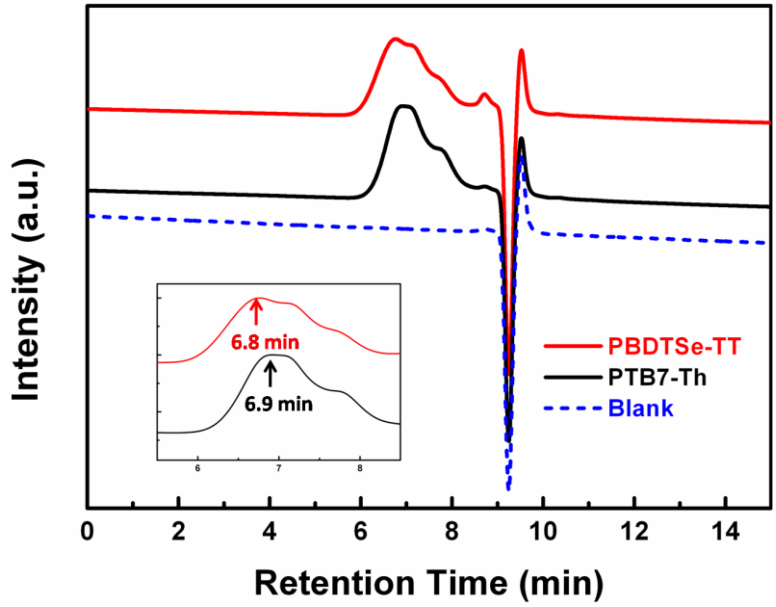

Figure 5-2. GPC trace curves of PTB7-Th and PBDTSe-TT. (Based on the blank chloroform injection, the positive and negative spikes at around 8.5-9.5 min can be identified as background system peaks. These peaks are excluded from the data evaluation.)

The ultraviolet–visible spectroscopy (UV-Vis) spectrum is shown in Figure 5-1b. After replacing the thiophene on the side-groups of BDT core unit with selenophene, the whole spectrum shows similar two bands spectra with nearly no observable shift of the peak positions. When PBDTSe-TT is dissolved in chloroform, a slightly blue-shifted absorption spectrum is found, indicating that the commonly observed good solubility of the PTB7-related polymers is kept after selenium substitution on the side-chain. The UV-Vis result points out that the current modification does not affect the PTB7-Th's optical E_g. The main transition peaks of band 1, however, are less resolved after selenium substitution. That is, the relative intensity of 0-0 vibrational peak (compared to 0-1 vibrational peak) is decreased. The same phenomenon was also found in our previous work.[6b]

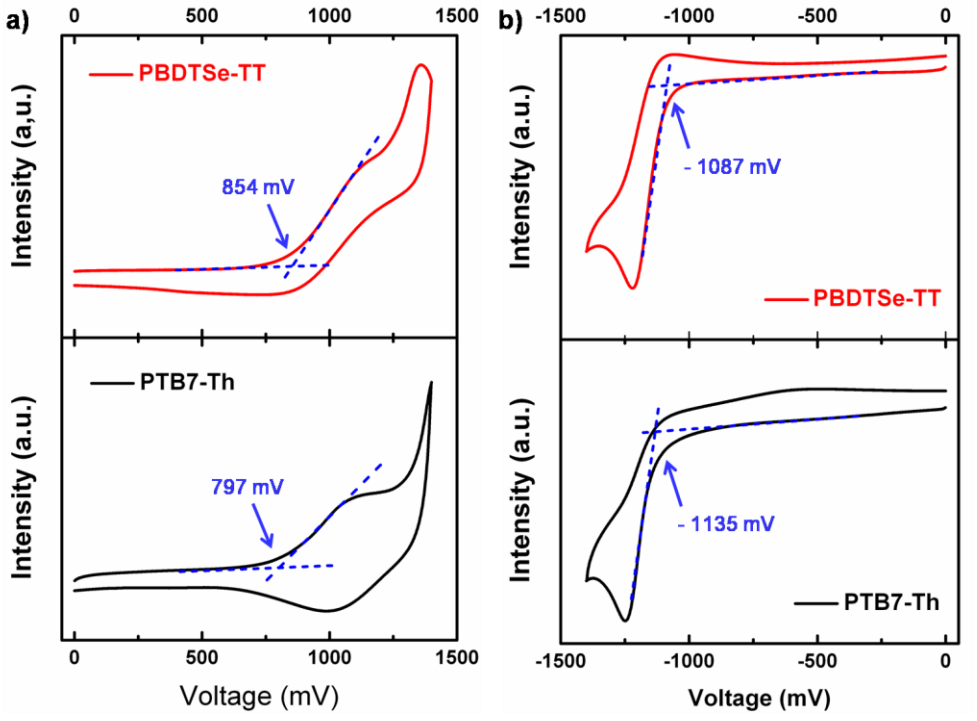

Figure 5-3. Cyclic voltammograms of PTB7-Th, and PBDTSe-TT polymer thin films (a) oxidation, and (b) reduction.

We speculate that this could be a sign of increased aggregation in the solid state, and more study need to be carried out in order to confirm this hypothesis. The energy level of the polymers is investigated through cyclic voltammertry measurement (Figure 5-3). Both HOMO and LUMO are found to be shifted downwards after selenium replacement, where HOMO/LUMO of 5.14 eV/3.21 eV and 5.19 eV/3.25 eV is found for PTB7-Th and PBDTSe-TT, respectively. Note that our observation of the energy level change through selenium replacement is different from that of observed by Warnan *et al*., where they replace the sulfur in PBDTTTPD polymer with selenium.[9d] Based on their theoretical calculation, the HOMOs of single BDTT and BDTSe molecules should be nearly the same. The result is mainly attributed to the twisting of heterocyclic ring and BDT core so satisfy the molecules' geometric optimized state; thus the influence of different electron donating ability for thiophene and selenophene is not prominent. We therefore postulate that the effect of selenium-replaced BDTT on the whole polymer should also take the acceptor building block into account. That is, through different combinations, the bulk phase of the resulting polymer can be affected, and therefore its electronic property as well. A clear reason behind this observation is however not known at this stage. Summarized from the above, the newly synthesized PBDTSe-TT shows quite similar optical properties as the PTB7-Th, though a deeper HOMO experimentally determined.

5.3.2 Single junction solar cell performance

Single junction solar cell device was firstly investigated via inverted architecture of indium tin oxide (ITO)/zinc oxide (ZnO)/Polymer:$PC_{71}BM$/molybdenum trioxide (MoO_3)/aluminum (Al). The PTB7-Th and PBDTSe-TT are both prepared in CB with polymer to $PC_{71}BM$ weight ratio of 1:1.5. The polymer concentration is fixed as 1.2 wt% and 3% DIO is added as additive.

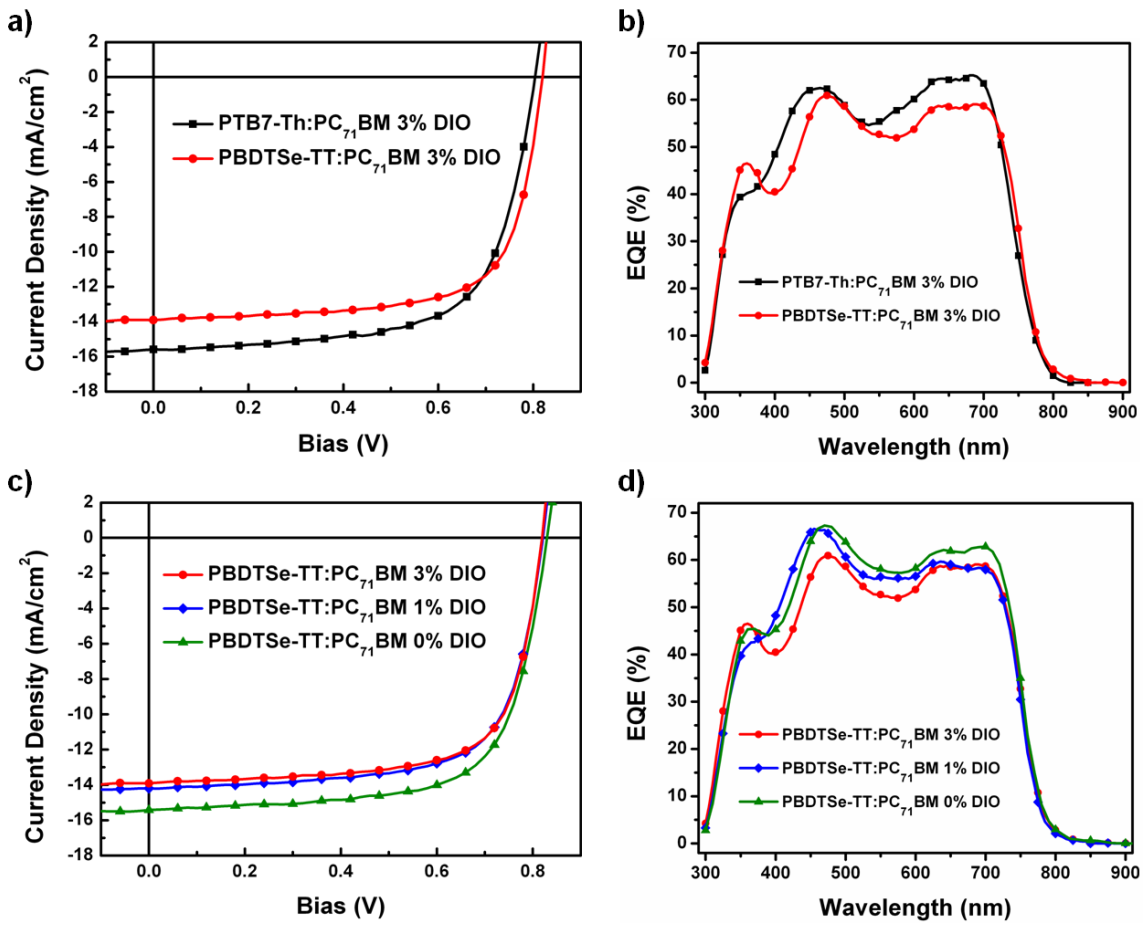

Figure 5-4. Current density-voltage characteristics of polymer:$PC_{71}BM$ solar cells under AM1.5G illumination (100 mW/cm^2), (a) PTB7-Th and PBDTSe-TT with 3% DIO content, (c) PBDTSe-TT with 3%, 1% and 0% DIO content. EQEs of the corresponding devices, and (b) PTB7-Th and PBDTSe-TT with 3% DIO content; d) PBDTSe-TT with 3%, 1% and 0% DIO content.

Figure 5-4a and 5-4b shows the current density-voltage and external quantum efficiency (EQE) characterization of the resulting devices, respectively. The PTB7-Th based device shows similar character as the one reported previously by Liao *et al.*, which indicates the credibility of the baseline of the current study.[8] It should be noted that, as expected, BHJ solar cell fabricated from PTB7-Th without solvent additive achieved PCE constantly less than 7 %. The PBDTSe-

TT based device processed with 3% DIO, on the other hand, shows a PCE of 8.0%. Compared to PTB7-Th based device processed with additives, it has a slightly larger V_{OC} of 0.82 eV, which could be benefit from a deeper HOMO energy level as we have discussed above. The EQE result shown in Figure 2b corresponds well with the photocurrent, where an average photon to electron efficiency of 55 % for PBDTSe-TT and 60 % for PBDT-Th is found. We attribute the lower EQE of PBDTSe-TT based device (processed with 3% DIO) to the unoptimized BHJ phase-separation with $PC_{71}BM$ and will discuss more below.

To illustrate the polymer's photovoltaic property without additive, we carried out a systematic study on the performance of PBDTSe-TT based device along with DIO content. In contrast to previously reported PTB7 or other PBDT-TT (PTB) based polymers, PBDTSe-TT performs even better in the absence of DIO. As shown in Figure 5-4c, the V_{OC} remains nearly the same as the DIO content decreases. The J_{SC}, on the other hand, progresses from 13.9 to 15.4 mA/cm^2 while the DIO content decreases from 3% to 0%. As a result, the non-DIO based device yields a high PCE of 8.8 %. The J_{SC} improvement is also confirmed by EQE measurement, where the average EQE is enhanced from 55 % to 60 % after removing the DIO. All device parameters characterized are summarized in Table 5-1 (the V_{OC}, J_{SC} and FF% are recorded from the champion cell). Note that a commonly used surface modifier, such as poly [(9,9-bis(3′-(N,N-dimethylamino)propyl)-2,7-fluorene)-alt-2,7-(9,9–dioctylfluorene)] (PFN), is excluded in the current study.[2b] It should be also noted that the condition is optimized in terms of different polymer:$PC_{71}BM$ blend ratio, and 1:1.5 is primarily observed to be the best condition. Comparing to the work by Warnan *et al.*, the effect of similar structural modification seems to be different on PBDTTPD polymers, where DIO is still required in order to arrive at an optimized morphology.[9d] This recalls our postulation in the discussion of energy level above, where the

bulk thin-film property may be different for dissimilar polymer design, even though the same building block is used.

From the device results, first, the effect of selenium substitution on the side-chain is very different that of on the main-chain. Replacing the sulfur with selenium on the side groups does not contribute much to the photocurrent as the backbone substitution does.[6b,10] This also correlates well with the UV-Vis measurement, where the bandgap stays the same after the modification. On the other hand, the current strategy seems to increase the intermolecular interaction between the polymer chains, which has also been observed by previous studies.[9a-c,10] This outcome renders us the opportunity to tackle the morphological problem in PTB polymers, and more information can be seen in the following discussion.

Table 5-1. Photovoltaic properties of single layer BHJ solar cells.

Polymer[a]	DIO Conc. (v/v, %)	V_{OC} (V)	J_{SC} (mA/cm^2)	FF (%)	$PCE_{max/avg}$ (%)
PTB7-Th	3	0.80	15.6	67	8.3/8.1
PBDTSe-TT	-	0.83	15.4	69	8.8/8.5
PBDTSe-TT	1	0.82	14.2	69	8.0/7.9
PBDTSe-TT	3	0.82	13.9	71	8.0/7.7
PBDTSe-TT[b]	-	1.64	8.8	69	9.9/9.6

[a] All prepared by: 1.2 wt% in chlorobenzene, polymer:$PC_{71}BM$ = 1:1.5, ~ 1500 rpm.
[b] Tandem device with identical sub-cells.

5.3.3 Thin film morphology study

To illustrate the reason behind this finding, the BHJ thin film morphology of the corresponding devices were imaged by transmission electron microscopy. From Figure 5-5a and 5-5b, it is apparent that without DIO's assistance, thin film morphology of PTB7-Th:$PC_{71}BM$ results in a highly unfavorable large phase segregated nanostructure. Upon addition of DIO, a

favorable morphology is observed. The morphological study on PTB7-Th shows similar result to those on PTB7.[2a]

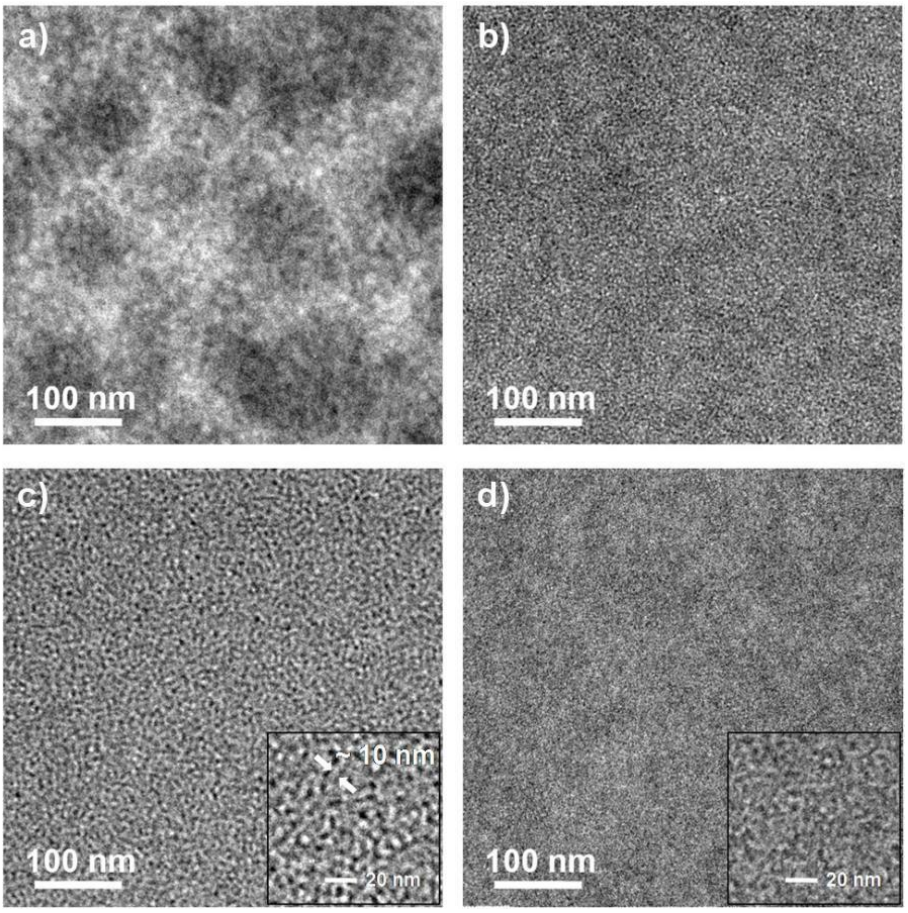

Figure 5-5. TEM image of (a) PTB7-Th:$PC_{71}BM$, (b) PTB7-Th:$PC_{71}BM$ with 3% DIO content, (c) PBDTSe-TT:$PC_{71}BM$, and (d) PBDTSe-TT:$PC_{71}BM$ with 3% DIO content blend thin film. (Scale bar: 100 nm)

The carrier transport property was also measured through photo-induced charge carrier extraction in a linearly increasing voltages method (Photo-CELIV, Figure 5-6).[12] It is shown that charge mobility of PTB7-Th based device is improved after addition of DIO (ca. 1.71×10^{-4} $cm^2V^{-1}s^{-1}$ and 3.00×10^{-4} $cm^2V^{-1}s^{-1}$ for the device without and with DIO, respectively), which corelates well with their morphology. The PBDTSe-TT, on the other hand, shows a different

scenario. Without DIO, device active layers exhibit nanoscale phase segregation with the acceptors. The dimension of different domains is found to be around 10 nm, which is believed to be critical in BHJ PSCs (see inset figure of Figure 5-5c).[1d-e,1g-i,2a,2c,7c] When DIO is incorporated, the phase-separation stays near the same (Figure 5-5d). Based on the Photo-CELIV results, however, a slight drop in charge mobility is observed after the addition of DIO in PBDTSe-TT based devices (ca. 7.59×10^{-4} $cm^2V^{-1}s^{-1}$ and 6.94×10^{-4} $cm^2V^{-1}s^{-1}$ for the device without and with DIO, respectively). Combined with the aforementioned device results, the thin-film morphology formed with DIO in this case could be less favorable to the BHJ photovoltaic device. Furthermore, It is important to note that charge mobilities of PBDTSe-TT based devices are relatively enhanced compared to those of PTB7-Th based devices, which could be brought by selenium substitution.[6b,9-10]

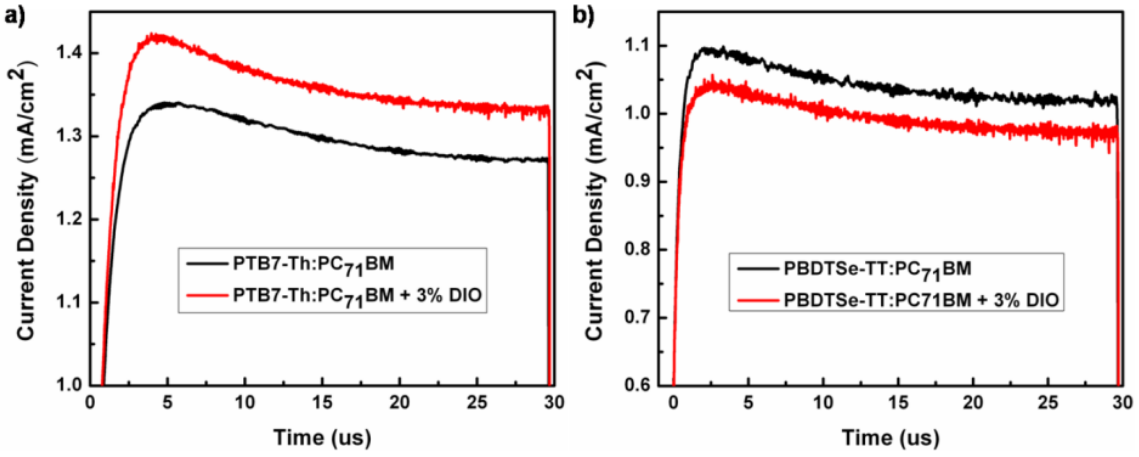

Figure 5-6. Photo-CELIV measurement of (a) PTB7-Th:$PC_{71}BM$ (with/without 3% DIO), and (b) PBDTSe-TT:$PC_{71}BM$ (with/without 3% DIO) solar cells.

These results shows that, due to a stronger intermolecular interaction of PBDTSe-TT polymer chains, the resulting BHJ thin film can arrive at an optimized morphology without

solvent additives. Addition of DIO, however, departs from the optimal bi-continuous separation structure, and thus could possibly reduce the charge-dissociation or charge transport efficiency.

5.3.4. Double Layer BHJ Solar Cell Performance, and the Benefit of Additive-Free Process

In order to fully utilize the solar spectrum within the absorption range of PBDTSe-TT, we built a tandem device. Considering the high V_{OC} of the PBDTSe-TT, a tandem architecture with two identical sub-cells is adopted.[13] Before constructing the tandem device, the thermal stability of PBDSe-TT based device (processed without DIO) is investigated through thermal annealing. From Table 5-2, it is revealed that PBDTSe-TT based single junction device has a relatively good stability under thermal stress, where only ~ 10% degradation of the overall efficiency is observed even after heating at 100^{o}C for 10 min; this makes it a good choice for fabricating the tandem device as at least 1 min of annealing is required for the processing of the interlayer.[13d]

Table 5-2. Thermal stability of single layer BHJ solar cells.

Polymer[a]	Annealing Temperature (^{o}C)	Annealing Time (min)	V_{OC} (V)	J_{SC} (mA/cm^2)	FF (%)	PCE_{avg} (%)
PBDTSe-TT	100	1	0.85	14.9	61	7.7
	100	5	0.84	14.6	59	7.3
	100	10	0.84	14.5	59	7.3

[a] All prepared by: 1.2 wt% in chlorobenzene, polymer:$PC_{71}BM$ = 1:1.5, ~ 1500 rpm.

The present tandem cell's structure is shown in Figure 5-7a, and the resulting I-V characterization is presented in Figure 5-7b. It is worth noting that, compare to our previous work, the PBDTSe-TT could be a better choice for this kind of tandem cell. The usage of CB as the casting solvent instead of 1,2-chlorobenzene (DCB) and those of DIO-containing solvents improves the stability of the interlayer (MoO_3/m-PEDOT:PSS/ZnO) since it evaporates faster

due to its lower boiling point, and thus prevents it from damaging or penetrating through the interlayer. Device performance of tandem cell is also summarized in Table 1. It can be found that the V_{OC} of the tandem cell add up successfully from 0.83 V to 1.64 V. The J_{SC} is measured to be 8.8 mA/cm^2. This could be comparable to a single junction device with over 17 mA/cm^2 J_{SC}, indicating that the solar spectrum of the absorption range of PBDTSe-TT:$PC_{71}BM$ blend thin film has been utilized in more thoroughly way through a tandem structure design.[13d] With a FF% of 69%, the tandem cell achieved a high PCE of 9.9%. We note that, similar tandem device based on PTB7-Th (processed with 3% DIO) only increases the PCE to 8.6%, mainly because of low J_{SC} (Figure 5-8a). This could possibly cause by thermal degradation of the bottom-cell during the interconnecting layer fabrication. Besides, the interconnecting layer may not be robust enough for resisting the solvent additives during the top-cell deposition. A similar phenomenon is also observed in the case of PTB7 based device (Figure 5-8b). A conclusive reason for unsuccessful tandem cells based on DIO-containing active layers is however out of the scope of this work, and more study will be carried out in the future.

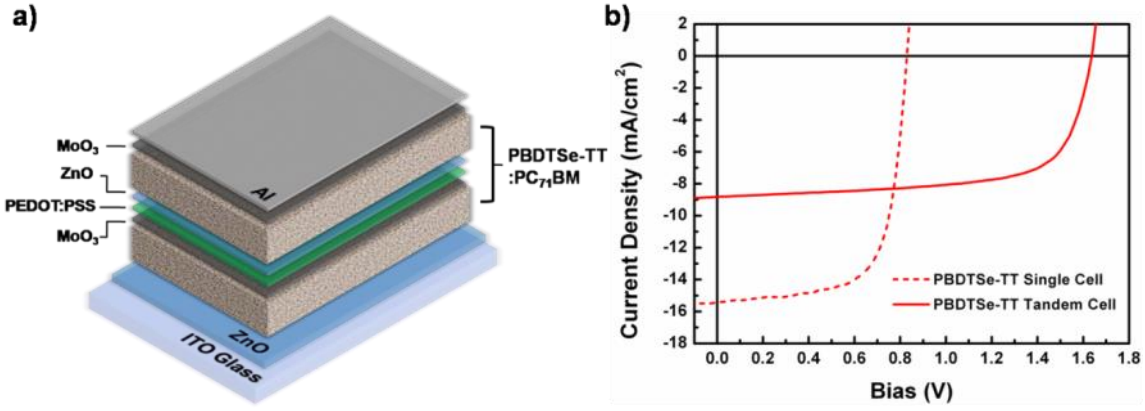

Figure 5-7. (a) PBDTSe-TT based tandem device architecture, and (b) the corresponding current density-voltage characteristics under AM1.5G illumination (100 mW/cm^2).

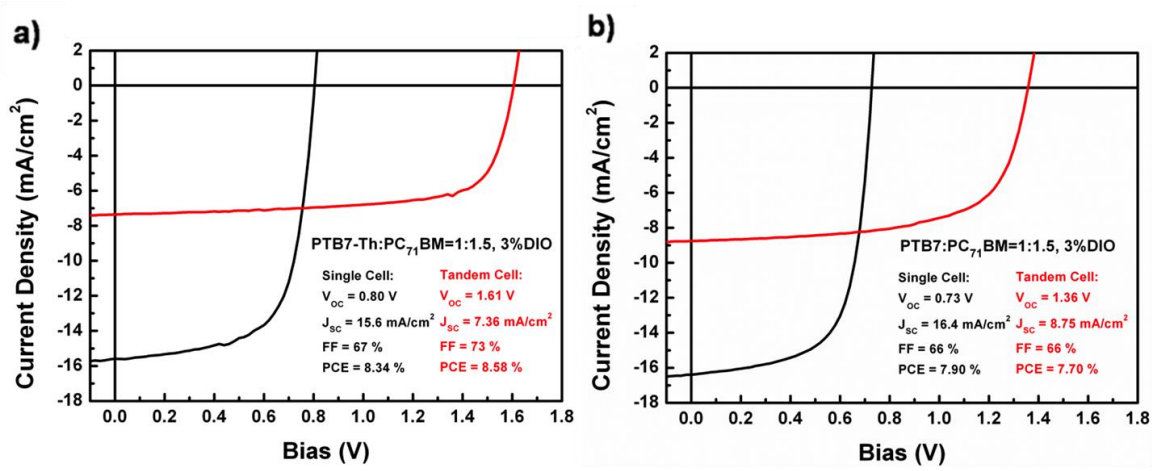

Figure 5-8. Current density-voltage characteristics of (a) PTB7-Th:$PC_{71}BM$, and (b) PTB7:$PC_{71}BM$ solar cells (processed with 3% DIO) under AM1.5G illumination (100 mW/cm^2).

5.4 Summary and outlook

To conclude, we present a newly synthesized selenium containing polymer, PBDTSe-TT, with E_g ~ 1.6 eV. The selenium substitution on the PTB7-Th is shown to affect the BHJ morphology with $PC_{71}BM$ greatly, and therefore an optimized phase-separation is obtained without the assistant from high boiling point additive, such as commonly used DIO. We note that this approach may not be applicable to every polymer system in terms of eliminating the need of solvent additives, the actual device performance should refer to the morphology of the resulting polymer:$PC_{71}BM$ blend. Combined with enlarged V_{OC}, a high PCE of 8.8 % is achieved through a simplified processing procedure. Furthermore, the non-DIO based device shows a relatively improved thermal stability, making it tolerable for tandem cell fabrication, and a high performing tandem solar cell with two identical PBDTSe-TT based sub-cells is successfully demonstrated. The selenium insertion is therefore proven to be an effective way to improve the property of PTB series photovoltaic polymers.

References:

[1] (a) Yu, G. *et al. Science* **1995,** *270*, 1789-1791. (b) Halls, J. J. M. *et al. Nature* **1995**, *376*, 498-500. (c) Brabec, C. J. *et al. Adv. Funct. Mater.* **2001,** *11*, 15-26. (d) Li, G. *et al. Nat. Mater.* **2005**, *4*, 864-868. (e) Ma, W. L. *et al. Adv. Funct. Mater.* **2005**, *15*, 1617-1622. (f) Thompson, B. C. *et al. Angew. Chem. Int. Ed.* **2008**, 47, 58-77. (g) Krebs, F. C. *Sol. Energy Mater. Sol. Cells* **2009**, *93*, 394-412. (h) Li, G. *et al. Nat. Photon.* **2012**, *6*, 153-161. i) Dou, L. *et al. Adv. Mater.* **2013**, *25*, 6642-6671.

[2] (a) Liang, Y. *et al. Adv. Mater.* **2010,** *22*, E135-E138. (b) He, Z. *et al. Nat. Photon.* **2012**, *6*, 591-595. (c) Lu, L. *et al. Adv. Mater.* **2014**, DOI: 10.1002/adma.201400384.

[3] Wu, C.-G. *et al. J. Mater. Chem. A*, **2014**, *2*, 5295-5303.

[4] (a) Kim, J. Y. *et al. Science* **2007**, 317, 222-225. (b) Dou, L. *et al. Nat. Photon.* **2012**, *6*, 180-185. (c) You, J. *et al. Nat. Commun.* **2013**, DOI: 10.1038/ncomms2411.

[5] (a) Lee, J. K. *et al. J. Am. Chem. Soc.*, **2008**, *130*, 3619-3623. (b) Lou, S. J. *et al. J. Am. Chem.Soc.* **2011**, *133*, 20661-20663.

[6] (a) Dou, L. *et al. J. Am. Chem. Soc.* **2012,** *134*, 10071-10079. (b) Dou, L. *et al. Adv. Mater.* **2013**, *25*, 825-831. (c) Dou, L. *et al. Macromolecules* **2013**, *46*, 3384-3390. (d) Gao, J. *et al. Adv. Energy Mater.* **2014**, *4*, 1300739. (e) Chang, W.-H. *et al. Adv. Energy Mater.* **2014**, *4*, 1300864. (f) Gao, J. *et al. Adv. Mater.* **2014**, DOI: 10.1002/adma.201400411; (g) Chen, C.-C. *et al. ACS Nano*, **2012**, *6*, 7185-7190. (h) Chen, C.-C. *et al. Energy Environ. Sci.* **2013**, *6*, 2714-2720.

[7] (a) Li, W. *et al. J. Am. Chem. Soc.*, **2013**, *135*, 5529-5532. (b) Hendriks, K. H. *et al. Angew. Chem. Int. Ed.* **2013**, *52*, 8341-8344. (c) Li, W. *et al. J. Am. Chem. Soc.*, **2013**, *135*, 18942-18948.

[8] Liao, S.-H. *et al. Adv. Mater.* **2013**, *25*, 4766-4771.

[9] (a) Byun, Y.-S. *et al. Synt. Met.* **2013**, *168*, 23–30. (b) Chakravarthi, N. *et al. Sol. Energ. Mat. Sol. Cells* **2014,** *122*, 136-145. (c) Kim, Y. J. *et al. J. Mater. Chem. C*, **2014**, *2*, 4937-4946. (d) Warnan, J. *et al. Chem. Mater.* **2014**, *26*, 2299-2306.

[10] (a) Ha, J. S. *et al. J. Am. Chem. Soc.* **2011**, *133*, 10364-10367. (b) Kronemeijier, A. J. *et al. Adv. Mater.* **2012,** *24*, 1558-1565. (c) Shahid, M. *et al. Chem. Sci.* **2012**, *3*, 181-185. (d) Liu, Y. *et al. Adv. Mater.* **2013**, *25*, 4657-4662.

[11] Saadeh, H. A. *et al. ACS Macro Lett.* **2012**, *1*, 361-365.

[12] Mozer, A. J. *et al. Appl. Phys. Lett.* **2005**, 86, 112104.

[13] (a) Sun, X. W. *et al. Appl. Phys. Lett.* **2010**, *97*, 053303. (b) Puetz, A. *et al. Org. Electron.* **2012**, *13*, 2696-2701. (c) Moet, D. J. D. *et al. Org. Electron.* **2010**, *11*, 1821-1827. (d) You, J. *et al. Adv. Mater.* **2013**, *25*, 3973-3978.

CHAPTER 6

More on the Side-Chain: the Effect of Side-Chain Asymmetry on the Optoelectronic Properties of DPP-based Photovoltaic Polymers

In this chapter, the effect of photovoltaic polymer's side-chain asymmetry on the solar cell performance is studied. I will show that breaking the side chain symmetry of an existing diketopyrrolopyrrole-based polymer used for solar cell application led to a greatly increased photovoltaic performance in terms of short-circuit current with more than a 50% improvement seen for two different structures. The cause of this observation is proposed as an enhancement in light absorption and the formation of a more favorable nanoscale morphology in the polymer:$PC_{71}BM$ blend, which could be further correlated to the increased molecular dipole moment as a result of using asymmetric side chains. An all-solution process 3-terminal tandem structure was demonstrated to connect two high photocurrent cells in a parallel connection in order to harvest more photons and obtain a photocurrent density of 22 mA/cm^2, which is unprecedented for any 3-terminal tandem devices reported with polymer solar cells.

6.1 Introduction

Polymer solar cells (PSCs) provide an opportunity to efficiently generate energy from sunlight at reasonable cost.[1-3] A unique structure of binary bulk heterojuction (BHJ) is developed to utilize a mixed layer of p-type polymeric semiconductors and n-type fullerene

derivatives, such as [6,6]-phenyl-C_{71}-butyric acid methyl ester ($PC_{71}BM$), via solution processing[4-6] Owing to the vast research efforts over the past decade, the power conversion efficiencies (PCE) of single- and multi-junction PSCs have recently surpassed the 10% milestone.[7-11]

Generally speaking, a solar cell can be characterized by open-circuit voltage (V_{OC}), short-circuit current (J_{SC}), and fill factor (FF%). In PSCs, V_{OC} is closely related to the difference between the highest occupied molecular orbital (HOMO) and lowest unoccupied molecular orbital (LUMO) energy levels of p-type polymer and n-type materials, respectively. The J_{SC} is essentially determined by the bandgap (E_g) of the polymeric material and its light-absorbing capability (i.e. absorption coefficient, ε). The FF% can be correlated to charge separation and transportation properties within the device and is largely influenced by the BHJ morphology, where a nanoscale phase-separation is often required.[2-3]

Improving the output J_{SC} has been one of the most important challenges. Multiple approaches have been applied to tackle this issue, which can be categorized into two major standpoints: 1) device engineering/physics & optimization and 2) material design. Device optimization has been carried out extensively over the past decade; tactics such as controlling the active layer morphology[6-7, 12-14], use of solvent additives[15-16], development/fine-tuning of the interfacial layer between the active layer and electrode[17-19], as well as managing the optical density within the device[20-23] have all successfully resulted in an enhancement of device performance for existing polymers. This makes the innovation in photoactive polymer materials a central research theme in the field.[24-25]

Given a polymer backbone, where the E_g is typically set, the fragment in which a chemist can easily work with is the side chains.[26] As known, side chains are extremely important for

conjugated polymers since they affect the polymer solubility and resulting morphology when dried.[27-33] Side chains can also influence the electronic properties of the polymer, which has been observed by several groups.[34-37] In chapter 2, I have also successfully demonstrated a novel side chain modification approach using triethylene glycol (TEG) groups, for which the PCE was improved by more than 10%.[38] Therefore, optimizing polymer side chains presents a very effective route in improving existing photovoltaic polymers.

In the present chapter, the effect of polymer side chain asymmetry on the PSC's performance is specifically studied. We intentionally break the side chain symmetry on part of the polymer building block (diketopyrrolopyrrole, DPP) by using different side chains on the same moiety, where one is the traditional alkyl group and the other is a more polar TEG group.[39] We observe a significant enhancement in photocurrent by performing this modification on two different polymer backbone systems. Using numerous characterization techniques, we rationalize that the increase in molecular dipole moment (μ), as a result of the side chain asymmetry, leads to an enhancement in the molecule or polymer absorption coefficient as well as a more favorable morphology. As the approach is quite general, we believe that this methodology can be applied to other polymer backbone systems to further enhancing the solar cell as well.

6.2 Experimental method

6.2.1 Synthetic procedures

Materials: 4,8-Bis((2-butyloctyl)oxy)benzo[1,2-b:4,5-b']dithiophene-2,6-diyl)bis(trimethylstannane) (BDT) was purchased from SunaTech Inc. 2-(2-(2-methoxyethoxy)ethoxy)ethyl 4-methylbenzenesulfonate, 1, 2, 3, T and FDPP were synthesized

according to the literature.[28,39] [6,6]-phenyl-C_{71}-butyric acid methyl ester ($PC_{71}BM$) was purchased from Solarmer. Unless otherwise stated, all of the chemicals were purchased from Aldrich and used as received.

Scheme 6-1. Synthesis of DPP and DPP-a.

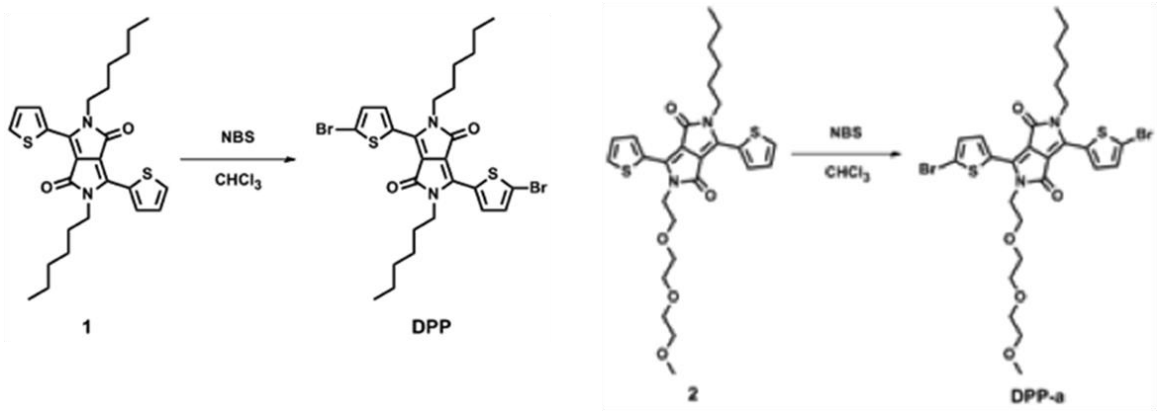

2,5-dihexyl-3,6-di(5-bromothien-2-yl)-1,4-diketo-pyrrolo[3,4-c]pyrrole (DPP): Compound 1 (0.13 g, 0.29 mmol) and N-bromosuccinimide (0.11 g, 0.60 mmol) were dissolved into chloroform (10 mL) in a two-neck round bottom flask under nitrogen protection, then the reaction mixture was prevented from light and stirred at room temperature overnight. The mixture was then extracted with chloroform and washed with water 2 times. After drying, the pure product was obtained through recrystallization from acetone:chloroform (~1:1) mixture as black solid (0.12 g, 67 %). ^{1}H NMR ($CDCl_3$, 400MHz) δ: 8.67 (d, J = 4.0 Hz, 2H), 7.24 (d, J = 4.0 Hz, 2H), 3.96-4.04 (m, 4H), 1.75-1.25 (br, 16H), 0.87 (m, 6H) ppm. DART-MS, *m/z*: Calcd, 627.02; Found, 627.01 (M+).

2-(hexyl)-5-(3,6,9-trioxadecyl)-3,6-di(5-bromothien-2-yl)-1,4-diketo-pyrrolo[3,4-c]pyrrole (DPP-a): Compound 2 (0.17 g, 0.32 mmol) and N-bromosuccinimide (0.12 g, 0.67 mmol) were dissolved into chloroform (10 mL) in a two-neck round bottom flask under nitrogen

protection, then the reaction mixture was prevented from light and stirred at room temperature overnight. The mixture was then extracted with chloroform and washed with water 2 times. After drying, the mixture was purified by silica gel chromatography using hexane:ethyl acetate (~7:3) mixture as eluent. The pure product was obtained as black solid (70 mg, 32 %). ^{1}H NMR ($CDCl_3$, 400MHz) δ: 8.65 (d, J = 4.2 Hz, 1H), 8.51 (d, J = 4.2 Hz, 1H), 7.24 (d, J = 4.2 Hz, 1H), 7.20 (d, J = 4.2 Hz, 1H), 4.17 (m, 2H), 3.97 (m, 2H), 3.78 (m, 2H), 3.63-3.47 (br, 6H), 3.34 (s, 3H), 1.71 (m, 2H), 1.34-1.25 (br, 8H), 0.90 (m, 3H) ppm. DART-MS, *m/z*: Calcd, 689.02; Found, 689.01 (M+).

Scheme 6-2. Synthesis of FDPP-a.

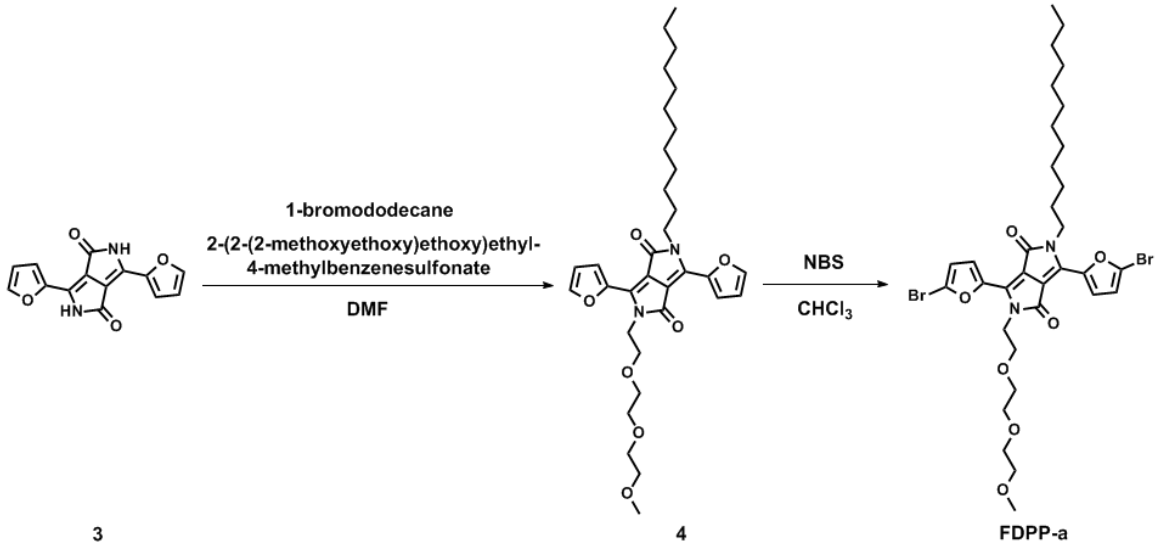

2-dodecyl-5-(3,6,9-trioxadecyl)-3,6-di(furan-2-yl)pyrrolo[3,4-*c*]pyrrole-1,4(2*H*,5*H*)-dione (4): Compound 3 (2 g, 7.5 mmol), 2-(2-(2-methoxyethoxy)ethoxy)ethyl 4-methylbenzenesulfonate (2.4 g, 7.4 mmol), 1-bromododecane (1.86 g 7.5 mmol), tetrabutylammonium bromide (0.12 g, 0.37 mmol) and anhydrous potassium carbonate (3.6 g, 26.0 mmol) were dissolved into N,N-dimethylformamide (50 ml) in a three-neck round flask under nitrogen protection, and then gradually heated to 90 °C after stirring at room temperature

for 3h. After 20 h, the solvent was removed and the mixture was extracted with chloroform. The combined extracts were washed with brine and water several times. After drying, the crude product was purified by silica gel chromatography using hexane:ethyl acetate (~3:2) mixture as eluent. The pure product was obtain as purple-red solid (1 g, 23 %). ^{1}H NMR ($CDCl_3$, 400MHz) δ: 8.28 (m, 2H), 7.63 (m, 2H), 6.68 (m, 2H), 4.35 (t, *J* = 6.3 Hz, 2H), 4.09 (t, *J* = 7.6 Hz, 2H), 3.75-3.46 (br, 8H), 3.34 (s, 3H), 1.68 (m, 2H), 1.38-1.24 (br, 20H), 0.89 (m, 3H) ppm. DART-MS, *m/z*: Calcd, 583.34; Found, 583.34 (M+).

2-dodecyl-5-(3,6,9-trioxadecyl)-3,6-di(5-bromofuran-2-yl)pyrrolo[3,4-*c*]pyrrole-1,4(2*H*,5*H*)-dione (FDPP-a): Compound 4 (0.30 g, 0.51 mmol) and N-bromosuccinimide (0.20 g, 1.12 mmol) were dissolved into chloroform (10 mL) in a two-neck round bottom flask under nitrogen protection, then the reaction mixture was prevented from light and stirred at room temperature overnight. The mixture was then extracted with chloroform and washed with water 2 times. After drying, the mixture was purified by silica gel chromatography using hexane:ethyl acetate (~1:1) mixture as eluent. The pure product was obtained as dark-purple solid (0.25 g, 65 %). ^{1}H NMR ($CDCl_3$, 400MHz) δ: 8.24 (m, 2H), 6.63 (m, 2H), 4.30 (t, *J* = 6.0 Hz, 2H), 4.04 (t, *J* = 7.7 Hz, 2H), 3.76-3.46 (br, 8H), 3.34 (s, 3H), 1.68 (m, 2H), 1.42-1.25 (br, 20H), 0.89 (m, 3H) ppm. DART-MS, *m/z*: Calcd, 741.16; Found, 741.15 (M+).

Polymerization for PBD: BDT (0.0885 g, 0.1000 mmol), and DPP (0.0557 g, 0.1000 mmol) were dissolved into 5 mL toluene and 0.75 mL DMF in a flask protected by argon. The solution was flushed with argon for 10 minutes, then 5 mg of $Pd(PPh_3)_4$ was added into the flask. The solution was flushed with argon again for another 10 min before stirring for 1.25 h at 115 °C under an argon atmosphere.. Then, the mixture was cooled down to room temperature and the polymer was precipitated in ~100 ml methanol and the precipitated solid was collected and

purified by silica gel chromatography using chloroform as eluent. The polymer was obtained as dark purple-black solid, yield ~ 30 %. Mn = 27.4 k; polydispersity = 2.0.

Polymerization for PBD-a: BDT (0.0807 g, 0.1000 mmol), and DPP-a (0.0628 g, 0.1000 mmol) were dissolved into 5 mL toluene and 0.75 mL DMF in a flask protected by argon. The solution was flushed with argon for 10 minutes, then 5 mg of $Pd(PPh_3)_4$ was added into the flask. The solution was flushed with argon again for another 10 min before stirring for 1.67 h at 115 °C under an argon atmosphere. Then, the mixture was cooled down to room temperature and the polymer was precipitated in ~100 ml methanol and the precipitated solid was collected and purified by silica gel chromatography using chloroform as eluent. The polymer was obtained as dark purple-black solid, yield ~ 30 %. Mn = 57.8 k; polydispersity = 2.5.

Polymerization for PTFD: T (0.0503 g, 0.1200 mmol), and FDPP (0.0930 g, 0.1200 mmol) were dissolved into 5 mL chlorobenzene in a flask protected by argon. The solution was flushed with argon for 10 minutes, then 2.2 mg of $Pd_2(dba)_3$ and 2.9 mg $P(o\text{-}tol)_3$ were added into the flask. The solution was flushed with argon again for another 10 min before stirring for 24 h at 110 °C under an argon atmosphere. Then, the mixture was cooled down to room temperature and the polymer was precipitated in ~100 ml methanol and the precipitated solid was collected and purified by silica gel chromatography using chloroform as eluent. The polymer was obtained as dark purple-black solid, yield ~25 %. The polymer can be readily dissolved into chloroform, chlorobenzene or dichlorobenzene, etc. Mn = 25.4 k; polydispersity = 1.5.

Polymerization for PTFD-a: T (0.0507 g, 0.1200 mmol), and FDPP-a (0.0917 g, 0.1200 mmol) were dissolved into 5 mL chlorobenzene in a flask protected by argon. The solution was flushed with argon for 10 minutes, 2.2 mg of $Pd_2(dba)_3$ and 2,9 mg $P(o\text{-}tol)_3$ were added into the flask. The solution was flushed with argon again for another 10 min before stirring for 24 h at

110 °C under an argon atmosphere. Then, the mixture was cooled down to room temperature and the polymer was precipitated in ~100 ml methanol and the precipitated solid was collected and purified by silica gel chromatography using chloroform as eluent. The polymer was obtained as dark purple-black solid, yield ~ 25%. Mn = 82.6 k; polydispersity = 3.0.

6.2.2 Materials Characterization

Instrumentation: ^{1}H NMR spectra were measured on a Bruker ARX-400 spectrometer. Absorption spectra were taken on a Varian Cary 50 ultraviolet-visible spectrometer. The molecular weight and polydispersity of the polymers were determined by the gel permission chromatography (GPC) method through Agilent Infinity 1260 system. Polystyrene was used as standard and chloroform was used as eluent (flow rate: 1.0 mL/min; column temperature: 40 °C). The electrochemical cyclic voltammetry (CV) was conducted with Pt disk, Pt plate, and Ag/AgCl electrode as working electrode, counter electrode, and reference electrode, respectively, in a 0.1 mol/L tetrabutylammoniumhexafluorophosphate (Bu_4NPF_6) acetonitrile solution. For calibration, the redox potential of ferrocene/ferrocenium (Fc/Fc^+) was measured under the same conditions, and it is located at 0.39 V vs. the Ag/AgCl electrode. It is assumed that the redox potential of Fc/Fc^+ has an absolute energy level of -4.80 eV to vacuum. The energy levels of the highest (HOMO) and lowest unoccupied molecular orbital (LUMO) were then calculated according to the following equations,

$$E_{HOMO} = -(\varphi_{ox} + 4.34)\ (eV)$$

$$E_{LUMO} = -(\varphi_{re} + 4.34)\ (eV)$$

where φ_{ox} is the onset oxidation potential vs Ag/AgCl and φ_{re} is the onset reduction potential vs Ag/AgCl. Grazing incidence wide angle X-ray scattering (GIWAXS) measurements were

performed at the 8ID-E beamline at the Advanced Photon Source (APS), Argonne National Laboratory, using X-rays with a wavelength of λ = 1.6868 Å and a beam size of ~200 μm (horizontal) × 20 μm (vertical). A two-dimensional PILATUS 1M-F detector was used to capture the scattering patterns and was located 208.7 mm from the samples. All samples were prepared on PEDOT:PSS-modified Si substrates to emulate the fabrication condition for OPV devices. Typical GIWAXS patterns were taken at an incidence angle of 0.20°, above the critical angles for polymer:$PC_{71}BM$ blends and below the critical angle of the Si substrate. Transmission electron microscopy (TEM) measurement was conducted with T12 cryo-electron microscope, 120 kV was used. Atomic force microscopy (AFM) images were taken by Bruker dimension icon scanning probe microscope, taping mode with SCM-PIT tip from Bruker was used.

6.2.3 Device fabrication and measurement

Single junction solar cell (inverted): PBD, PBD-a, PTFD, or PTFD-a was co-dissolved with $PC_{71}BM$ in chloroform (CF)/1,2-dichlorobenzene (DCB) (v/v = 4/1) with a concentration of 10 mg/mL polymer and 20 mg/mL $PC_{71}BM$, and 3% DIO was added as additives. ITO-coated glass substrates (15Ω/cm^2) were cleaned stepwise in detergent, water, acetone, and isopropyl alcohol under ultrasonication for 15 min each and subsequently dried in an oven for 5 h. A thin layer (~30 nm) of PEDOT:PSS (Clevios P VP AI 4083) was spin-coated onto the ITO surface which was pretreated by ultraviolet ozone for 15 min. Low-conductivity PEDOT:PSS was chosen to minimize measurement error from device area due to lateral conductivity of PEDOT:PSS. After being baked at 120 ºC for ~ 20 min, the substrates were transferred into a nitrogen-filled glove box (<0.1 ppm O_2 and H_2O). A polymer/$PC_{71}BM$ composite layer (ca. ~100 nm thick) was then spin-coated from the blend solutions at ~1500 rpm on the ITO/PEDOT:PSS substrate without further special treatments. Then, the film was transferred into a thermal

evaporator located in the same glovebox. A calcium layer (20 nm) and an aluminium layer (100 nm) were deposited in sequence under a vacuum of 2×10^{-6} torr. The effective area of the device was measured to be 0.10 cm^2.

3-terminal Tandem device fabrication: The device architecture of the tandem solar cell is shown in Fig. 5a. A 20-nm-thick ZnO layer was spin-coated on ITO-glass from nanoparticle solution and baked 150C ºC for ~ 20 min.[10] The PBD-a layer for the bottom sub-cell were fabricated via same process as single-junction cells. Then modified PEDOT:PSS (Clevios PH500 with 5% DMSO and 10% IPA) were spin-coated on photoactive layer to form a layer of ~50 nm thick. Approximately 100-nm-thick silver nanowire (IPA dispersion from BlueNano) is spray-coated on PEDOT:PSS. Then the silver nanowire network is fused by a droplet of TiO_2 nanoparticle. Then, same modified PEDOT:PSS were spin-coated on silver nanowire again. The PTFD-a layer for the top subcell was then spin-coated. The active layer thickness of front cell and back cell are ~100 nm. After that, a thin layer of ZnO was spin coated. The device fabrication was completed by thermal evaporation of 100 nm Al as cathode under high vacuum (~2×10^{-6} torr). The PBD/PTFD based 3-termainal tandem device was fabricated in the same procedure.

Current-voltage measurement: The current density-voltage (J-V) characteristics of photovoltaic devices were obtained by a Keithley 2400 source-measure unit. The photocurrent was measured under AM 1.5 G illumination at 100 mW cm^{-2} under a Newport Thermal Oriel 91192 1000 W solar simulator. In order to obtain trustable results, we have 1) scratched out the empty area in between each device on the same substrate to avoid parasitic photocurrent, and 2) compared the measured J_{SC} to that of derived by EQE, where two values are comparable. Note that no mask was used during the measurement. The light intensity was calibrated by a calibrated

KG5-filtered Mono-silicon reference diode traceable to NREL. EQEs were measured using a lock-in amplifier (SR830, Stanford Research Systems) with current preamplifier (SR570, Stanford Research Systems) under short-circuit conditions. The devices were illuminated by monochromatic light from a xenon lamp passing through a monochromator (SpectraPro-2150i, Acton Research Corporation) with a typical intensity of 10 μW. The photocurrent signal is then amplified by an SR570 and detected with an SR830. A calibrated mono-silicon diode with known spectral response is used as a reference.

Hole mobility: Hole mobility was measured using the space charge limited current model (SCLC), using a diode configuration of ITO/ PEDOT:PSS/polymer:$PC_{71}BM$/Au and taking current-voltage measurements in the range of 0-7 V and fitting the results to a space charge limited form, where the SCLC is described by

$$J=(8/9)\varepsilon_r\varepsilon_0\mu_e(V^2/L^3)$$

where ε_0 is the permittivity of free space, ε_r is the dielectric constant of the polymer, μ is the hole mobility, V is the voltage drop across the device ($V = V_{appl} - V_r - V_{bi}$, where V_{appl} is the applied voltage to the device, V_r is the voltage drop due to contact resistance and series resistance across the electrodes, and V_{bi} is the built-in voltage due to the difference in work function of the two electrodes), L is the polymer thickness. The dielectric constant ε_r is assumed to be 3, which is a typical value for conjugated polymers. The thickness of the polymer:$PC_{71}BM$ films is measured by using a Dektakprofilometer.

6.2.4 Computational calculation

The geometry of modeling molecules was subjected to density functional theory (DFT) optimizations by Gaussian 03 software package. The hybrid three-parameter B3LYP functional

combined with 6-31G(d,p) basis set was used for ground state calculation. Note that before the computation, conformational search for both DPP and FDPP core units were carried out. In addition, due to limited computational source, one donor-acceptor repeat unit with shorter alkyl and glycol side chain was carried out as representative for each polymer. The ground state geometry optimization results as well as the direction/magnitude of ground state dipole moments (μ_g) (obtained from the output file) for all molecules are shown in Figure 6-7 – 6-8. The ground to excited state oscillator strength (*f*) was acquired by performing time-dependent density functional theory (TDDFT) calculation using DFT optimized geometry; note that same functional/basis set was used for all molecules. The excited state dipole moment (μ_e) was attained by CIS calculation with 6-31G(d,p) basis set, and the result is used for extracting the change in dipole moment during the excitation ($\Delta\mu_{ge}$).

6.3 Result and discussion

6.3.1 Polymer design, synthesis and characterization

Figure 6-1a displays the polymer structures in this study. PBD and PTFD represent the conventional symmetric side chain polymers, where the side chains on the DPP and FDPP building blocks are the same. PBD-a and PTFD-a are two newly synthesized structures with different side chains on each DPP and FDPP segment, namely DPP-a and FDPP-a. We note that, in the PBD system, this strategy was initially intended to apply to our best performing benzodithiophene (BDT)-DPP based polymer, where alkylthienyl groups are used as side chains for BDT moiety.[38] Unfortunately, the solubility had became an issue for that polymer and thus an alkoxy group was used instead to proof our concept in the present work.

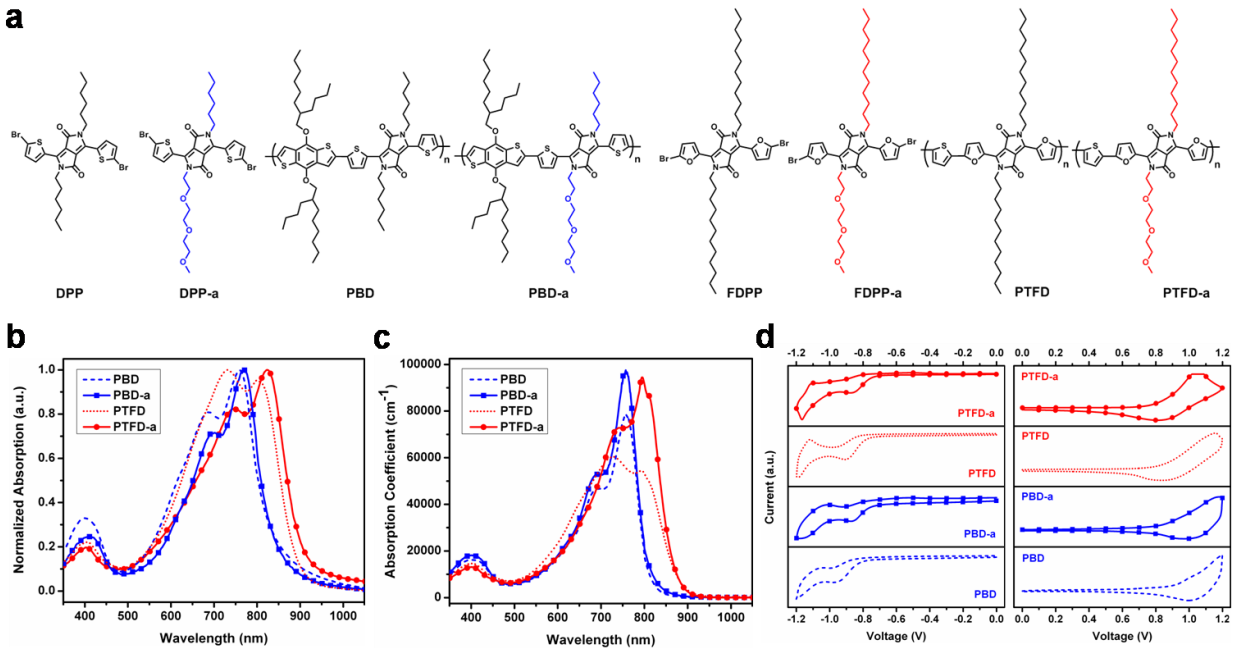

Figure 6-1. (a) Molecular structures of key monomers used to construct polymers, PBD, PBD-a, PTFD, and PTFD-a, (b) Normalized UV/Vis absorption of PBD, PBD-a, PTFD, and PTFD-a in thin films, (c) Measured absorption coefficient of PBD, PBD-a, PTFD, and PTFD-a, and (d) CV characteristics of PBD, PBD-a, PTFD, and PTFD-a.

A one-to-one side chain feeding ratio was used in synthesizing the asymmetric side chain monomers in a single batch. The polymers were synthesized via Stille coupling polymerization. The molecular weight, determined by GPC, are 27.4, 57.8, 25.4, 82.6 kg/mol for PBD, PBD-a, PTFD, PTFD-a, with corresponding PDI calculated as 2.0, 2.5, 1.5, 3.0, respectively. From the ^{1}H NMR spectra of the polymers, signals corresponding to the hydrogen on the TEG groups prove that PBD-a and PTFD-a indeed have both kinds of side chains (Figure 6-2 – 6-5). The optical properties of the polymers were studied by UV-Vis spectrometry. As shown in Figure 6-1b, slightly red-shifted spectra are found in both the PBD-a and PTFD-a thin-films compared to their original version. According to the onset of the thin film absorption spectra, the optical E_g of

PBD, PBD-a, PTFD, and PTFD-a are calculated to be 1.49, 1.48, 1.39, and 1.37 eV, respectively. In comparing the absorption coefficients (Figure 6-1c), we further found that the asymmetric side chain polymers have a higher light absorbing capability. Note that since the solid-state absorption coefficient of a polymer is difficult to determine accurately, here we adopt the method introduced by Reynold *et al*., where we calculate the thin-film absorption coefficient by measuring the mass extinction coefficient of the polymer solution with the assumption that the density of the polymer is equal to 1.[40] Based on our result, it seems that introducing the asymmetric side chain on the DPP unit could increase the numbers of photons absorbed, which will be discussed in further detail in the following section. The energy levels of the polymers were studied by electrochemical cyclic voltammetry (CV) measurements. From the experimental CV data (Figure 6-1d), the LUMO levels are slightly decreased after applying the asymmetric side chain, moving the PBD system from -3.52 to -3.58 eV, and PTDF system form -3.56 to -3.60 eV. The HOMO levels, on the other hand, showed a different trend. After breaking the side chain symmetry, they increased from 5.24 to 5.14 eV and 5.18 to 5.16 eV for the PBD and PTDF systems, respectively. This might be due to the weak electron-donating effect of the TEG side chains to the polymer backbone. From the above results we can see that properties of the polymers such as solubility, optical responses, and energy levels were changed after introducing asymmetric side chains into these systems.

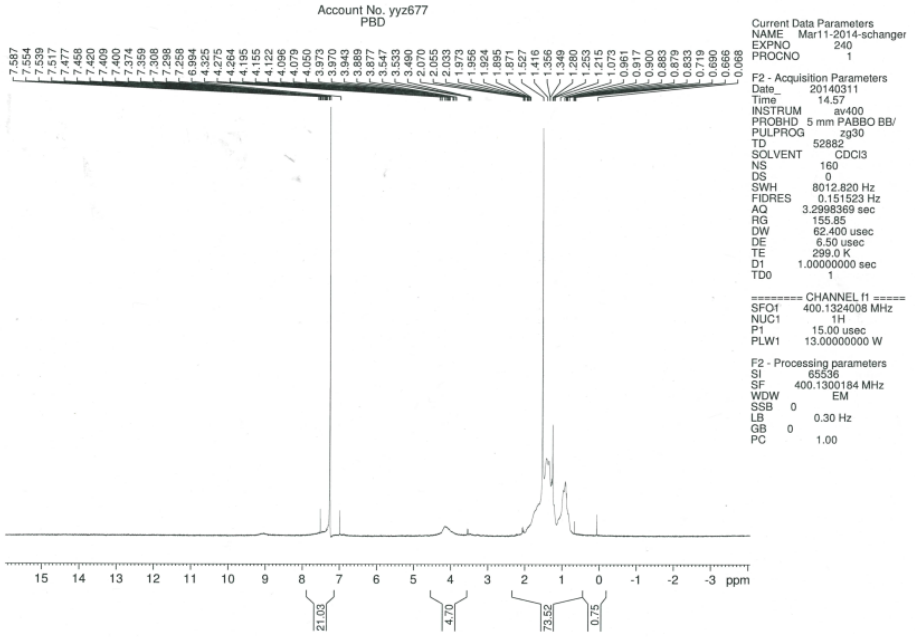

Figure 6-2. ^{1}H NMR spectrum of PBD at 298 K.

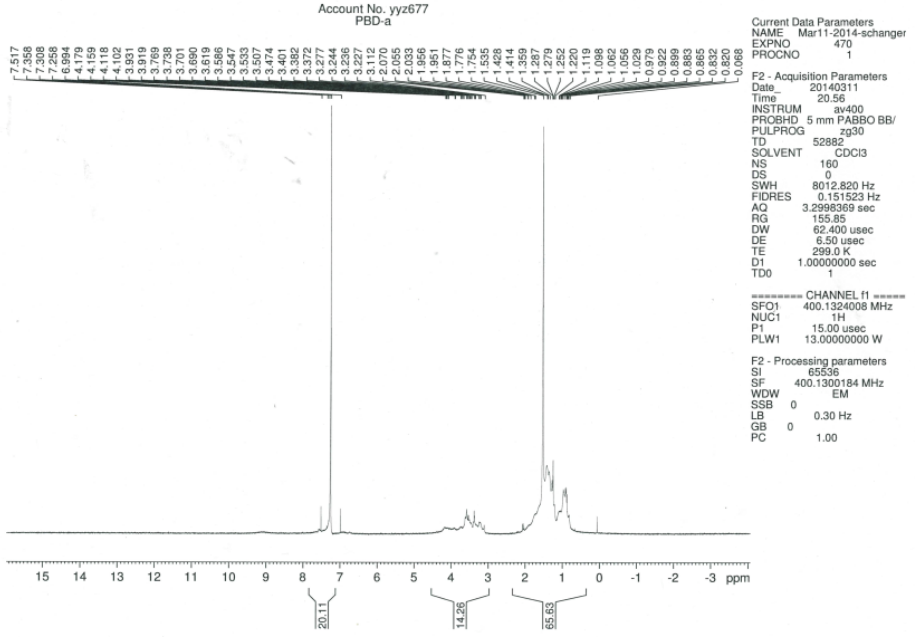

Figure 6-3. ^{1}H NMR spectrum of PBD-a at 298 K.

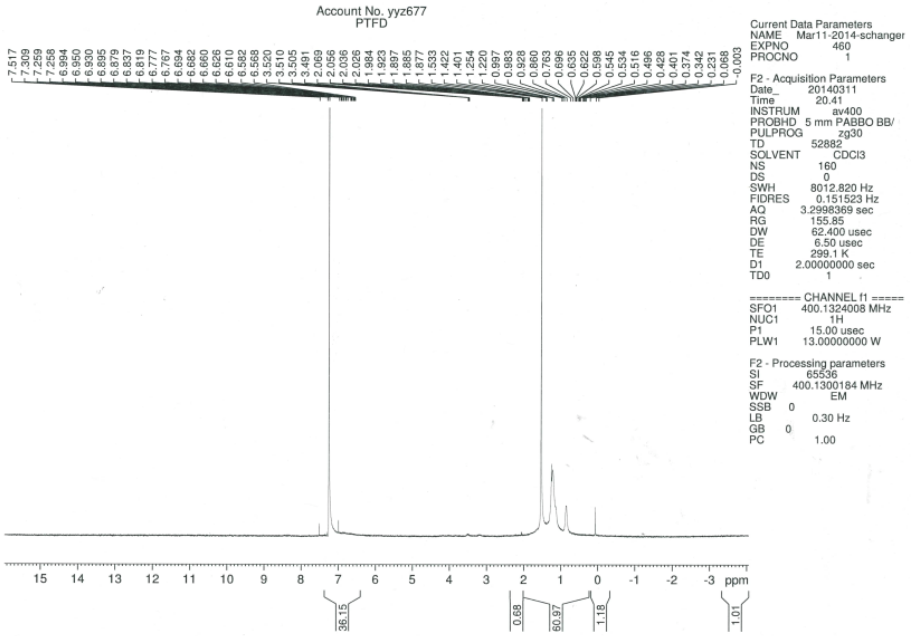

Figure 6-4. ^{1}H NMR spectrum of PTFD at 298 K.

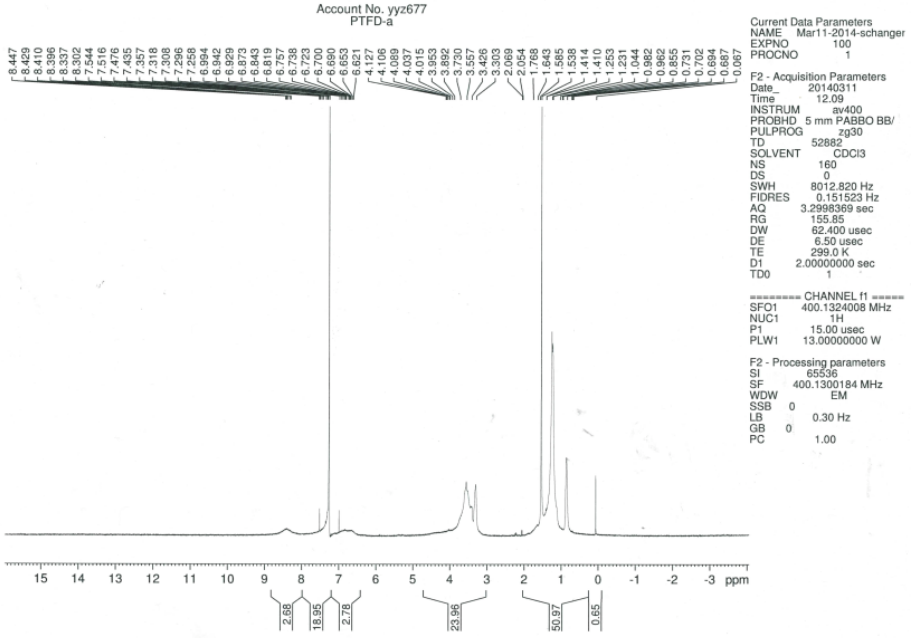

Figure 6-5. ^{1}H NMR spectrum of PTFD-a at 298 K.

6.3.2 Single junction solar cell performance

Single junction BHJ solar cells with a structure of indium-doped tin oxide (ITO)/poly(3,4-ethylenedioxythiophene) polystyrene sulfonate (PEDOT:PSS)/polymer:$PC_{71}BM$/Calcium (Ca)/Aluminium (Al) was used to investigate the photovoltaic properties of the polymers. The devices were tested under AM1.5G illumination (100 mW/cm^2). Details of device fabrication and measurement can be found in the Method. Typical current density-voltage (J-V) curves are shown in Figure 6-6a, and the corresponding external quantum efficiency (EQE) data are presented in Figure 6-6b. The device results are summarized in Table 6-1. The original PBD and PTFD based devices are comparable to reported values with minor differences in structure and processing condition.[28,41]

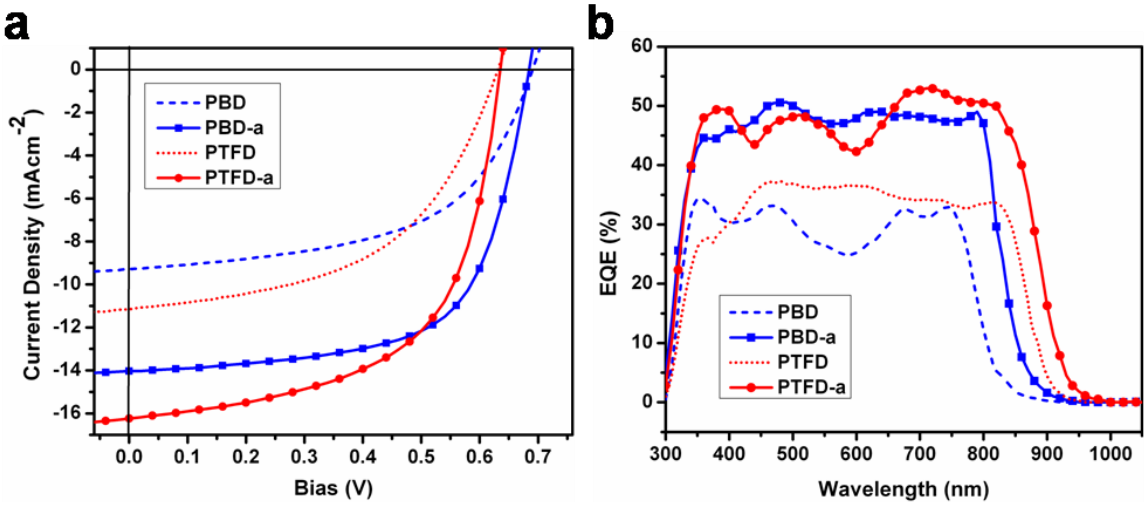

Figure 6-6. (a) Current density-voltage characteristics of polymer:$PC_{71}BM$ solar cells under AM1.5G illumination (100 mW/cm^2), and (b) EQEs of the corresponding polymer:$PC_{71}BM$ devices. Integrated J_{SC} for PBD, PBD-a, PTFD, and PTFD-a based devices are calculated to be 8.1, 13.9, 11.0 and 15.8 mA/cm^2, respectively.

As shown in Figure 6-6a and 6-6c, the V_{OC} of both polymer systems remain nearly the same through use of different side chains. Therefore, the slight increase in the HOMO level derived from the CV measurement seems to not affect the resulting V_{OC} of the device. The J_{SC}, on the other hand, is enhanced for both systems from 9.3 mA/cm^2 to 14 mA/cm^2, and 10.6 mA/cm^2 to 16.2 mA/cm^2 for PBD and PTFD, respectively. Similarly, the EQE results clearly show the improvement in current density of the newly synthesized PTFD-a and PBD-a based devices compared to their original version. On average, this value is nearly 50% higher than the non-modified polymer controlled device (average EQE increased from 30% to 50%). Moreover, we found that the onset of the EQE also red-shifted compared to the original version, showing that the red-shifted absorption induced by side chain modification does actively contribute to photocurrent.

Table 6-1. Photovoltaic properties of single layer BHJ solar cells.

Polymer[a]	V_{oc} (V)	J_{sc} (mA/cm^2)	FF (%)	PCE_{avg}(%)
PBD	0.70	9.3	54	3.9
PBD-a	0.68	14.0	65	6.2
PTFD	0.64	10.6	50	3.4
PTFD-a	0.64	16.2	59	6.1
PBD/PTFD[b]	0.64	13.2	54	4.6
PBD-a/PTFD-a[b]	0.64	22.2	59	8.4

[a] 1.0 wt% in CF/1,2-dichlorobenzene, 3% DIO, Polymer:$PC_{71}BM$ = 1:2, ~3000 rpm.
[b] Result from 3-terminal tandem device.

Each device was analyzed by conducting space charge limited current (SCLC) measurements (for hole-only devices) in order to determine the reason behind the higher EQE of

the PBD-a and PTFD-a based cells. From our experiment, mobilities of the resulting polymer:$PC_{71}BM$ blend of PBD-a and PTFD-a were higher than their non-modified counterpart, which were calculated to be around 5.01×10^{-5}, 1.12×10^{-4} $cm^2/V\cdot s$ compared to 2.3×10^{-6}, 9.1×10^{-6} $cm^2/V\cdot s$, respectively. These findings show that breaking the side chain symmetry may result in boosting the photocurrent. We hypothesis that such phenomena is a result of increased photon absorptivity and enhanced molecular packing, which will be discussed more in the later sections.

6.3.3 Effect of Asymmetric Side Chain on the Molecular Optoelectronic Property

To examine the effect of breaking the side chain symmetry on the molecule's optoelectronic properties, a series of theoretical calculations were carried out through a combination of density functional theory/time-dependent density functional theory (DFT/TDDFT) and Configuration Interaction Singles (CIS) with a Gaussian 03 package. Note that in order to minimize the calculation time, one repeating unit of the polymer was calculated and the sizes of the side chains were reduced.

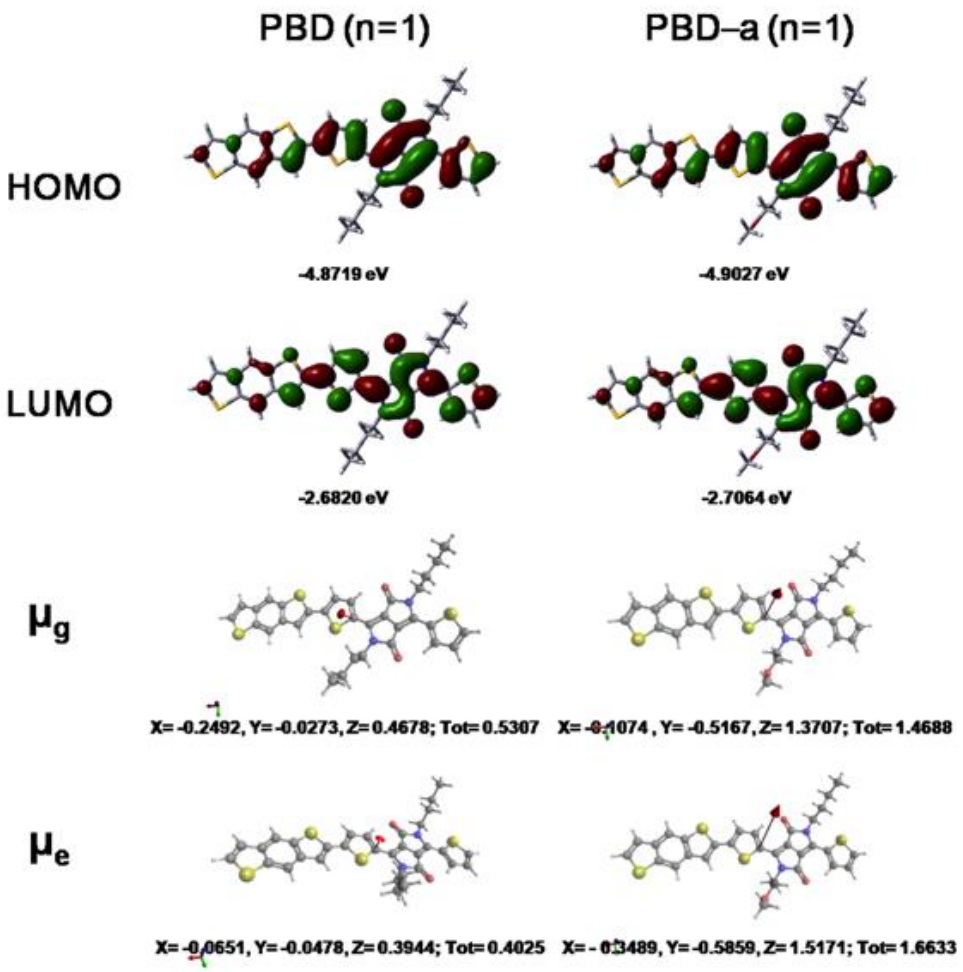

Figure 6-7. Summary of calculation results for PBD (n=1) and PBD-a (n=1), including optimized ground state geometry, HOMO/LUMO molecular orbital, ground state dipole moment (obtained from DFT calculation) and excited state dipole moment (obtained from CIS calculation). The visualization of dipole moments was done by Avogadro software (version 1.1.1).

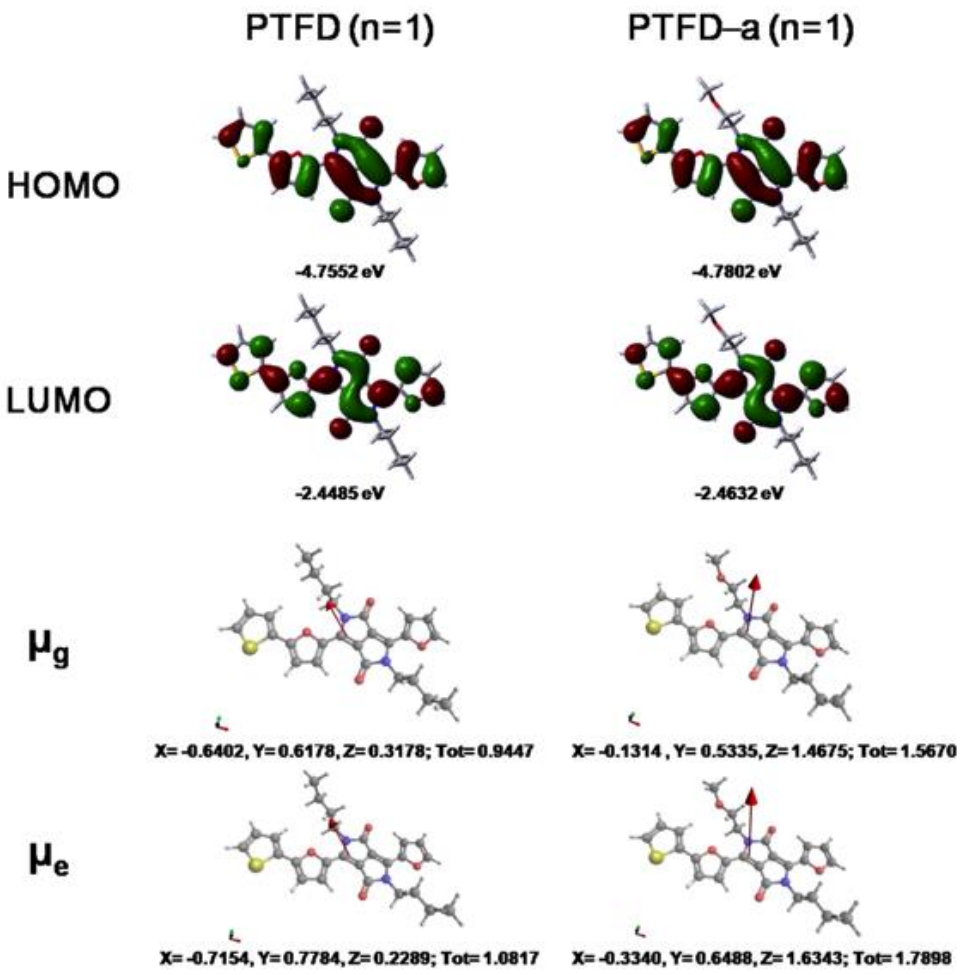

Figure 6-8. Summary of calculation results for PTFD (n=1) and PTFD-a (n=1), including optimized ground state geometry, HOMO/LUMO molecular orbital, ground state dipole moment (obtained from DFT calculation) and excited state dipole moment (obtained from CIS calculation). The visualization of dipole moments was done by Avogadro software (version 1.1.1).

The ground state dipole moment (μ_g), based on our study, apparently increased when asymmetric side chains were applied (1.4688 and 1.5670 D compared to 0.5307 and 0.9447 D for PBD and PTFD, respectively; Figure 6-7 – 6-8 and Table 2). We first hypothesized that increasing the molecular dipole moment might raise the charge-separation efficiency as

mentioned by different groups[42-43]; and thus an increase in photocurrent may be expected. However, according to our calculation, the difference between ground- and excited-state dipole moment ($\Delta\mu_{ge}$), which can be correlated to charge-separation efficiency, does not alter significantly after the side chain symmetry is broken (2.4-3.5% increment; Table 6-2). Thus, the improvement in device performance is unlikely to come from the improved charge-separation efficiency via increasing molecular dipole moment.

Table 6-2. Calculated dipole moments for polymers

Polymer[a]	μ_g (D)	μ_e (D)	$\Delta\mu_{ge}$ (D)	f
PBD	0.5307	0.4025	0.1992	1.1678
PBD-a	1.4688	1.6633	0.2907	1.2089
TFD	0.9447	1.0817	0.1984	0.8227
TFD-a	1.5670	1.7898	0.2866	0.8422

[a] One repeating unit is used and the size of polymer side chain is reduced

Of all other calculated parameters, we further identify that the oscillator strength (*f*) seems to increase by enlarging the dipole moment of the molecule (Table 6-2). This finding is interesting because this parameter can be correlated to absorption coefficient (ε) by the relationship $f \approx 4.31\times10^{-9} \int \varepsilon \, \mathrm{d}v$.[42] Indeed, from Figure 6-1b, we observe an increase in absorption coefficient experimentally from PBD and PTFD to PBD-a and PTFD-a, respectively. Moreover, the extinction coefficient of the pristine polymer thin-film as well as the polymer:$PC_{71}BM$ also shows the same trend (Figure 6-9). Therefore, we postulate that these asymmetric structures, formed by using conventional alkyl and highly polar TEG groups on each side of the DPP/FDPP building blocks have an enlarged absorption capability as a result of an increased molecular dipole moment.

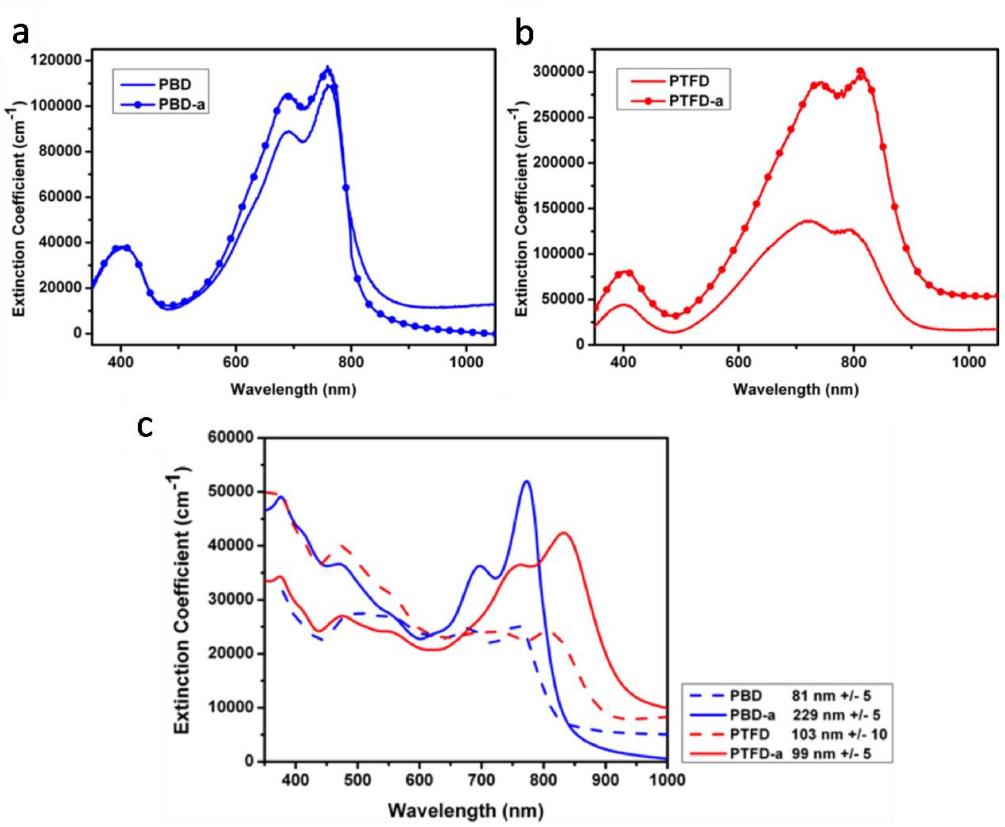

Figure 6-9. (a), and (b) Calculated pristine polymer thin film extinction coefficient. The thickness was determined by AFM measurement (PBD, d_{avg} = 84.4 nm; PBD-a, d_{avg} = 232.8 nm; PTFD, d_{avg} = 46.84 nm; PTFD-a, d_{avg} = 29.68 nm). (c) Calculated polymer/$PC_{71}BM$ blend thin film extinction coefficient. The thickness of the polymer:$PC_{71}BM$ films is determined by using a Dektakprofilometer.

To further check the hypothesis, four small molecules with symmetric vs. asymmetric side chains, DPP, DPP-a, FDPP and FDPP-a, were synthesized in order to examine molecular polarities and optical properties (Fig. 6-10). By using these molecules, we were able to exclude the effects of donor moiety presented in the polymer as well as the natural complexity brought by polymers such as molecular weight, polymer entanglement, and remaining impurities, etc. We

compared the relation of dipole moment and oscillator strength of these molecules through a combination of theoretical calculations and experimentally obtained absorption coefficients.

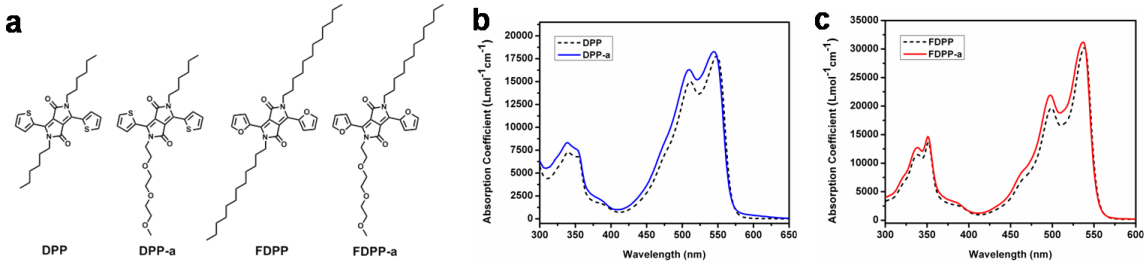

Figure 6-10. (a) Structures of monomers used to study optical properties of DPP, DPP-a, FDPP and FDPP-a. Measured absorption coefficients for (b) DPP, DPP-a, and c., FDPP, FDPP-a.

On the basis of the geometry optimization results (Table 6-3 and Fig. 6-11), it was confirmed that DPP-a and FDPP-a have a higher ground state dipole moment (1.6431 and 1.4985 compared to 0.5061 and 0.3640 for DPP and FDPP, respectively). Following from the geometric optimization, TDDFT was performed in order to find the first three transition energies for each molecule. Our results show that both DPP-a and FDPP-a have relatively higher oscillator strength than their original version (Table 6-3). Moreover, the oscillator strengths of second and third transitions all show a higher value in the case of the asymmetric system, although the strength is much lower than the first transition.

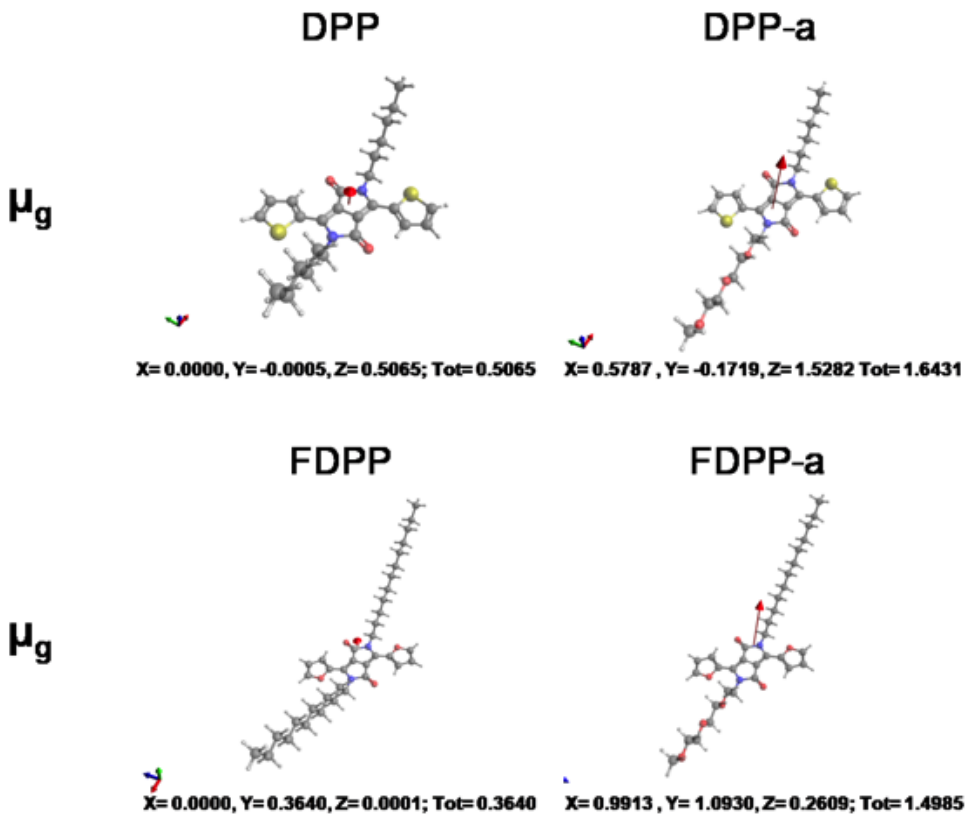

Figure 6-11. DFT optimized ground state geometry and molecular dipole moment for DPP, DPP-a, FDPP, and FDPP-a. The visualization of dipole moments was done by Avogadro software (version 1.1.1).

The experimentally measured absorption coefficient follows nearly the same trend as the simulation predicts, where it increases from 17.8 and 30.2 $\times 10^3$ $Lmol^{-1}cm^{-1}$ to 18.2 and 31.2 $\times 10^3$ $Lmol^{-1}cm^{-1}$ (Figure 6-10b-c and Table 6.3). In order to reduce the effect of molecular packing on the absorption coefficient measurement, the solution used for determination was relatively diluted (~ 1×10^{-5} M). Note that the absorption spectra tend to become flat at higher concentrations (Figure 6-12). The result from the model small molecules clearly shines light on the difference in absorption coefficient in more complicated real polymer systems, which can at least provide partial explanation behind the improvement of device performance.

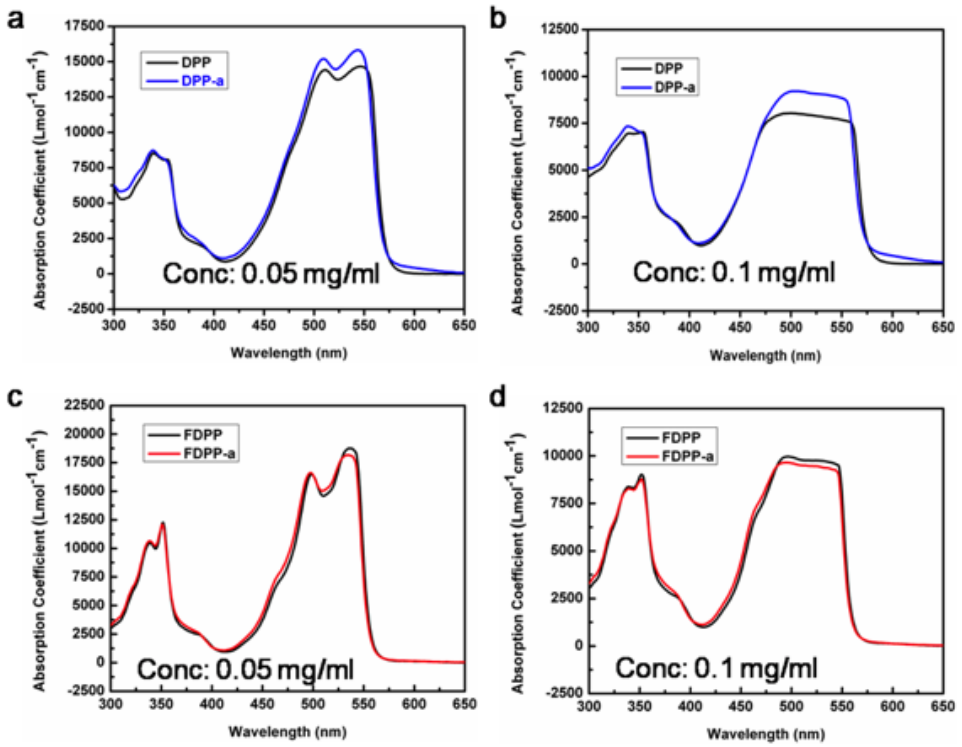

Figure 6-12. Measured absorption coefficient for (a) DPP, DPP-a and (b) FDPP, FDPP-a at 0.05 mg/ml CF solution; and (c) DPP, DPP-a and (d) FDPP, FDPP-a at 0.1 mg/ml CF solution.

Table 6-3. Calculated dipole moment, and oscillator strength, measured absorption coefficients for studied molecules

Monomer	μ_g (D)	f^{1st}	f^{2nd}	f^{3rd}	ε_{max} ($\times 10^3$Lmol^{-1}cm^{-1})
DPP	0.5065	0.4900	0.0001	0.0000	17.8
DPP-a	1.6431	0.4997	0.0010	0.0002	18.2
FDPP	0.3640	0.4950	0.0002	0.0001	30.2
FDPP-a	1.4985	0.5000	0.0012	0.0002	31.2

6.3.4. Thin-film morphology

Molecular packing also affects the polymer thin-film properties as well as device performance in a profound way. In order to study the effects of side chain asymmetry on the

molecular stacking, Grazing Incidence Wide Angle X-Ray Scattering (GIWAXS), Atomic Force Microscope (AFM), and Transmission Electron Microscope (TEM) were employed. Figure 6-13 shows the two-dimensional (2D) GIWAXS patterns of pristine polymer thin films. The polymers were spin-casted on a PEDOT:PSS modified Silicon (Si) substrate. From the 2D scattering patterns, it is clear that the crystallinity and orientation of polymer crystals change significantly after the symmetry of side chains are broken. From the linecuts along with the out-of-plane direction (Fig. 6-13b), in the case of PBD series, the observed crystal peaks (100), (200), and (300) are more pronounced in the PBD-a thin-film than that of PBD. Based on the peak position of (100), PBD-a's lamellar spacing is calculated to be 17.7 Å (q_z = 0.358 $Å^{-1}$), while PBD shows a lamellar spacing of 17.1 Å (q_z = 0.368 $Å^{-1}$), which is slightly shorter. According to (010) peaks, the π-π stacking distance is found to be 3.8 Å for both PBD and PBD-a thin films. Other than the distance, the information of crystallite size (crystalline correlation length, *D*) can be acquired via Scherrer equation using an experimentally determined full width at half-maximum (FWHM) of the peaks of interests.[44-45] Assuming the orientation of PBD and PBD-a is face-on and edge-on preferential, respectively, we find that the D_{100} is decreased from 14.4 nm to 6.7 nm by changing from symmetric to asymmetric structures. Overall, in the case of asymmetric PBD-a, the lamella distance is slightly larger than that of its un-modified version. On the other hand, the linecuts along with the in-plane direction for PBD and PBD-a thin films display that the (010) peak is significantly more pronounced after introducing different side chains, along with a decrease in (100) peak's intensity. Combined with the linecut analyses, we observe a more well-defined crystalline structure after asymmetric side chains are introduced. Moreover, the orientation of the polymer crystals changed to an edge-on preference from face-on. For the PTFD polymer system, breaking the side chain's symmetry shows a slightly different story.

Based on the out-of-plane linecuts, it is difficult to assign peaks for both polymers, while a more pronounced (010) peak is observed for PTFD-a thin film, with a distance of around 3.7 Å (q_z = 1.693 $Å^{-1}$), which belongs to π-π stacking. Weak (100) peaks of around 24 Å (q_{xy} ~ 0.260 $Å^{-1}$) were observed for both polymers, with PTFD having a more distinct (010) peak. Based on the observations for the PTFD series, we judge that the crystal orientation has changed from edge-on to face-on. It is noted that this structural change along with the side chain modification is preserved after blending with the $PC_{71}BM$ (Figure 6-14).

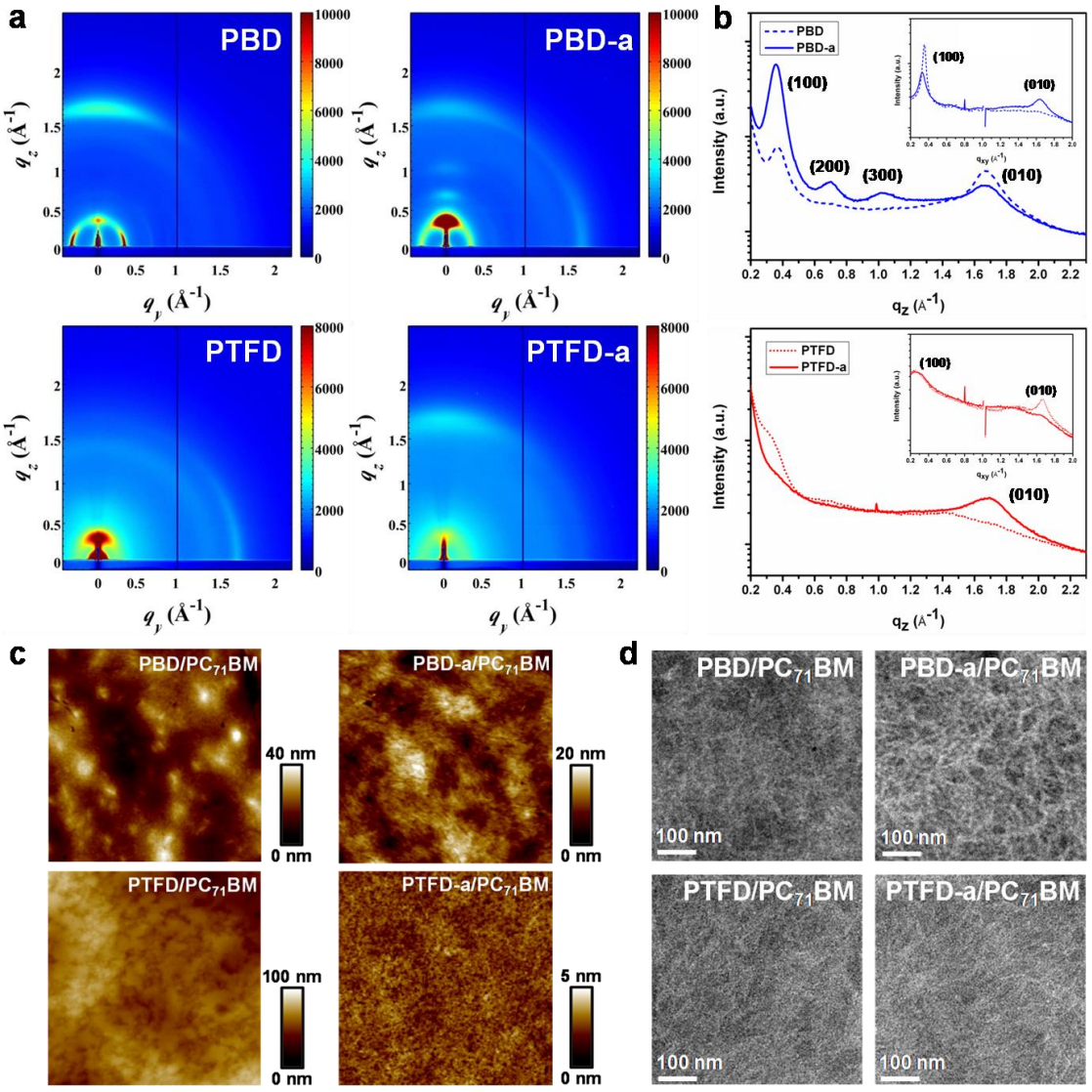

Figure 6-13. (a) GIWAXS patterns of pristine polymer PBD, PBD-a, PTFD, and PTFD-a, (b) lincuts of the corresponding GIWAXS patterns, (c) AFM height images of PBD:$PC_{71}BM$, PBD-a:$PC_{71}BM$, PTFD:$PC_{71}BM$, and PTFD-a:$PC_{71}BM$ blends (scale of the figure: 2.5 μm), and (d) TEM images of PBD:$PC_{71}BM$, PBD-a:$PC_{71}BM$, PTFD:$PC_{71}BM$, and PTFD-a:$PC_{71}BM$ blends.

To further visualize the BHJ thin film morphology, tapping-mode AFM was taken for each sample. From Fig. 6.13c, it is clear that after modifying the side chains, both polymer:$PC_{71}BM$ thin films show a relatively smoother surface with a slightly finer structure

(R_{RMS} = 5.62, 2.52, 6.22, and 0.83 nm for PBD, PBD-a, PTFD, and PTFD-a:$PC_{71}BM$ blend thin film, respectively). This is further confirmed by thin-film TEM measurement, showing that the aggregation is indeed more pronounced. We thus attribute the enhanced photocurrent in solar cell device to a more favorable morphology formed. This morphology transformation is believed to be induced by side chain asymmetry as well as the existing of the easier-to-crystalized TEG groups. Summarized from the morphological analysis, a dramatic change in polymer crystal structure and orientation was observed after breaking the side chain symmetry for both polymer systems. The blend thin-film, benefiting from the asymmetrical side chains, shows the formation of more favorable morphology, which is beneficial for PSC.

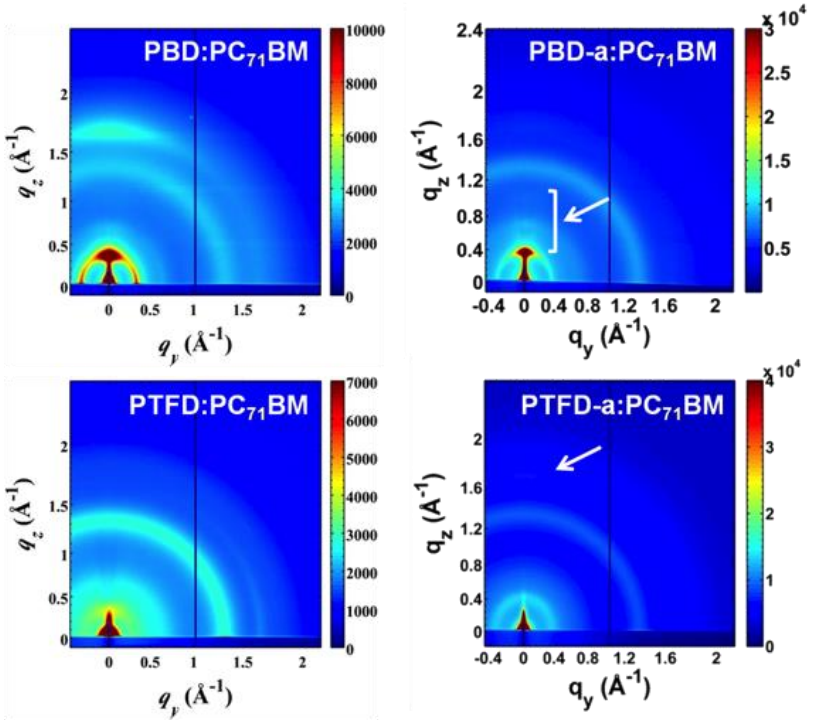

Figure 6-14. GIWAXS patterns of PBD:$PC_{71}BM$, PBD-a:$PC_{71}BM$, PTFD:$PC_{71}BM$, and PTFD-a:$PC_{71}BM$. Blend ratio, polymer:$PC_{71}BM$ = 1:2.

6.3.5. All solution process 3-Terminal parallel tandem solar cell devices

Tandem structure is a critical step towards high solar cell efficiency. While monolithic integrated series tandem is the mainstream, the current matching restriction increases the difficulty for its application. Parallel tandem removes the current matching restriction, but the highly conductive and transparent interconnection layer was traditionally achieved through vacuum deposition of thin metal or transparent conductive oxides. Removing the vacuum process is critical to achieve cost effectiveness. Here, we successfully demonstrated a vacuum free all solution process 3-terminal parallel tandem solar cell device using these two polymers PBD-a and PTFD-a as model subcells.[46-47] The device architecture is shown in Figure 6-15a, where a silver nanowire (AgNW)-based common electrode was used as the interconnecting layer (device structure: ITO/zinc oxide (ZnO)/PBD-a/PEDOT:PSS/AgNWs:Titanium oxide (TiO_2)/PEDOT:PSS/PTFD-a/ZnO/Al). The embedded silver nanowire mesh network can dramatically enhance the conductivity of common middle electrode at lowest cost of transparency.[48-49] By sandwiching AgNWs in between PEDOT:PSS and TiO_2, the chance of AgNWs penetrating through other layers and causing electrical short circuit becomes little. Furthermore, our 3-terminal tandem solar cell device also complies with full solution processing requirement, making it as attractive as other 2-terminal (series-connected) tandem solar cells.[9-11,50] Unlike 2-terminal tandem devices, a perfectly complementary spectrum is not necessary in the present tandem structure since current matching is not a critical factor.

Here, we demonstrate the universal compatibility of our tandem design with different material systems. From the device results (Table 6-1), we observe a high J_{SC} of 22 mA/cm^2 using PBD-a and PTFD-a in 3-terminal tandem solar cell. The V_{OC} of tandem cell is measured to be 0.64 V, which is similar to that observed in PTFD-a based single junction device. Along with a

FF% of 59, a PCE of 8.4 % was achieved, which is the highest number reported for 3-terminal tandem device structure. The overall EQE of the tandem device has a highest value of over 80 %), indicating that most of the visible photons has successfully been converted into electricity. Note that a tandem cell based on PBD and PTFD without asymmetry side chain design has been fabricated as reference and a 4.6 % PCE has been recorded (Table 6-1). In brief, all solution process 3-terminal tandem solar cell utilizes the spectrum overlapping to its own advantage. This development also paves another way to obtain high performing organic solar cells without using the high-cost and scarce polymer materials.

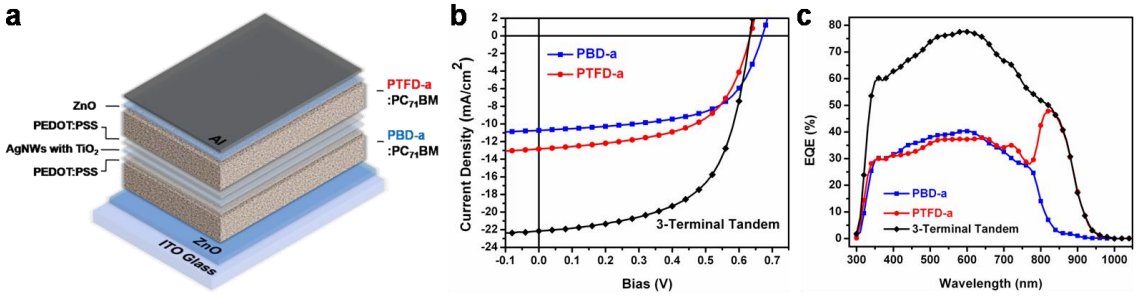

Figure 6-15. (a) all solution process 3-Terminal tandem device architecture, (b) current density-voltage characteristics of PBD-a and PTFD-a based 3-terminal tandem solar cells under AM1.5G illumination (100 mW/cm^2), and (c) EQE of the corresponding tandem device. Integrated J_{SC} for tandem device is calculated to be 21.3 mA/cm^2.

6.5 Summary and outlook

In conclusion, this work explores the effects of side chain asymmetry on the optoelectronic properties and corresponding photovoltaic performance of conjugated polymers. Two different polymer backbone systems, PBD and PTFD, with different E_g were demonstrated to have higher solar cell J_{SC} after breaking the side chain symmetry, while the V_{OC} remained the same. We speculate that the increased dipole moment, as a result of replacing one alkyl-chain

with TEG groups, could be the main reason for this enhancement. Supported by a detailed investigation on absorption capability of the corresponding DPP and FDPP molecules, we find that increasing the dipole moment may lead to stronger light absorption. Moreover, the increased dipole moment may also strengthen the ordering between the molecules, which is evidenced by a series of morphological studies. This ordering is also responsible for better charge transport, where the transportation of the carriers is found to be faster by SCLC measurement. In utilizing these polymers, we successfully demonstrated an all-solution processed 3-terminal tandem device using PEDOT:PSS/AgNW:TiO_2/PEDOT:PSS as the common transparent middle electrodes. A high J_{SC} of 22 mA/cm^2 was achieved with a maximum EQE of ~ 80%. The present contribution thus provides an effective way to adjust polymer's optoelectronic and photovoltaic properties with low requirement from polymer's single-junction performance. We envision that this strategy can provide even higher performance boost with the help from other material systems and a PCE as high as 10% can be expected in the near future.

References:

[1] Li, G. *et al. Nature Photon.*, **6**, 153 (2012).

[2] Dou, L. *et al. Adv. Mater.*, **25**, 6642 (2013).

[3] Heeger, A. J. *Adv. Mater.*, **26**, 10 (2014).

[4] Yu, G. *et al. Science,* **270**, 1789 (1995).

[5] Halls, J. J. M. *et al. Nature*, **376**, 498 (1995).

[6] Li, G. *et al. Nat. Mater*., **4**, 864 (2005).

[7] Liu, Y. *et al*. *Nature Commun*., **5**, 5293 (2014).

[8] He, Z. *et al. Nature Photonics*, **9**, 174 (2015).

[9] You, J. *et al. Nature Commun.*, **4**, 1446 (2013).

[10] Chen, C.-C. et al. *Adv. Mater*., **26**, 5670 (2014).

[11] bin Mohd Yusoff, A. R., *et al. Energy Environ. Sci.*, **8**, 303 (2015).

[12] Ye, L. *et al. Adv. Mater.*, **24**, 6335 (2012)

[13] Gao, J. *et al. Adv. Mater.*, **26**, 3142 (2014).

[14] Zhou, H. *et al. Adv. Mater*., **25**, 1646 (2013).

[15] Peet, J. *et al. Nat. Mater.*, **6**, 497 (2007).

[16] Liang, Y. *et al. Adv. Mater.*, **22**, E135 (2010).

[17] He, Z. *et al. Adv. Mater.*, **23**, 4636 (2011).

[18] He, Z. *et al. Nature Photon.*, **6**, 591 (2012).

[19] Chueh, C.-C. *et al. Energy Environ. Sci.*, **8**, 1160 (2015).

[20] Esiner, S. *et al. Adv. Energy Mater.*, **3**: 1013 (2013).

[21] Morfa, A. J. *et al. Appl. Phys. Lett.*, **92**, 13504 (2008).

[22] Wu, J. L. *et al. ACS Nano*, **5**, 959 (2011).

[23] Janković, V. *et al. ACS Nano*, **7**, 3815 (2013).

[24] Cheng, Y. J. *et al. Chem. Rev.*, **109**, 5868 (2009)

[25] Dou, L. *et al. Chem. Rev.*, DOI: 10.1021/acs.chemrev.5b00165 (2015).

[26] Mei, J. *et al. Chem. Mater.*, **26**, 604 (2014).

[27] Liang, Y. *et al. J. Am. Chem. Soc.*, **131**, 7792 (2009).

[28] Yiu, A. T. *et al. J. Am. Chem. Soc.*, **134**, 2180 (2012).

[29] Cabanetos, C. *et al. J. Am. Chem.Soc.*, **135**, 4656 (2013).

[30] Li, W. *et al. Adv. Mater.*, **25**, 3182 (2013).

[31] Meager, I. *et al. J. Am. Chem. Soc.*, **135**, 11537 (2013).

[32] Fang, L. *et al. Chem. Mater.*, **25**, 4874 (2013).

[33] Chang, W.-H. *et al. Macromolecules*, **48**, 562 (2015).

[34] Chen, H.-Y. *et al. Nat. Photon.*, **3**, 649 (2009).

[35] Huo, L. *et al. Angew. Chem. Int. Ed.*, **123**, 9871 (2011).

[36] Li, W. *et al. J. Am. Chem. Soc.*, **135**, 5529 (2013).

[37] Cui, C. *et al. Energy Environ. Sci.*, **7**, 2276 (2014).

[38] Chang, W.-H. *et al. Adv. Energy Mater.*, 4: 1300864 (2014).

[39] Naik, M. A. *et al. J. Phys. Chem. C*, **116**, 26128 (2012).

[40] Beaujuge, P. M. *et al. Acc. Chem. Res.*, **43**, 1396 (2010).

[41] Huo, L. *et al. Macromolecules*, **42**, 6564 (2009).

[42] Carsten, B. *et al. J. Am. Chem. Soc.*, **133**, 20468 (2011).

[43] Homyak, P. D. *et al. Macromolecules*, **46**, 8873 (2013).

[44] Chen, W. *et al. Nano Lett.*, **11**, 3707 (2011).

[45] Rivnay, J. *et al. Phys Rev. B*, **84**, 045203 (2011).

[46] Sista, S. *et al. Adv. Mater*., **22**, E77 (2010).

[47] Guo, F. *et al. ACS Nano*, **8**, 12632 (2014).

[48] Chen, C.-C. *et al. ACS Nano*, **6**, 7185 (2012).

[49] Chen, C.-C. *et al. Energy Environ. Sci*., **6**, 2714 (2013).

[50] Chen, C.-C. *et al. Mater. Horiz*., **2**, 203 (2015).

CHAPTER 7

Conclusion

Polymer solar cells (PSCs) provide an opportunity to efficiently generate energy from sunlight at a reasonable cost. Via solution processing, a unique structure binary bulk heterojuction (BHJ) structure can be developed to utilize a mixed layer of p-type polymeric semiconductors and n-type fullerene derivatives, such as [6,6]-phenyl-C71-butyric acid methyl ester ($PC_{71}BM$). Owing to the vast research efforts over the past decade, the power conversion efficiencies (PCE) of single- and multi-junction PSCs have recently surpassed the 10% milestone.

Materials development, driven by the desire to overcome the constraint of P3HT, has played an important role in advancing this technology. To date, several state-of-the-art polymers, such as PTB7, PDPP3T, PBDTDPP and PffBT4T, have shown remarkable performance. In order to keep this momentum going, further improvements and deeper insights into materials' property are certainly required. In this dissertation, we focus on improving the properties of several state-of-the-art photovoltaic polymers by overcoming their limitations using novel organic synthetic approaches.

In Chapter 3, we aim to enhance the performance of the solar cell based on the PBDTT-DPP:$PC_{71}BM$ blend by attempting to increase the generated photocurrent. We show that this goal can be achieved by substituting part of the sulfur atoms along the polymer backbone with

selenium atoms. This approach leads to two results: a polymer bandgap reduction and a charge transport property enhancement in the blend thin film, both of which contribute to the improved photocurrent. The newly synthesized polymer, PBDTT-SeDPP (Eg = 1.38 eV), shows an excellent single junction solar cell PCE of over 7%, a tandem polymer solar cell PCE of 9.5%, and a visibly transparent solar cell PCE of 4.5%. These results from different types of solar cell are all superior to those based on PBDTT-DPP.

Balancing the trade-off between a semiconductive polymer's solubility and its easiness to aggregate is always a difficult issue. In Chapter 4, we use a triple component random copolymerization approach to precisely control the amount of triethylene glycol (TEG) side chain, which can be regarded as a stack-inducing agent, being introduced into a given polymer backbone without affecting its solubility. TEG side chains result in a more favorable morphology in a polymer:fullerene blend. Based on PBDTT-DPP polymer series, this approach can bring an overall 10% improvement in PCE.

Chapter 5 addresses the common morphological issue observed in PTB7-based PSC devices by a selenophene-modified side-chain. The structure adjustment carried out by alkylselenophene substitution on the BDT moiety of PTB7-Th can affect the energy levels. Therefore, a solar cell based on the new polymer, PBDTSe-TT, shows an enlarged V_{OC}. More importantly, the PBDTSe-TT:$PC_{71}BM$ bulk-heterojunction thin film morphology is also optimized through this modification. As a consequence, an efficient PCE of 8.8% is achieved without using any solvent additive or special interfacial layer. The PBDTSe-TT-based device is thus relatively stable under thermal stress, making it a good candidate for fabricating stacked cells.

In Chapter 6, we provide more insights on how a polymer's side chains can affect its photovoltaic properties. We find that breaking the side chain symmetry of an existing DPP-based photovoltaic polymer can lead to a greatly enhanced photovoltaic performance. Using this strategy, more than a 50% photocurrent improvement is seen for two different structures. The cause of this observation is proposed as an enhancement in light absorption and the formation of a more favorable nanoscale morphology in the polymer:$PC_{71}BM$ blend, which could be further correlated to the increased molecular dipole moment as a result of using asymmetric side chains. An all-solution process 3-terminal tandem structure was demonstrated to connect two high photocurrent cells in a parallel connection in order to harvest more photons and obtain a photocurrent density of 22 mA/cm^2, which is unprecedented for any 3-terminal tandem device reported with polymer solar cells.

The current dissertation provides several new polymer design strategies to the field. Adjustments of materials' optoelectronic properties and their device processing conditions have been demonstrated to be viable through chemistry modification at the molecular scale. We hope that the accompanied insights of this work can contribute to the field by giving rise to more high-performing photovoltaic polymers in the future.